
Article:
Sobala, Lukasz F. orcid.org/0000-0002-3807-6452, Speciale, Gaetano, Zhu, Sha et al. (17 more authors) (2020) An epoxide intermediate in glycosidase catalysis. ACS Central Science. pp. 760-770. ISSN: 2374-7943

https://doi.org/10.1021/acscentsci.0c00111

An epoxide intermediate in glycosidase catalysis

Lukasz F. Sobala,[1,†] Gaetano Speciale,[2,†] Sha Zhu,[3,†] Lluís Raich,[4,5,†] Natalia Sannikova,[6] Andrew J Thompson,[1] Zalihe Hakki,[2] Dan Lu,[3] Saeideh Shamsi Kazem Abadi,[7] Andrew R. Lewis,[6] Víctor Rojas-Cervellera,[4,5] Ganeko Bernardo-Seisdedos,[9] Yongmin Zhang,[3] Oscar Millet,[9] Jesús Jiménez-Barbero,[9,10] Andrew J. Bennet,[6,7]* Matthieu Sollogoub,[3]* Carme Rovira,[4,5]* Gideon J Davies,[1]* Spencer J. Williams,[2]*

[1] York Structural Biology Laboratory, Department of Chemistry, University of York YO10 5DD, U.K.

[2] School of Chemistry and Bio21 Molecular Science and Biotechnology Institute, University of Melbourne, Parkville, Victoria 3010, Australia

[3] Sorbonne Université, CNRS, Institut Parisien de Chimie Moléculaire, UMR 8232, 4 place Jussieu, 75005 Paris, France

[4] Departament de Química Inorgànica i Orgànica (Secció de Química Orgànica) & Institut de Química Teòrica i Computacional (IQTCUB), Universitat de Barcelona, Martí i Franquès 1, 08028 Barcelona, Spain

[5] Institució Catalana de Recerca i Estudis Avançats (ICREA), Pg. Lluís Companys 23, 08010 Barcelona, Spain

[6] Department of Chemistry, Simon Fraser University, 8888 University Drive, Burnaby, British Columbia, V5A 1S6, Canada

[7] Department of Biochemistry and Molecular Biology, Simon Fraser University, 8888 University Drive, Burnaby, British Columbia, V5A 1S6, Canada

[8] Ikerbasque, Basque Foundation for Science, Mariá Dıáz de Haro 3, 48013 Bilbao, Spain

[9] Molecular Recognition and Host−Pathogen Interactions, CIC bioGUNE, Bizkaia Technology Park, Building 800, 48160 Derio, Spain

E-mail: sjwill@unimelb.edu.au, gideon.davies@york.ac.uk, matthieu.sollogoub@sorbonne-universite.fr, c.rovira@ub.edu

† These authors contributed equally.

G.J.D and S.J.W conceived the project; C.R., M.S., A.J.B., G.J.D., and S.J.W. designed the experiments; G.S., Z.H., D.L., S.Z., and Y.Z. synthesized ligands and substrates; N.S., S.S.K.A., A.R.L., and A.J.B. measured KIEs and analysed results; L.F.S., A.J.T., Z.H., G.J.D. conducted X-ray crystallography and analysed results; L.F.S, S.Z performed

enzymatic reactions and analyzed results; G.B.-S., L.F.S., O.M., J.J.-B. performed NMR measurements of ligand affinities; L.R., V.R.-C. and C.R. performed computational studies; C.R., A.J.B., G.J.D., and S.J.W. wrote the manuscript.

Abstract:

Retaining glycoside hydrolases cleave their substrates through stereochemical retention at the anomeric position. Typically, this involves two-step mechanisms using either an enzymatic nucleophile via a covalent glycosyl enzyme intermediate, or neighboring group participation by a substrate-borne 2-acetamido neighboring group via an oxazoline intermediate; no enzymatic mechanism with participation of the sugar 2-hydroxyl has been reported. Here, we detail structural, computational and kinetic evidence for neighboring group participation by a mannose 2-hydroxyl in glycoside hydrolase family 99 *endo*-α-1,2-mannanases. We present a series of crystallographic snapshots of key species along the reaction coordinate: a Michaelis complex with a tetrasaccharide substrate; complexes with intermediate mimics, a sugar-shaped cyclitol β-1,2-aziridine and β-1,2-epoxide; and a product complex. The 1,2-epoxide intermediate mimic displayed hydrolytic and transfer reactivity analogous to that expected for the 1,2-anhydro sugar intermediate supporting its catalytic equivalence. Quantum mechanics/molecular mechanics modelling of the reaction coordinate predicted a reaction pathway through a 1,2-anhydro sugar via a transition state in an unprecedented flattened, envelope (E_3) conformation. Kinetic isotope effects (k_{cat}/K_M) for anomeric-^{2}H and anomeric-^{13}C support an oxocarbenium ion-like transition state and that for C2-^{18}O (1.052 ± 0.006) directly implicates nucleophilic participation by the C2-hydroxyl. Collectively, these data substantiate this unprecedented and long-imagined enzymatic mechanism.

Introduction

Glycoside hydrolases (glycosidases) catalyze the transfer of the glycosyl group of glycosides to water or another nucleophilic molecule.[1] One major group of glycosidases are those that cleave their glycoside substrates with a net retention of anomeric configuration. Retaining glycosidases typically operate through two-step mechanisms involving a covalent glycosyl enzyme intermediate formed from a nucleophilic amino acid residue (Asp, Glu or Tyr) (**Fig. 1a**). Alternatively, certain retaining hexosaminidases act through a mechanism involving neighboring-group participation by the 2-acetamido (or glycolylamido) group of the substrate.

While there is extensive evidence for neighboring group participation by a 2-acetamido group in hexosaminidases, these are the only glycosidases for which neighboring group participation is accepted. Interestingly, there is a large body of evidence supporting neighboring group participation by a glycoside 2-hydroxyl in the alkaline cleavage of 1,2-*trans* glycosides and glycosyl fluorides and 1,2-anhydro sugars (a 1,2-epoxide) as intermediates. This data includes the well-known differences in the rate of alkaline hydrolysis of 1,2-*cis*- versus 1,2-*trans*-glycosides, the reduced rate of alkaline hydrolysis of otherwise identical 2-alkylated 1,2-*trans*-glycosides,[2] and retention of anomeric stereochemistry in the alkaline methanolysis of 1,2-*trans*-glycosyl fluorides whereas 2-alkylated 1,2-*trans*-glycosyl fluorides react with inversion.[3] Kinetic isotope effects for the alkaline hydrolysis of 4-nitrophenyl α-D-mannopyranoside have given direct evidence for neighboring-group participation by a C2-oxyanion.[4] Neighboring group participation by a 2-hydroxyl has also been proposed for other glycoside hydrolases,[5-6] but none have withstood cursory, let alone detailed, mechanistic scrutiny.[7-9]

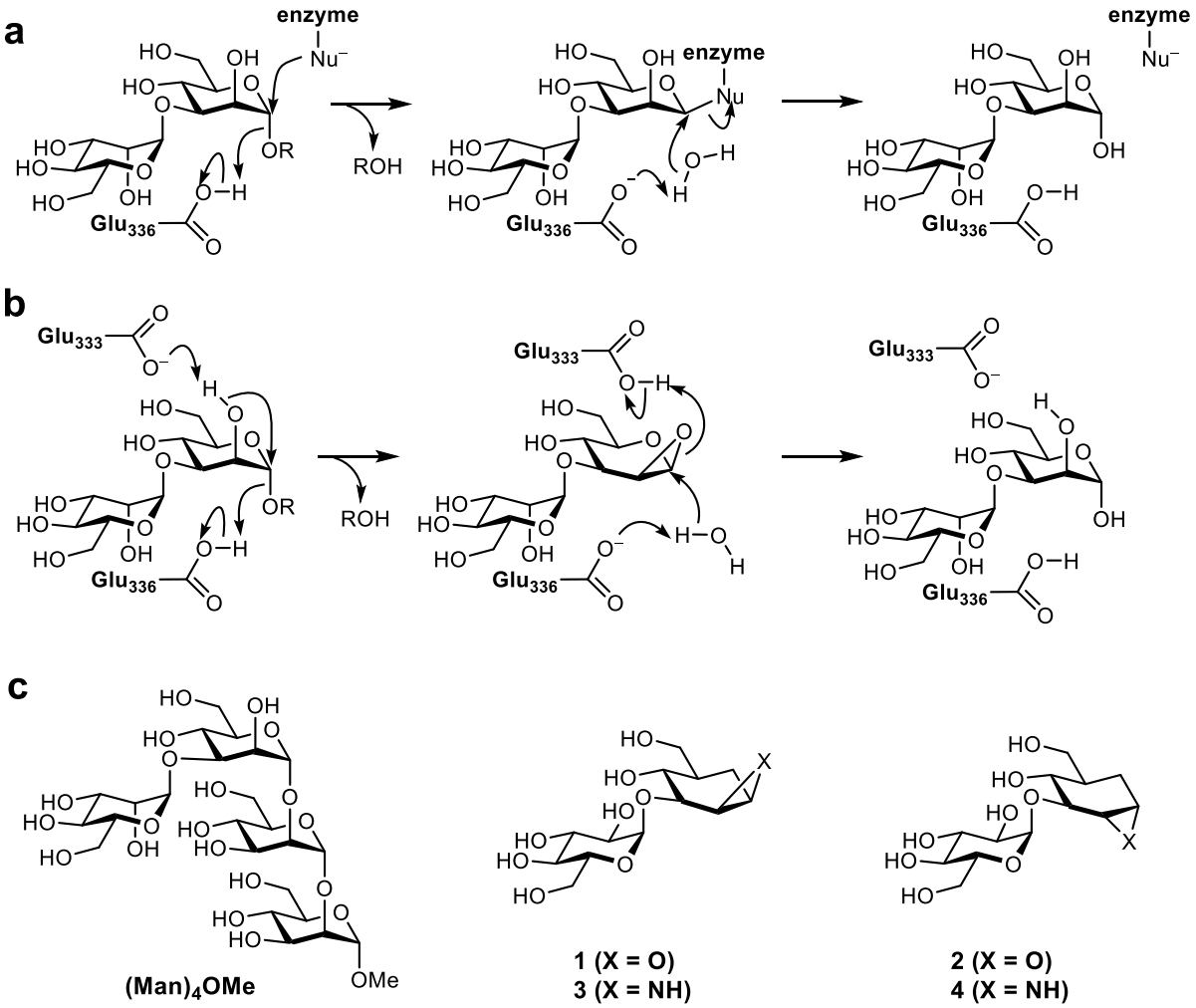

Figure 1. Proposed mechanisms for a retaining glycoside hydrolase applied to a GH99 endo-α-1,2-mannanase. a, Classical Koshland mechanism involving an enzymatic nucleophile and a glycosyl enzyme intermediate. Residue numbering is for *Bt*GH99. **b**, Alternative mechanism involving neighboring group participation by the 2-hydroxy group and a 1,2-anhydro sugar intermediate. **c,** Structures of ligands used in this study.

Glycoside hydrolases of CAZY (see www.cazy.org; www.cazypedia.org)[10-11] family 99 are *endo*-acting retaining glycosidases that cleave α-mannosidic linkages within α-mannans in the yeast cell wall (*endo*-α-1,2-mannanases)[12] and mammalian glucosylated high-mannose N-glycans (*endo*-α-1,2-mannosidases).[13-15] These enzymes have important roles in fungal cell wall degradation in the human gut microbiota[16] as well as processing of glucosylated

intermediates in N-glycan biosynthesis,[17] respectively. For both types of enzyme, the minimum substrate for these enzymes is a disaccharide in which the reactive, –1 mannosyl residue is modified at the 3-position with either an α-mannosyl or α-glucosyl residue. The first X-ray structures of members of GH family 99, *endo*-α-1,2-mannanases from *Bacteroides thetaiotaomicron* and *Bacteroides xylanisolvens*, *Bt*GH99 and *Bx*GH99, respectively, provided hints of an atypical mechanism.[18] These bacterial representatives act on both α-glucosyl- and α-mannosyl-1,3-α-mannosides (with around 10-fold preference for the latter), and structural studies using substrate-like ligands were applied to identify the enzymatic catalytic machinery. However, 3-dimensional structures of wild-type *Bt*GH99 in complex with the isofagomine-derived inhibitors GlcIFG[18] and ManIFG,[12] and a disabled non-catalytic mutant in complex with a substrate[12] failed to identify a likely enzymatic nucleophile appropriately situated near the fissile anomeric bond. Enticingly, complexes with deoxymannojirimycin-derived inhibitors GlcDMJ[18] and Man-2-amino-DMJ,[19] noeuromycin-derived inhibitors GlcNOE[18] and ManNOE,[20] and of the E333Q mutant with substrate,[12] highlighted an interaction between a carboxylate residue and the 2-hydroxyl of the –1 mannosyl residue. Collectively, these data were suggestive of an alternative mechanism involving a 1,2-anhydro sugar intermediate (**Fig. 1b**); however, no studies have provided direct evidence for participation of O2 or insight into the proposed epoxide intermediate.

Here, we present an analysis of the reaction mechanism of GH99 *endo*-α-1,2-mannanases. X-ray data of molecular probes, designed to mimic species along the reaction coordinate, provides a snapshot of key catalytic states. These results are extended by applying quantum mechanics/molecular mechanics (QM/MM) methods to study the enzyme-catalyzed reaction, giving computational support for the formation of a 1,2-anhydro sugar intermediate. We also show that a cyclitol epoxide mimic of the 1,2-anhydro sugar exhibits reactivity that is consistent with the expected reactivity of this intermediate. Finally, we measure kinetic isotope

effects that provide direct experimental support for neighboring-group participation by the substrate 2-hydroxy group in *Bt* and *Bx*GH99.

Results

Structures of the 'Michaelis' and product complexes of *Bx*GH99

As a first step in the mechanistic dissection of GH99 enzymes, and to provide structural data for computational approaches to study the reaction coordinate, we sought to define, at near atomic resolution, the two ends of the reaction coordinate. We thus determined substrate ('Michaelis') and product complexes of *Bx*GH99. A catalytically-inactive variant, E333Q, was used to obtain a complex with the substrate Man_4OMe (representing a fragment of the yeast mannan that is the substrate for this bacterial enzyme),[12] at a resolution of 1.07 Å, **Fig. 2a** (for X-ray data collection and refinement statistics see **Table S1**). The intact tetrasaccharide occupies the –2 to +2 subsites,[21] spanning the active site.

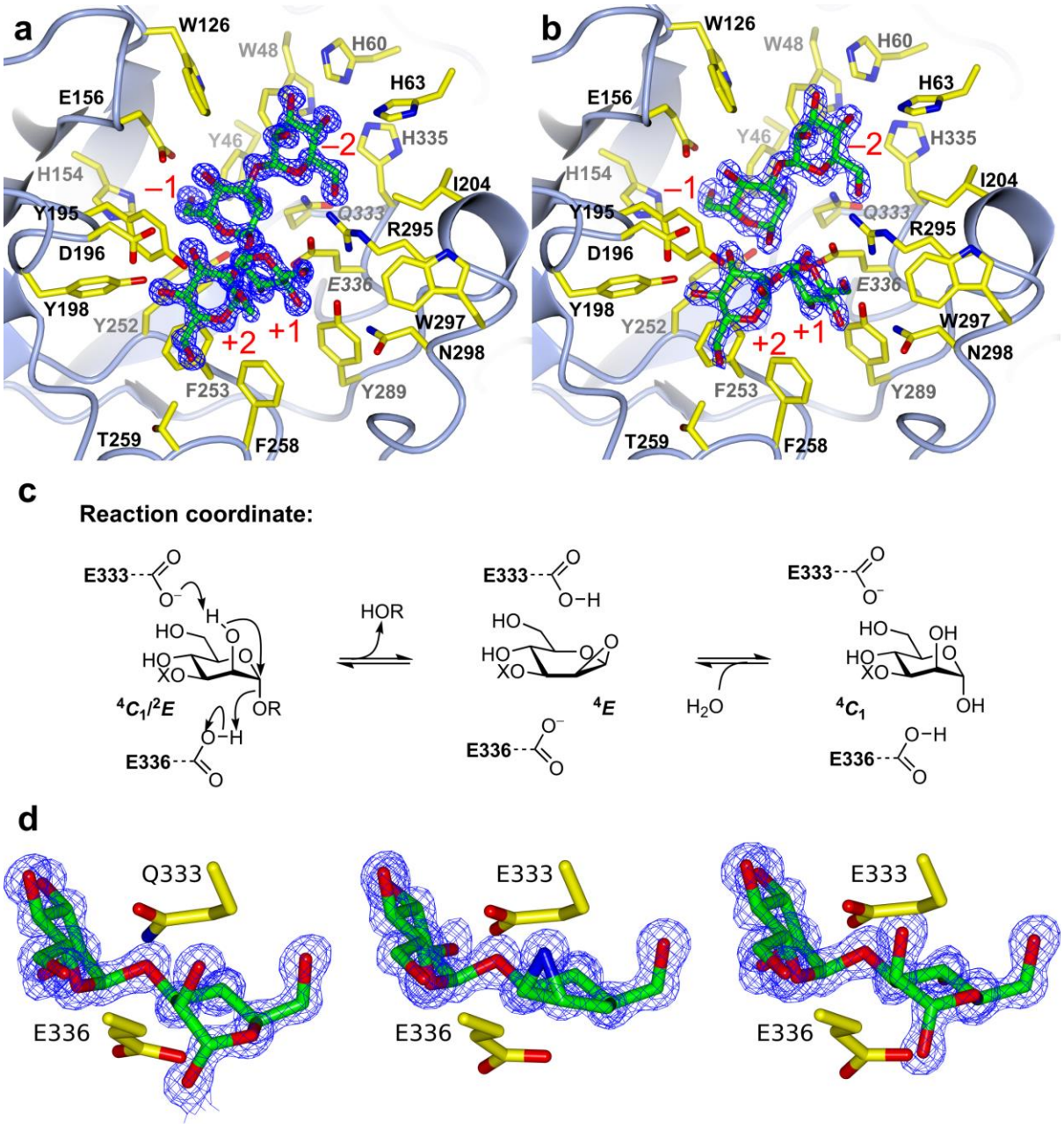

Figure 2. X-ray snapshots along the *Bx*GH99 reaction coordinate. X-ray structures of **a**, *Bx*GH99-E333Q bound to αMan-1,3-αMan-1,2-αMan-1,2-αMan-OMe [$(Man)_4OMe$]; **b**, *Bx*GH99-E333Q bound to α-1,3-mannobiose and α-1,2-mannobiose. Mutated active site residue in italics. **c**, Proposed reaction coordinate of the GH99 catalyzed reaction (X = αMan). **d**, X-ray structures showing the –2/–1 subsites for the Michaelis complex: *Bx*GH99-E333Q with $(Man)_4OMe$; intermediate complex: wildtype with cyclohexane β-1,2-aziridine **1**; and product complex: α-1,3-mannobiose and α-1,2-mannobiose with wildtype. $2mF_o$-F_c weighted electron density maps contoured at 0.8 $e^-/Å^3$ in all cases.

Within the Michaelis complex, the –1 mannoside residue adopts a $^4C_1$ conformation that is slightly distorted towards ^2E; this distortion can be confidently assigned at the atomic resolution of the data. There is no major protein conformational change (indeed, none has been seen in any GH99 structure) and, as seen in previous disaccharide and inhibitor complexes, no candidate enzymatic nucleophile is located near the reactive anomeric C1 carbon. Tyr252 is approx. 4 Å away from C1 in *Bx*GH99 and mutagenesis of the equivalent residue in human *endo*-α-mannosidase (39% sequence identity to *Bx*GH99) gave a mutant enzyme that maintained its ability to perform transglycosylation, excluding the possibility that this residue provides nucleophilic catalysis.[22] Of note is the interaction, 2.8 Å, between the Nε2 of the introduced Gln333 with the O2 of the –1 subsite mannoside. The natural Glu at this position is proposed to act as catalytic base for the deprotonation of O2 during the formation of the 1,2-anhydro sugar intermediate (**Fig. 1b**). The Michaelis complex shows that this residue is ideally placed, consistent with the complete loss of activity when Glu333 is substituted by Gln.[18]

The final enzyme-bound state of the reaction coordinate was determined through studies of product complexes. We solved ternary complexes of wildtype and E333Q variant *Bx*GH99 enzymes with the two products of hydrolysis: α-1,3-mannobiose and α-1,2-mannobiose, at 1.08 Å and 1.65 Å resolution, respectively. In both complexes, α-1,3-mannobiose bound in the –2, –1 subsites, and α-1,2-mannobiose bound in the +1, +2 subsites (**Fig. 2b, Fig. S1**). Comparison of the Michaelis and product complexes reveals that in the latter complex, the –1 sugar is in a relaxed $^4C_1$ conformation, which is consistent with the lack of a covalent bond connecting the –2/–1 and +1/+2 sugars, and the +1 mannose residue is shifted, such that it makes different hydrogen bonds to the protein. Thus, in the substrate complex the +1 mannose O3 hydrogen bonds to E336 O1, whereas in the product complex O3 is hydrogen bonded with Y289 and a water molecule resides where O3 sat in the substrate. Similarly, in the

substrate complex the +1 mannose O4 hydrogen bonds with water whereas in the product complex hydrogen bonds with the Y289 oxygen (see **Fig. S2**).

Both the 'Michaelis' and product complexes are thus consistent with a reaction mechanism involving neighboring-group participation by the substrate 2-hydroxy group, activated through deprotonation by Glu333 and with Glu336 acting as the catalytic acid for leaving group departure. Given this enticing structural support for this mechanism, we next sought to dissect the reaction coordinate using a computational approach.

QM/MM metadynamics simulations of the *endo*-α-1,2-mannanase-catalyzed reaction

To probe the potential neighboring-group participation by the substrate 2-hydroxy group, we modelled the reaction mechanism of the *endo*-α-1,2-mannanase-catalyzed reaction using classical molecular dynamics (MD) and QM/MM metadynamics simulations (see **Supplementary Methods**).[23-24] This approach accounts for the room temperature motion of the enzyme during the reaction while providing QM (DFT) accuracy for the description of the active site atoms. It has been used with success to model reaction mechanisms in a wide range of carbohydrate-active enzymes,[25] including Golgi α-mannosidase II.[26] Two collective variables (CVs) were used to define the reaction coordinate starting with the Michaelis complex, described above. These variables were chosen as to include the main bonds that are to be made/broken during the reaction (Figure 2c). The first collective variable (CV1, representing *nucleophilic attack*) was defined as the distance difference between C1-O1 and O2-C1. The second collective variable (CV2, *glycosidic bond protonation*) was defined as the distance between O1-H_{E336} and H_{E336}-O_{E336}.

The free energy landscape reconstructed from the simulation (**Fig. 3a**) shows that the Michaelis complex evolves to the product *via* a 1,2-anhydro sugar intermediate. An energy barrier of $\Delta G^{\ddagger} \approx 15$ kcal/mol between the Michaelis complex (MC) and the transition state (TS)

leads to the formation of a 1,2-anhydro sugar (EPO; local minimum on the right-hand-side). The computed free energy barrier is in good agreement with the available kinetic data;[16] the reaction is therefore both feasible and favored. The two minima located in the reactants region (MC and MC') correspond to alternative arrangements of the Michaelis complex in which the O-H bond of the acid/base residue E336 twists to point either towards the glycosidic oxygen or the +1 saccharide. The calculated TS is dissociative, with the glycosidic bond elongated (C1–O1 = 1.88 ± 0.06 Å; **Fig. 3b** and **Table S2**) and the O2 atom at an early stage of attack on the anomeric carbon (C1–O2 = 2.29 ± 0.06 Å), causing weakening of the C2–O2 bond. Analysis of the structures along the reaction coordinate (**Fig. 3c,d**) reveals distortion of the –1 mannosyl ring during the reaction, following a $^{2}E/^{2}H_{3} \rightarrow [E_{3}]^{\ddagger} \rightarrow {}^{4}E/^{4}H_{5}$ itinerary during the first half of the reaction, which can be considered an 'electrophilic migration' of C1 from the leaving group oxygen in the Michaelis complex, to the nucleophilic O2 in the EPO complex (**Fig. S3**). The conformation of the MC ($^{2}E/^{2}H_{3}$) is similar to the one obtained from the X-ray structure (between $^{4}C_{1}$ and ^{2}E; see **Fig. S4**), with only slight differences that can be attributed to the E333Q mutation in the X-ray structure altering the nature of the interaction of this residue with the substrate 2-OH. The conformation of the –1 mannosyl residue at the TS (E_{3}) achieves planarity of C2–C1–O–C5, as required for an oxocarbenium-ion-like transition state.[1] Finally, the calculated 1,2-anhydro sugar intermediate is in a $^{4}E/^{4}H_{5}$ conformation, in agreement with the X-ray structure of the wildtype enzyme in complex with cyclohexane β-1,2-aziridine (*vide infra*).

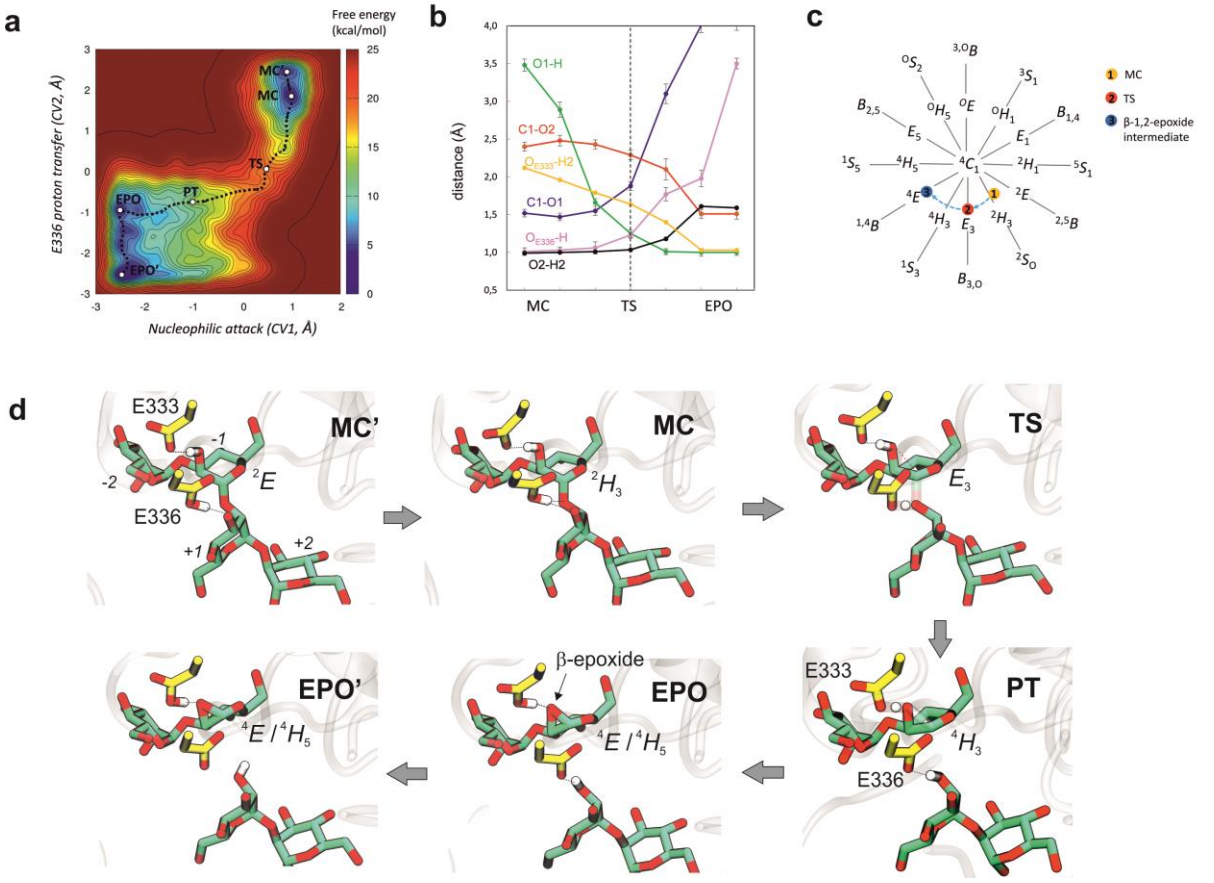

Figure 3. QM/MM metadynamics modelling of the *Bx*GH99 *endo*-α-1,2-mannanase catalyzed reaction. a, Free energy landscape (FEL) of the enzymatic reaction with respect to the two collective variables described in the text. Contour lines are at 0.5 kcal/mol. **b**, Evolution of relevant distances along the minimum free energy pathway (reaction coordinate). Averages over all configurations sampled for each point on the pathway are considered. Error bars correspond to standard deviations. **c**, Conformational itinerary of the α-mannoside at the –1 subsite along the reaction coordinate projected into Stoddart's diagram. **c**, Representative snapshots of the main states along the reaction coordinate (MC, MC', Michaelis complexes; TS, transition state; PT, proton transfer; EPO, EPO', 1,2-anhydro sugar.

To explore other possible mechanisms, we performed simulations with different collective variables. In particular, we quantified whether the canonical Koshland-type mechanism is a viable alternative mechanism for *Bx*GH99. To do so, an additional

metadynamics simulation was performed in which the O2 atom was not included in the CV set, thereby excluding any bias towards the epoxide formation. Specifically, we considered common CVs used to describe a classical Koshland double displacement reaction (i.e. considering the O_{E333}-C1 and C1-O1 distances as CV1 with the same CV2 as in the previous simulation).[27] The results, shown in the Supporting Information, reveal that even in this case, a double displacement reaction is not favorable; instead E333 acts as a base to abstract a proton from the 2-OH, leading to the same epoxide intermediate (**Fig. S5**). Altogether, our simulations provide computational support for a neighboring-group participation mechanism for *Bx*GH99 *endo*-α-1,2-mannanase.

Structures and reactivity of intermediate-mimicking complexes

To study the interactions and reactivity of the intermediate, we designed and synthesized compounds that mimic the GH99 Glc/Man-α-1,3-linked β-1,2-anhydrosugar intermediate. To improve their chemical stability, we replaced the endocyclic oxygen with methylene (CH_2), as previous work showed that the affinity of a glycal inhibitor was similar to that of the corresponding cyclohexene.[20] Thus, we synthesized cyclohexane-β-1,2-epoxide **1** and cyclohexane-β-1,2-aziridine **3** (**Fig. 1c**). To demonstrate stereospecificity, and to control for potential promiscuous reactivity of epoxides, we also synthesized the α-isomers: cyclohexane-α-1,2-epoxide **2** and cyclohexane-α-1,2-aziridine **4**.[28]

As reactivity of an intermediate mimic can provide strong evidence for mechanism, the ability of *Bt*GH99, *Bx*GH99 wild-type, E333Q and E336Q to catalyze reactions of these compounds was studied by mass spectrometry. The only enzyme-catalyzed reaction observed was for the β-1,2-epoxide **1**, which was converted to an M+18 species (**Fig. 4**, **Fig. S6**); the α-1,2-epoxide **2** and both α- and β-1,2-aziridines, **3** and **4** were inert (see **Fig. S7** for data for other compounds). The lack of reactivity of α-1,2-epoxide **2**, which stands in contrast to the

reactivity observed for β-1,2-epoxide **1**, is consistent with stereochemical specificity of GH99 enzymes, and provides evidence that there is not a nucleophilic enzymatic residue situated 'above' the sugar ring. The rate of formation of the M+18 species was linear as a function of time and was proportional to enzyme concentration. Using mass spectrometry the rates of product formation were 0.090 s^{-1} for *Bt*GH99 and 0.047 s^{-1} for *Bx*GH99, in concordance with data showing GlcManF is turned over more slowly by *Bx*GH99 than *Bt*GH99.[18] ^{1}H NMR spectroscopy of the product of the reaction revealed it to be a vicinal diol with an α-configuration **5** matching that of the product of the endomannanase reaction (**Supporting methods**). Thus, the cyclohexane β-1,2-epoxide exhibits reactivity expected for a 1,2-anhydro sugar intermediate, but with a rate of turnover approximately 1/30th of that of Glc-Man fluoride[18] at the same concentration, a result consistent with a reduced reactivity arising from the reduced charge-stabilization at the transition state because of the absence of an endocyclic oxygen. Notably, the α-1,2-epoxide **2** did not react with the GH99 enzyme to yield a covalently labelled enzyme, as might be expected if GH99 enzymes used an enzymatic nucleophile based on similar precedents with variants of cyclophellitol epoxide and its aziridine.[29]

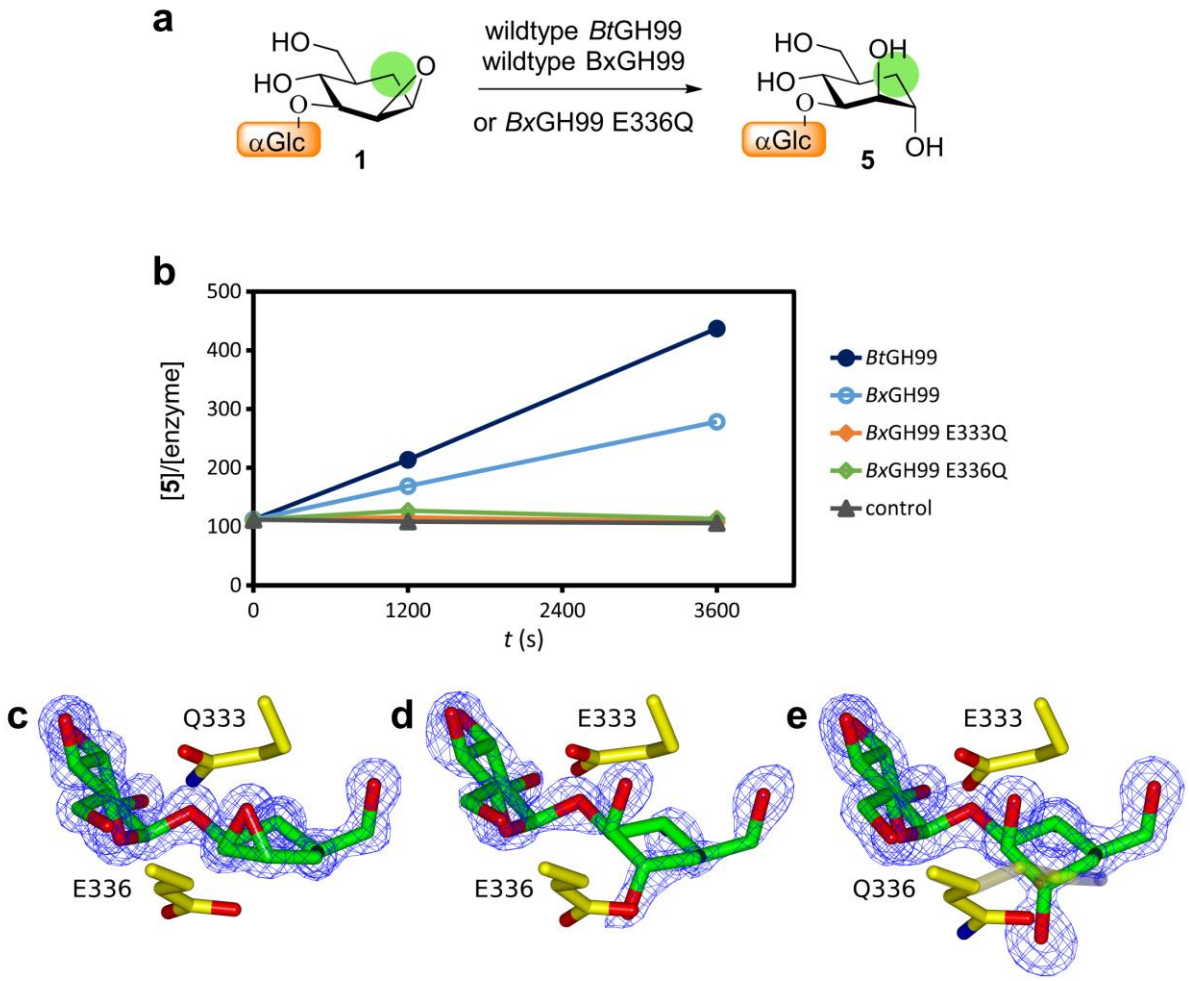

Figure 4. Structure and reactivity of cyclohexane β-1,2-epoxide. a, Enzyme-catalyzed reaction of cyclohexane β-1,2-epoxide. **b,** Monitoring of enzyme-catalyzed reaction of cyclohexane β-1,2-epoxide by mass spectrometry with wildtype and E333Q and E336Q mutants. X-ray structures of **c**, Cyclohexane β-1,2-epoxide with *Bx*GH99 E333Q mutant (2mF_o-DF_c at 0.8 e$^-$/Å^3); **d**, Hydrolysis product *trans*-1,2-diol with wildtype (2mF_o-DF_c at 0.5 e$^-$/Å^3) and with **e**, E336Q mutant (2mF_o-DF_c at 0.5 e$^-$/Å^3).

The stability of the β-1,2-aziridine **3** to enzyme action (unlike β-epoxide **1**) enabled the measurement of a binding constant (K_D) of 17.7 ± 1.3 μM for *Bt*GH99 using NMR, as described previously[20] (**Fig. S8**). The 3-D structure of aziridine **3** bound to GH99 provides the first

structural insight into an intermediate-mimicking complex (**Fig. 2d**). The complex of the wildtype enzyme with the β-1,2-aziridine was obtained at 1.25 Å resolution and subsequently at 1.07 Å for a ternary complex including α-1,2-mannobiose. The –1 pseudosugar is observed in a ^{4}E conformation, as predicted by QM/MM calculations, and consistent with the proposed $^{2}E/^{2}H_{3} \rightarrow [E_{3}]^{\ddagger} \rightarrow {}^{4}E/^{4}H_{5}$ conformational itinerary. Within both structures the aziridine N–E333 Oε distance is 2.6 Å, supportive of a role for E333 as acid/base residue.

The greater reactivity of the epoxide species, and its regioselectivity for enzyme-catalyzed ring opening, matches that expected for the putative 1,2-anhydro sugar intermediate and prompted efforts to obtain an epoxide co-complex with *Bx*GH99. Crystal structures of the cyclohexane β-1,2-epoxide **1** were subsequently obtained with the wildtype and both the E333Q and E336Q mutants, at resolutions of 1.28 Å, 1.12 Å and 1.34 Å, respectively (**Fig. 4c**). Consistent with the proposed mechanism in which E333 is the base required for epoxide opening, the epoxide remained intact for the E333Q mutant, and was opened to the *trans*-1,2-diol **5** with both wildtype and the E336Q mutant. As with the aziridine, the epoxide binds in a ^{4}E conformation, matching the QM/MM calculations. The *trans*-diaxially-opened cyclohexanediol was α-configured and in a product-mimicking $^{4}C_{1}$ conformation. These results confirm that the β-1,2-epoxide ring is opened by GH99 yielding an α-configured product, and that the E333 residue is required for this activity. For a direct comparison of the structures of complexes with the intermediate mimics, see **Fig. S9**.

Human *endo*-α-1,2-mannosidase catalyses glycosylation of α-1,2-mannobiose with retention of stereochemistry using Glc-Man fluoride as donor to yield GlcManManMan, and it is proposed that this reaction proceeds through a 1,2-anhydro sugar intermediate.[22] Incubation of *Bt*GH99 and *Bx*GH99 wildtype enzymes with the β-epoxide **1** and α-1,2-mannobiose yielded

a product with mass spectrometric data consistent with a Glc-carbamannose-Man_2 tetrasaccharide (*m/z* of 883.4 assigned to the permethylated M+Na species detected using MALDI-MS, see **Fig. S10** and **Supporting Methods**). The proposed alkylation reaction mechanism is shown in **Fig. S11**.

Kinetic isotope effect analysis of substrate cleavage

The foregoing structural and reactivity data with substrate, product and putative intermediate mimics and the accompanying computational data are collectively consistent with the proposed neighboring group participation by O2 but do not directly demonstrate the involvement of this residue in the enzymatic mechanism. Kinetic isotope effects (KIEs) are a powerful method to directly study transition state structure as they allow differences in rate of isotope-substituted substrates to report on hybridization, bond order and geometry changes between the ground and the transition states. Unlike substrate variation studies, KIE studies utilize isotopologues that vary only in the number of neutrons at specific sites, and thus constitute a minimal perturbation to the substrate. We recently reported KIEs at six sites (C1, O1, H1, and C2, O2, and H2) for the alkaline solvolysis of PNPMan, which proceeds through a C2-oxyanion *en route* to a 1,2-anhydro sugar.[4] Among the most characteristic KIEs were a strikingly large $^{16}O/^{18}O$ KIE for O2 of 1.044 ± 0.006, $^{12}C/^{13}C$ KIEs for C1 of 1.026, and $^{1}H/^{2}H$ KIE for H1 of 1.112 (**Fig. 5b**). These data are supportive of nucleophile participation by an O2 oxyanion, rate-limiting C1–O_{LG} bond cleavage, and an exploded transition state arising from the late build-up in strain of the epoxide of the intermediate. These KIEs represent benchmark data against which to compare KIE data at the equivalent sites for enzymatic cleavage, noting that alkaline solvolysis is a specific base-catalyzed process whereas the enzymatic process is likely to involve both general-acid and general-base catalysis.

a

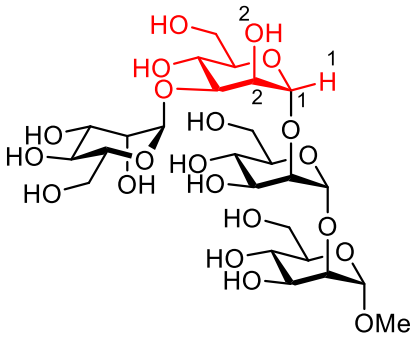

αMan-1,3-αMan-1,2-αMan-1,2-αMan-OMe
[(Man)$_4$OMe]

site of KIE measurement	'light' substrates	'heavy' substrates
H1	(1-^{13}C)	(1-^{2}H,1-^{13}C)
O2	(2-^{13}C)	(2-^{13}C,2-^{18}O)
C1	(2-^{13}C)	(1,2-^{13}C$_2$)

b

	Experimental KIEs	
position	***Bt*GH99 catalyzed (this work)**	**base promoted hydrolysis of PNPMan (Ref.[4])**
1-^{2}H	1.123 ± 0.012	1.112 ± 0.004
1-^{13}C	1.030 ± 0.005	1.026 ± 0.006
2-^{18}O	1.052 ± 0.006	1.044 ± 0.006

c

distance (Å)	**TS structure for *Bx*GH99 hydrolysis of (Man)$_4$OMe**	**TS structure for PNPMan hydrolysis (Ref. [4])**
C1…O1	1.9	2.3
C1…O2	2.3	2.0
O2…O	2.7	2.7

Figure 5. Substrate structures and kinetic isotope effect measurements. a, Structure of substrate and table of isotopologues required for measurement of ^{2}H-, ^{13}C- and ^{18}O-KIEs. **b**, Table of KIEs (± standard error) for the *Bt*GH99 catalyzed hydrolysis of the tetrasaccharide substrate; and published KIEs (± standard error) for the base-promoted hydrolysis of 4-nitrophenyl α-D-mannopyranoside (PNPMan). **c**, Calculated critical interatomic distances for the calculated transition states for *Bt*GH99 catalyzed hydrolysis of the tetrasaccharide substrate; and published KIEs for the base-promoted hydrolysis of PNPMan.

Chan *et al.* reported the development of a highly sensitive competitive NMR method that allows the high precision measurement of KIEs on milligram quantity mixtures of light and heavy isotopologues each possessing an NMR active probe nucleus (typically ^{13}C) that reported on an adjacent site labelled with light and heavy isotopes.[30] An NMR spectrometer is used to measure competitive KIEs for the second-order rate constant (k_{cat}/K_M) by monitoring reaction mixtures of isotopologue substrates. Owing to redundancies, measurement of KIEs using this technique at the C1, H1 and O2 positions requires just 4 isotopologues labelled at one or two positions. Prior work showed that simple aryl disaccharides are poor substrates for *Bt* and *Bx*GH99.[12] Thus, we elected to synthesize the tetrasaccharide **(Man)$_4$OMe** as a preferred substrate. A reliable 24-step synthesis (13 of which were on isotope-labelled intermediates) was developed and applied for the synthesis of five isotopologues, plus the parent unlabelled tetrasaccharide. Despite its length, the efficiency of this approach allowed conversion of less than 100 mg of isotopically-labelled D-mannoses to sufficient amounts of tetrasaccharide for measurement of KIEs using the competitive NMR technique.

KIE measurements were performed by acquisition of quantitative ^{13}C NMR spectra of the *Bt*GH99-catalyzed hydrolysis of mixtures of approximately 1 mg each of the ^{13}C-labelled pair of compounds possessing light or heavy isotopes at the adjacent position (**Fig. 5a**). Due to the presence of a minor ^{13}C-labelled impurity, which was impervious to GH99 catalysis, the spectrum for the reaction at completion was subtracted from the spectra acquired earlier, on the same sample, at varying degrees of completion. Following processing and normalization of data, KIE effects were calculated (**Table S3, Fig. S12, S13, S14**). The KIE values reveal the $^{1}H/^{2}H$ KIE for H1 of 1.123, $^{12}C/^{13}C$ KIEs for C1 of 1.030, and $^{16}O/^{18}O$ KIE for O2 of 1.052 (**Fig. 5b**). While these KIE measurements are less precise than we would have wished due to the unknown ^{13}C-labelled impurity they show that there are significant zero-point energy

changes at C1 and O2 and these KIE values are clearly consistent with nucleophilic participation by O2 that leads to formation of an epoxide intermediate.

Strikingly, the enzymatic KIE values are essentially identical to that measured for the base-promoted (non-enzymatic) reaction, providing support for a similar transition state structure and reaction mechanism. The anomeric ^{13}C-KIE of 1.030 is in the range associated with S_N2 reactions on glycosides that proceed through 'exploded' dissociative transition states. The α-secondary deuterium KIE for glycosidic bond fission originates mainly from changes in bending vibrations as the anomeric carbon undergoes rehybridization from sp^3 to sp^2 at the transition state. The ^{1}H/^{2}H KIE for H1 of 1.123 is smaller than for reactions that proceed through bona fide glycopyranosylium ions, consistent with an exploded S_N2-like transition state, as also predicted by the QM/MM simulations. The non-unity ^{16}O/^{18}O KIE of 1.052 for O2 indicates TS involvement of O2 as a nucleophile. The magnitude of this KIE reflects vibrational frequency changes between the ground state and the transition state leading to epoxide formation. For both the enzyme-catalyzed and base-promoted reactions the formation of the three-membered epoxide ring involves the build-up of significant angle strain (~27 kcal mol^{-1})[31] and this results in weakening of the C2-oxygen bond.

At first glance there appears to be a difference between the calculated GH99 TS structure, where epoxide formation occurs after traversal of the TS, and the magnitude of the heavy atom KIEs, which implicate significant motion of the C2-oxygen atom as well as a weakening of the O2-H bond. However, we note that the free energy profile in the vicinity of the transition state (**Fig. 3a**) is relatively flat and the reaction coordinate includes a shortening of the C1–O2 distance (**Fig. 3b**), which is associated with the bending C1–C2–O2 bending vibration, as well as a tightening of the O_{333} to O2 distance, which results in a significant shortening of the distance between H2 and the general-base glutamate, a motion that will also result in zero point vibrational changes at the labelled O2 site.

Comparison of the structures calculated for the TS of the enzyme-catalyzed process using QM/MM methods (*vide supra*) and that calculated using *ab initio* methods, calibrated with the KIE measurements, for the hydroxide-promoted hydrolysis of PNPMan[4] provide insights into the structure and timing of the respective transition states (**Fig. 5c**). Qualitatively the data (**Fig. 5c**; sum of O2…C1 and C1…O1 distances) suggests similar nucleophile to leaving group distances at the two respective TSs, with that for the specific base-promoted oxyanion being later, and slightly looser, than that for the GH99 *endo*-mannosidase-catalyzed reaction. We conclude that each of/all of the KIE, computational, and structural studies are consistent this enzyme-catalyzed reaction forming an obligatory epoxide intermediate, and that both theory and experiment (KIE) entail similar, synchronized, heavy atom motions at the TS that are coupled to proton transfer events.

Discussion

Enzyme-catalyzed hydrolytic cleavage of the glycosidic bond can occur through a spectrum of mechanisms that are unified by oxocarbenium ion like transition states.[1] Reactions that proceed with retention of configuration involve two-step reaction with either participation by an enzymic nucleophile (classical retaining glycosidases) or one borne on the substrate (neighboring group participation glycosidases). The case for neighboring group participation is convincing for various 2-acetamido-hexosaminidases, where the substrate 2-acetamido group acts as a nucleophile assisting departure of the leaving group and formation of an oxazoline (or oxazolinium ion) intermediate,[32] which is hydrolyzed in the second step.[33] Over 40 years ago, Wallenfels proposed the biological equivalent of this reaction for LacZ β-galactosidase involving nucleophilic participation by a pyranoside 2-hydroxy group to form a 1,2-anhydro sugar (or 1,2-epoxide) intermediate;[34] subsequently this enzyme was shown to utilize a standard retaining mechanism with an enzymatic nucleophile.[7] The present work provides a body of evidence in support of a neighboring group participation mechanism for

GH99 involving nucleophilic participation by the 2-hydroxyl group and formation of a 1,2-anhydro sugar intermediate, a mechanism proposed for GH family 99 endo-α-1,2-mannosidases/mannanases[18] and recently invoked for α-L-rhamnosidases of GH family 145.[35]

The structures presented here collectively define a series of snapshots along the reaction coordinate of stable molecules that mimic the substrate, intermediate or product. Comparison of the start and end structures reveals that the key change in these complexes is the shift in the position of the leaving group (O2 of the +1 mannose) as the covalent bond to C1 is cleaved. Computational studies suggest that the conformation of the –1 sugar in the Michaelis complex is perturbed by the very action of making an inactive mutant for X-ray crystallographic study and predicts a $^{2}E/^{2}H_{3}$ conformation. This conformation in the Michaelis complex is unusual for mannosidases, which in all other cases adopt distorted $^{O}S_{2}$, $^{1}S_{5}$, $^{3}S_{1}$ or $^{1}C_{4}$ conformations that alleviate the steric interaction between the 2-OH and the incoming nucleophile, providing an unfettered nucleophilic trajectory.[36] Notably, in the Michaelis complexes, the -1 subsite sugar adopts a $^{2}E/^{2}H_{3}$ conformation in which the 2-OH sits in between the E333 residue and the anomeric carbon, preventing direct nucleophilic attack at C1, and clearly an alternative strategy must be employed by GH99 enzymes to catalyze glycosidic bond cleavage.

The X-ray structure of the Michaelis complex reveals that $^{2}E/^{2}H_{3}$ conformation of the –1 mannosyl residue positions O2 in a near-axial orientation, where it is poised to act as an internal nucleophile to displace the anomeric group. Our QM/MM metadynamics simulations show that this leads to a reaction involving nucleophilic attack by O2 on the anomeric carbon, forming a 1,2-anhydro sugar intermediate and exclude the classical Koshland double-displacement mechanism involving an enzymatic nucleophile. As mimics of the highly reactive 1,2-anhydro sugar intermediate, we explored more stable cyclohexane analogues: a β-1,2-epoxide **1** and a β-1,2-aziridine **3**. The β-1,2-aziridine **3** proved sufficiently stable to allow acquisition of a complex with *Bx*GH99 (and with the β-1,2-epoxide for a catalytically disabled

mutant), providing insight into the conformation of a 1,2-anhydro sugar mimic. Both complexes gave evidence for the 1,2-anhydro sugar intermediate binding in a ^4E conformation, as predicted computationally, and showed the proposed catalytic machinery E333 and E336 positioned appropriately to assist nucleophilic attack by water and provide general acid catalysis to open the ring.

The cyclohexane β- and α-1,2-epoxides **1** and **2** exhibit reactivity that suggests that only the former acts as a bona fide mimic of the proposed 1,2-anhydro sugar intermediate. In particular, only **1** was a substrate for *Bt*GH99, and underwent regioselective hydrolysis as the position equivalent to the anomeric position, to give a 1,2-*trans* product **5**. The reactivity profile of β-1,2-epoxide **1** extends to reaction with 1,2-α-mannobiose, which yielded a pseudotetrasaccharide, a reaction analogous to the transglycosylation reaction of *Hs*GH99 using GlcManF with 1,2-α-mannobiose,[22] recapitulating the reactivity invoked for the 1,2-anhydrosugar intermediate.

Kinetic isotope effects are considered the gold standard for experimental investigations of transition state structure. Using a highly sensitive competitive NMR method we measured α-secondary KIEs for $^1H/^2H$ for H1 of 1.123 ± 0.012 and for $^{12}C/^{13}C$ of 1.030 ± 0.005, and a $^{16}O/^{18}O$ KIE for O2 of 1.052 ± 0.006. The α-secondary deuterium and primary anomeric ^{13}C-KIEs are consistent with that expected for a reaction center undergoing $sp^3 \rightarrow sp^2$ rehybridization at the TS such as that which occurs in an exploded S_N2-type reaction. In addition, the $^{16}O/^{18}O$ KIE indicates a primary KIE associated with O2 acting as a nucleophile at the experimentally observed TS. These KIEs are essentially identical to benchmark KIEs determined for the hydroxide-promoted hydrolysis of 4-nitrophenyl α-mannoside[4] (although are consistent with an earlier, looser transition state) and provide direct evidence for neighboring group participation by *Bx*GH99.

Conclusions

Collectively the 3-D structures, QM/MM calculations, KIE measurements, and the reactivity of cyclohexane epoxide intermediate mimics provide experimental evidence that GH99 enzymes achieve substitution with retention of stereochemistry through a neighboring group participation mechanism by O2 involving general base-assistance by E333 and leading to a 1,2-anhydro sugar intermediate, via a TS with oxocarbenium ion character. 3-D structures and QM/MM calculations are consistent with the enzyme achieving this outcome through a conformational itinerary along the reaction coordinate of ${}^{2}H_{3} \rightarrow [E_{3}]^{\ddagger} \rightarrow {}^{4}E$. This conformational pathway is distinct from that used by all other characterized mannosidases as it involves only minor distortion of the –1 sugar residue at the Michaelis complex, whereas pathways involving ${}^{3}H_{4}$ and $B_{2,5}$ transition state conformations require substantial distortion to alleviate nucleophile…O2 interactions. This work provides strong evidence for the existence of a 1,2-anhydro sugar mechanism in biological catalysis that is broadly equivalent to the 1,2-anhydro sugars that have long been implicated as intermediates in the base-promoted hydrolysis of *trans*-1,2-glycosides.

Associated content

Supporting Information

The Supporting Information is available free of charge at https://pubs.acs.org/doi/10.1021/acscentsci

Supplementary Methods describing protein crystallography, computational methods, enzymatic reactions and MS and NMR analysis of products, KIE measurements, synthetic methods and characterization data for synthesis of cyclohexane epoxides and aziridines, and of isotopologues used for KIE studies. NMR spectra for new compounds (PDF).

Supplementary Tables & Figures containing Tables S1-3 and Figures S1-14 (PDF).

Accession Codes

The coordinates and structure factors have been deposited in the Protein Data Bank (accession codes 6FWG, 6FWI, 6FWJ, 6FWL, 6FWM, 6FWO, 6FWP and 6FWQ).

Author Information

Corresponding authors

*E-mail: bennet@sfu.ca

*E-mail: matthieu.sollogoub@sorbonne-universite.fr

*E-mail: c.rovira@ub.edu

*E-mail: gideon.davies@york.ac.uk

*E-mail: sjwill@unimelb.edu.au

ORCID

Lukasz F. Sobala: 0000-0002-3807-6452

Ganeko Bernardo-Seisdedos: 0000-0002-1372-3844

Oscar Millet: 0000-0001-8748-4105

Jesús Jiménez-Barbero: 0000-0001-5421-8513

Andrew J. Bennet: 0000-0002-8378-6752

Matthieu Sollogoub: 0000-0003-0500-5946

Carme Rovira: 0000-0003-1477-5010

Gideon J Davies: 0000-0002-7343-776X

Spencer J. Williams: 0000-0001-6341-4364

Notes

The authors declare no competing interests

Acknowledgements

This work was supported by the Australian Research Council (FT130100103, DP120101396, DP180101957), the BBSRC (AJT), European Research Council (ERC-2012-AdG-322942 "Glycopoise"; LFS), Natural Sciences and Engineering Research Council of Canada (AJB Discovery Grant: 2017–04910), the Spanish Minister of Science, Innovation and Universities (MICINN) (CTQ2017-85496-P to C. R.), the Spanish Structures of Excellence María de Maeztu (MDM-2017-0767 to C.R.) and the Agency for Management of University and Research Grants of Generalitat de Catalunya (AGAUR) (2017SGR-1189 to C. R.). G.J.D is funded by the Royal Society "Ken Murray" Professorship. We are grateful to Sivanandam Veeramuthu for help with NMR. We thank Diamond Light Source for access to beamlines I02, I04 and I04-1 (proposals mx-9948 and mx-13587). In-house crystal screening was performed on X-ray equipment provided, in part, by the Wellcome Trust. The authors gratefully acknowledge the computer resources and technical support provided by the Barcelona Supercomputing Center (BSC-CNS, Barcelona, Spain).

Author contributions

G.J.D and S.J.W conceived the project; C.R., M.S., A.J.B., G.J.D., and S.J.W. designed the experiments; M.S. designed the syntheses of the mimics; G.S., Z.H., D.L., S.Z., and Y.Z. synthesized ligands and substrates; N.S., S.S.K.A., A.R.L., and A.J.B. measured KIEs and analysed results; L.F.S., A.J.T., Z.H., G.J.D. conducted X-ray crystallography and analysed results; L.F.S, S.Z performed enzymatic reactions and analyzed results; G.B.-S., L.F.S., O.M., J.J.-B. performed NMR measurements of ligand affinities; L.R., V.R.-C. and C.R. performed computational studies; C.R., A.J.B., G.J.D., and S.J.W. and wrote the manuscript with input from other authors.

References

(1) Sinnott, M. L., Catalytic mechanisms of enzymatic glycosyl transfer, *Chem. Rev.* **1990,** *90*, 1171-1202.

(2) Gasman, R. C.; Johnson, D. C., C-2 Oxyanion Participation in the Base-Catalyzed Cleavage of p-Nitrophenyl β-D-Galactopyranoside and p-Nitrophenyl α-D-Mannopyranoside, *J. Org. Chem.* **1966,** *31*, 1830-1838.

(3) Micheel, F.; Borrmann, D., Ein neues Verfahren zur Synthese höherer Saccharide, *Chem. Ber.* **1960,** *93*, 1143-1147.

(4) Speciale, G.; Farren-Dai, M.; Shidmoossavee, F. S.; Williams, S. J.; Bennet, A. J., C2-Oxyanion neighboring group participation: Transition state structure for the hydroxide-promoted hydrolysis of 4-nitrophenyl α-D-mannopyranoside, *J. Am. Chem. Soc.* **2016,** *138*, 14012-14019.

(5) Brockhaus, M.; Dettinger, H.-M.; Kurz, G.; Lehmann, J.; Wallenfels, K., Participation of HO-2 in the cleavage of β-D-galactosides by the β-D-galactosidase from *E. coli*, *Carbohydr. Res.* **1979,** *69*, 264-268.

(6) Johnson, R. W.; Marschner, T. M.; Oppenheimer, N. J., Pyridine nucleotide chemistry. A new mechanism for the hydroxide-catalyzed hydrolysis of the nicotinamide-glycosyl bond, *J. Am. Chem. Soc.* **1988,** *110*, 2257-2263.

(7) Gebler, J. C.; Aebersold, R.; Withers, S. G., Glu-537, not Glu-461, is the nucleophile in the active site of (lac Z) β-galactosidase from *Escherichia coli*, *J. Biol. Chem.* **1992,** *267*, 11126-11130.

(8) Egea, P. F.; Muller-Steffner, H.; Kuhn, I.; Cakir-Kiefer, C.; Oppenheimer, N. J.; Stroud, R. M.; Kellenberger, E.; Schuber, F., Insights into the Mechanism of Bovine CD38/NAD$^+$ Glycohydrolase from the X-Ray Structures of Its Michaelis Complex and Covalently-Trapped Intermediates, *PLOS One* **2012,** *7*, e34918.

(9) Handlon, A. L.; Xu, C.; Muller-Steffner, H. M.; Schuber, F.; Oppenheimer, N. J., 2'-Ribose Substituent Effects on the Chemical and Enzymic Hydrolysis of NAD+, *J. Am. Chem. Soc.* **1994,** *116*, 12087-12088.

(10) Lombard, V.; Golaconda Ramulu, H.; Drula, E.; Coutinho, P. M.; Henrissat, B., The carbohydrate-active enzymes database (CAZy) in 2013, *Nucleic Acids Res.* **2014,** *42*, D490-5.

(11) Ten years of CAZypedia: a living encyclopedia of carbohydrate-active enzymes, *Glycobiology* **2018,** *28*, 3-8.

(12) Hakki, Z.; Thompson, A. J.; Bellmaine, S.; Speciale, G.; Davies, G. J.; Williams, S. J., Structural and kinetic dissection of the *endo*-α-1,2-mannanase activity of bacterial GH99 glycoside hydrolases from *Bacteroides* spp, *Chem. Eur. J.* **2015,** *21*, 1966-77.

(13) Lubas, W. A.; Spiro, R. G., Evaluation of the role of rat liver Golgi endo-α-D-mannosidase in processing N-linked oligosaccharides, *J. Biol. Chem.* **1988,** *263*, 3990-3998.

(14) Moore, S. E.; Spiro, R. G., Demonstration that Golgi endo-α-D-mannosidase provides a glucosidase-independent pathway for the formation of complex N-linked oligosaccharides of glycoproteins, *J. Biol. Chem.* **1990,** *265*, 13104-13112.
(15) Moore, S. E.; Spiro, R. G., Characterization of the endomannosidase pathway for the processing of N-linked oligosaccharides in glucosidase II-deficient and parent mouse lymphoma cells, *J. Biol. Chem.* **1992,** *267*, 8443-8451.
(16) Cuskin, F.; Lowe, E. C.; Temple, M. J.; Zhu, Y.; Cameron, E. A.; Pudlo, N. A.; Porter, N. T.; Urs, K.; Thompson, A. J.; Cartmell, A.; Rogowski, A.; Hamilton, B. S.; Chen, R.; Tolbert, T. J.; Piens, K.; Bracke, D.; Vervecken, W.; Hakki, Z.; Speciale, G.; Munoz-Munoz, J. L.; Day, A.; Pena, M. J.; McLean, R.; Suits, M. D.; Boraston, A. B.; Atherly, T.; Ziemer, C. J.; Williams, S. J.; Davies, G. J.; Abbott, D. W.; Martens, E. C.; Gilbert, H. J., Human gut Bacteroidetes can utilize yeast mannan through a selfish mechanism, *Nature* **2015,** *517*, 165-169.
(17) Roth, J.; Ziak, M.; Zuber, C., The role of glucosidase II and endomannosidase in glucose trimming of asparagine-linked oligosaccharides, *Biochimie* **2003,** *85*, 287-94.
(18) Thompson, A. J.; Williams, R. J.; Hakki, Z.; Alonzi, D. S.; Wennekes, T.; Gloster, T. M.; Songsrirote, K.; Thomas-Oates, J. E.; Wrodnigg, T. M.; Spreitz, J.; Stutz, A. E.; Butters, T. D.; Williams, S. J.; Davies, G. J., Structural and mechanistic insight into N-glycan processing by endo-α-mannosidase, *Proc. Natl. Acad. Sci. USA* **2012,** *109*, 781-786.
(19) Fernandes, P. Z.; Petricevic, M.; Sobala, L.; Davies, G. J.; Williams, S. J., Exploration of Strategies for Mechanism-Based Inhibitor Design for Family GH99 endo-α-1,2-Mannanases, *Chem. Eur. J.* **2018,** *24*, 7464-7473.
(20) Petricevic, M.; Sobala, L. F.; Fernandes, P.; Raich, L.; Thompson, A. J.; Bernardo-Seisdedos, G.; Millet, O.; Zhu, S.; Sollogoub, M.; Jimenez-Barbero, J.; Rovira, C.; Davies, G. J.; Williams, S. J., Contribution of shape and charge to the inhibition of a family GH99 *endo*-α-1,2-mannanase, *J. Am. Chem. Soc.* **2017,** *139*, 1089–1097.
(21) Davies, G. J.; Wilson, K. S.; Henrissat, B., Nomenclature for sugar-binding subsites in glycosyl hydrolases, *Biochem. J.* **1997,** *321*, 557-559.
(22) Iwamoto, S.; Kasahara, Y.; Yoshimura, Y.; Seko, A.; Takeda, Y.; Ito, Y.; Totani, K.; Matsuo, I., Endo-alpha-Mannosidase-Catalyzed Transglycosylation, *ChemBioChem* **2017,** *18*, 1376-1378.
(23) Barducci, A.; Bonomi, M.; Parrinello, M., Metadynamics, *WIREs: Comp. Mol. Sci.* **2011,** *1*, 826-843.
(24) Laio, A.; Parrinello, M., Escaping free-energy minima, *Proc. Natl. Acad. Sci. USA* **2002,** *99*, 12562-12566.
(25) Ardèvol, A.; Rovira, C., Reaction Mechanisms in Carbohydrate-Active Enzymes: Glycoside Hydrolases and Glycosyltransferases. Insights from ab Initio Quantum Mechanics/Molecular Mechanics Dynamic Simulations, *J. Am. Chem. Soc.* **2015,** *137*, 7528-7547.

(26) Petersen, L.; Ardevol, A.; Rovira, C.; Reilly, P. J., Molecular mechanism of the glycosylation step catalyzed by Golgi α-mannosidase II: a QM/MM metadynamics investigation, *J. Am. Chem. Soc.* **2010,** *132*, 8291-8300.
(27) Biarnés, X.; Ardèvol, A.; Iglesias-Fernández, J.; Planas, A.; Rovira, C., Catalytic Itinerary in 1,3-1,4-β-Glucanase Unraveled by QM/MM Metadynamics. Charge Is Not Yet Fully Developed at the Oxocarbenium Ion-like Transition State, *J. Am. Chem. Soc.* **2011,** *133*, 20301-20309.
(28) Lu, D.; Zhu, S.; Sobala, L. F.; Bernardo-Seisdedos, G.; Millet, O.; Zhang, Y.; Jiménez-Barbero, J.; Davies, G. J.; Sollogoub, M., From 1,4-Disaccharide to 1,3-Glycosyl Carbasugar: Synthesis of a Bespoke Inhibitor of Family GH99 Endo-α-mannosidase, *Org. Lett.* **2018,** *20*, 7488-7492.
(29) Wu, L.; Armstrong, Z.; Schroder, S. P.; de Boer, C.; Artola, M.; Aerts, J. M.; Overkleeft, H. S.; Davies, G. J., An overview of activity-based probes for glycosidases, *Curr. Opin. Chem. Biol.* **2019,** *53*, 25-36.
(30) Chan, J.; Lewis, A. R.; Gilbert, M.; Karwaski, M. F.; Bennet, A. J., A direct NMR method for the measurement of competitive kinetic isotope effects, *Nat. Chem. Biol.* **2010,** *6*, 405-7.
(31) Whalen, D. L., Mechanisms of hydrolysis and rearrangements of epoxides, *Adv. Phys. Org. Chem.* **2005,** *40*, 247-298.
(32) Coines, J.; Alfonso-Prieto, M.; Biarnés, X.; Planas, A.; Rovira, C., Oxazoline or Oxazolinium Ion? The Protonation State and Conformation of the Reaction Intermediate of Chitinase Enzymes Revisited, *Chem. Eur. J.* **2018,** *24*, 19258-19265.
(33) Macauley, M. S.; Whitworth, G. E.; Debowski, A. W.; Chin, D.; Vocadlo, D. J., O-GlcNAcase uses substrate-assisted catalysis: kinetic analysis and development of highly selective mechanism-inspired inhibitors, *J. Biol. Chem.* **2005,** *280*, 25313-22.
(34) Wallenfels, K.; Weil, R., In *The Enzymes*, 3rd Edition ed.; Boxer, P. D., Ed. Academic Press: New York, 1972; Vol. 7, pp 617-663.
(35) Munoz-Munoz, J.; Cartmell, A.; Terrapon, N.; Henrissat, B.; Gilbert, H. J., Unusual active site location and catalytic apparatus in a glycoside hydrolase family, *Proc. Natl. Acad. Sci. USA* **2017,** *114*, 4936-4941.
(36) Davies, G. J.; Planas, A.; Rovira, C., Conformational analyses of the reaction coordinate of glycosidases, *Acc. Chem. Res.* **2012,** *45*, 308-316.

Graphical abstract

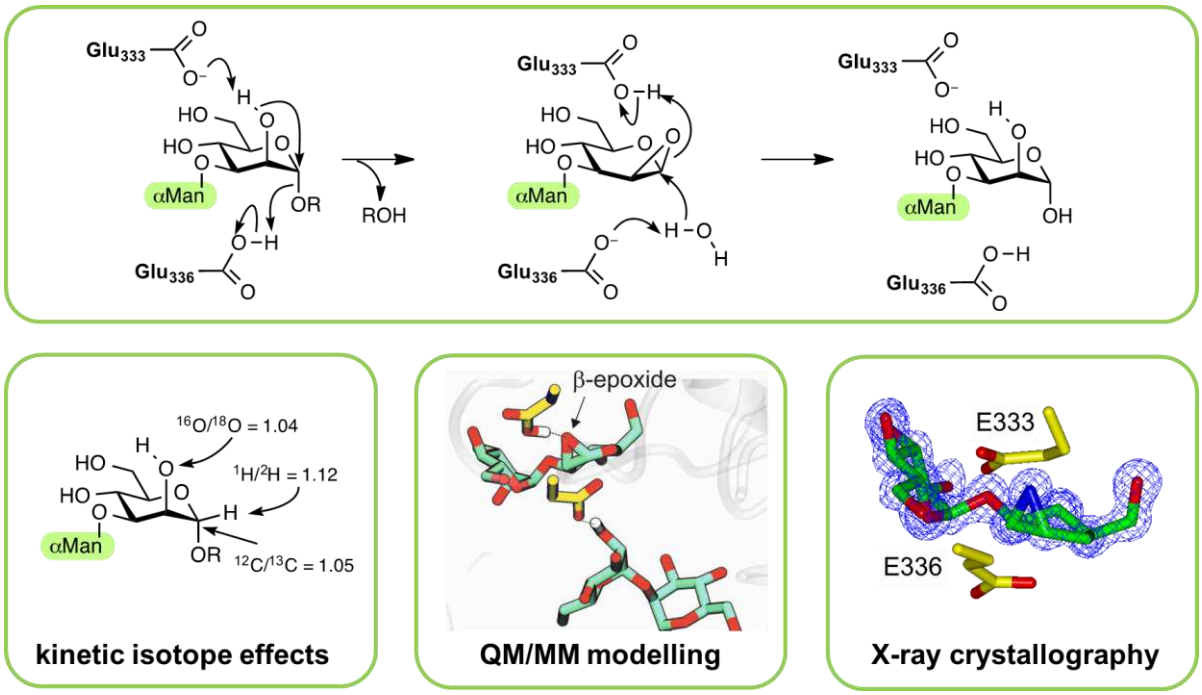

Synopsis

Mannosidases of glycoside hydrolase family 99 use a neighboring group participation mechanism involving the substrate 2-hydroxyl.

Supplementary Tables & Figures

An epoxide intermediate in glycosidase catalysis

Table S1 | X-ray data collection and refinement statistics.

	E333Q 'Michaelis' complex	WT + β-1,2-aziridine	WT + β-1,2-aziridine + α-1,2-mannobiose	E333Q + β-1,2-epoxide	WT + cyclohexane-diol	E336Q + cyclohexane-diol	WT product complex	E333Q product complex
Data collection								
Beamline	I02	I04-1	I02	I04	I04	I04	I04-1	I04-1
Space group	*I*4	*I*4	*I*4	*I*4	*I*4	*I*4	*I*4	*I*4
Cell dimensions								
a, *b*, *c* (Å)	107.9, 107.9, 67.6	108.5, 108.5, 68.0	108.6, 108.6, 67.6	108.2, 108.2, 67.4	108.3, 108.3, 67.5	107.6, 107.6, 67.5	108.9, 108.9, 68.5	108.7, 108.7, 68.8
α, β, γ (°)	90, 90, 90	90, 90, 90	90, 90, 90	90, 90, 90	90, 90, 90	90, 90, 90	90, 90, 90	90, 90, 90
Resolution (Å)*	57.30-1.07 (1.09-1.07)	39.49-1.25 (1.27-1.25)	57.42-1.04 (1.06-1.04)	76.53-1.12 (1.14-1.12)	57.25-1.28 (1.30-1.28)	57.17-1.34 (1.36-1.34)	58.00-1.08 (1.10-1.08)	76.83-1.65 (1.68-1.65)
R_{merge}	0.061 (1.531)	0.059 (1.664)	0.075 (1.346)	0.063 (1.387)	0.066 (1.445)	0.069 (1.278)	0.059 (1.455)	0.084 (1.014)
R_{pim}	0.026 (0.705)	0.022 (0.643)	0.030 (0.601)	0.027 (0.634)	0.028 (0.650)	0.029 (0.544)	0.025 (0.710)	0.047 (0.578)
CC(1/2)	0.997 (0.398)	0.998 (0.462)	0.993 (0.455)	0.999 (0.450)	0.999 (0.439)	0.999 (0.563)	0.999 (0.407)	0.995 (0.406)
I / σ I	10.6 (1.0)	17.4 (1.3)	9.5 (0.8)	9.8 (1.1)	10.7 (1.2)	10.6 (1.3)	10.1 (1.0)	8.2 (1.1)
Completeness (%)	100.0 (99.3)	99.4 (100.0)	98.8 (80.4)	100.0 (99.2)	100.0 (99.9)	99.9 (99.5)	99.9 (99.2)	99.6 (99.8)
Redundancy	6.3 (5.5)	8.2 (7.6)	7.5 (5.5)	6.4 (5.7)	6.4 (5.9)	6.5 (6.3)	6.3 (5.1)	4.0 (4.1)
Refinement								
Resolution (Å)	76.28-1.07	76.69-1.25	76.82-1.04	76.53-1.12	76.56-1.28	76.10-1.34	77.03-1.08	76.83-1.65
No. reflections all / free	170019 / 8420	108087 / 5400	185423 / 9152	149020 / 7398	100095 / 4977	86250 / 4416	170757 / 8460	47947 / 2376
R_{work} / R_{free}	0.120 / 0.138	0.126 / 0.147	0.128 / 0.147	0.126 / 0.146	0.138 / 0.164	0.126 / 0.161	0.126 / 0.137	0.146 / 0.189
No. atoms								

Protein	3067	3045	3150	3165	3129	3034	3080	2980
Ligand/ion	54	38	60	30	27	31	81	47
Water	344	270	382	416	381	278	277	161
B-factors (Å^2)								
Protein	16.4	17.3	16.3	16.6	18.4	20.6	16.4	27.8
Ligand/ion	16.8	22.4	16.4	17.4	22.8	25.3	18.1	26.3
Water	34.6	33.2	33.3	32.7	32.9	36.0	33.5	40.5
R.m.s. deviations								
Bond lengths (Å)	0.0103	0.0091	0.0133	0.0113	0.0092	0.0111	0.0128	0.0142
Bond angles (°)	1.539	1.424	1.772	1.557	1.391	1.493	1.411	1.411
PDB ID	6FWG	6FWI	6FWJ	6FWL	6FWM	6FWO	6FWP	6FWQ

*Values in parentheses are for highest-resolution shell

Table S2 | Lengths (Å) of important bonds along the calculated reaction pathway.[a]

	C1-O1	C1-O2	O1-H_{E336}	O_{E336}-H_{E336}	O2-H2	H2-O_{E333}
MC'	1.53±0.05[a]	2.40±0.06	3.48±0.08	1.01±0.05	0.99±0.03	2.12±0.28
MC	1.47±0.05	2.48±0.07	2.89±0.10	1.03±0.04	1.00±0.02	1.96±0.25
TS	1.88±0.06	2.29±0.06	1.25±0.05	1.23±0.04	1.04±0.03	1.64±0.10
PT	3.1±0.13	2.1±0.14	1.01±0.04	1.77±0.09	1.18±0.17	1.40±0.20
EPO'	4.01±0.10	1.51±0.06	1.00±0.05	1.98±0.11	1.61±0.10	1.03±0.03
EPO	4.03±0.09	1.51±0.07	1.00±0.04	3.50±0.07	1.59±0.11	1.03±0.03

[a] Standard deviation

Table S3 | KIEs measured on *Bx*GH99-catalyzed hydrolysis of Man_4OMe at pH = 7.0, 25°C.

Effect	Run 1	Run 2	Run 3	Run 4	Mean ± SD
1-^{2}H	1.129 ± 0.012	1.121 ± 0.009	1.118[a]	-	1.123 ± 0.012
1-^{13}C	1.032 ± 0.002	1.030 ± 0.005	1.028[a]	-	1.030 ± 0.005
2-^{18}O	1.052 ± 0.006	1.048 ± 0.007	1.055 ± 0.004	1.052 ± 0.005	1.052 ± 0.006

[a] Fits from experiments containing more enzyme, which resulted in fewer data points and more scatter.

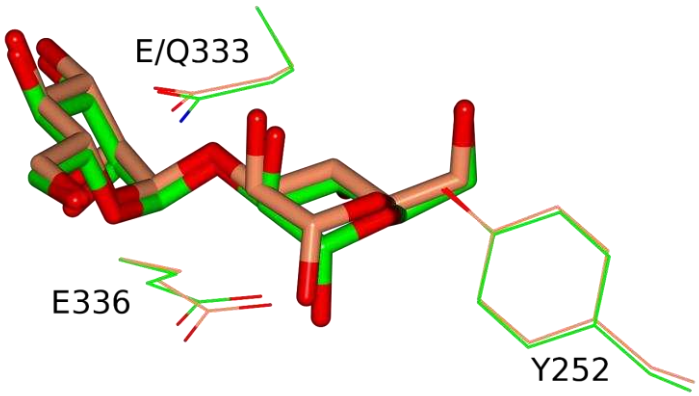

Fig. S1 | Superposition of the –2/–1 subsite ligands in product complexes of wildtype and E333Q *Bx*GH99.
The product sits deeper in the binding cleft of the wildtype. Wildtype complex colored coral and E333Q mutant complex colored green. The models were aligned in ccp4mg[1] using the mainchain atoms of residues 333 to 336.

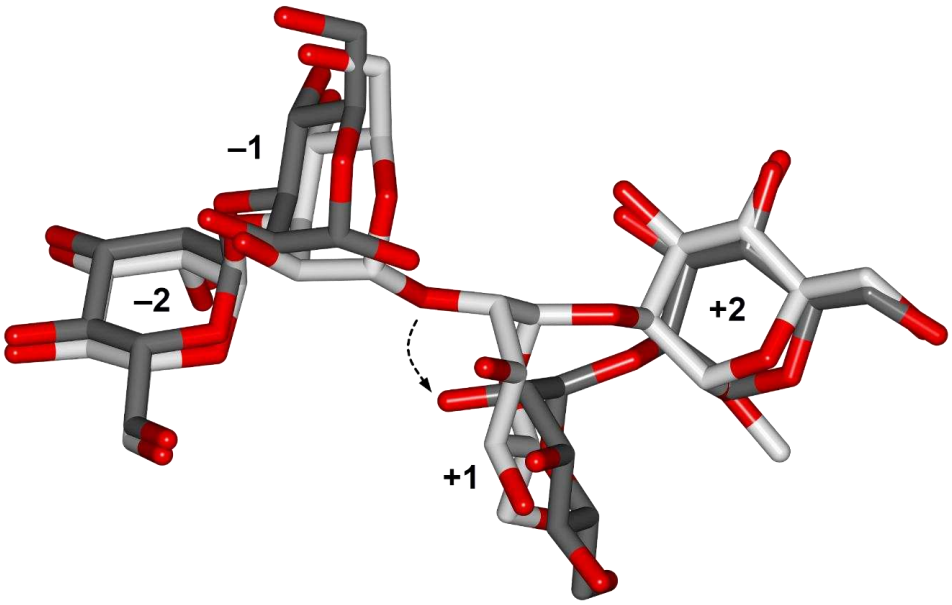

Fig. S2 | Comparison of substrate and product complexes showing reorganization in the active site.
Structures of *Bx*GH99 E333Q-bound (white) $(Man)_4OMe$ and (grey) α-1,3-mannobiose + α-1,2-mannobiose. The arrow highlights the change in position of oxygen-2 of the +1 mannose. Figure assembled in ccp4mg.[1]

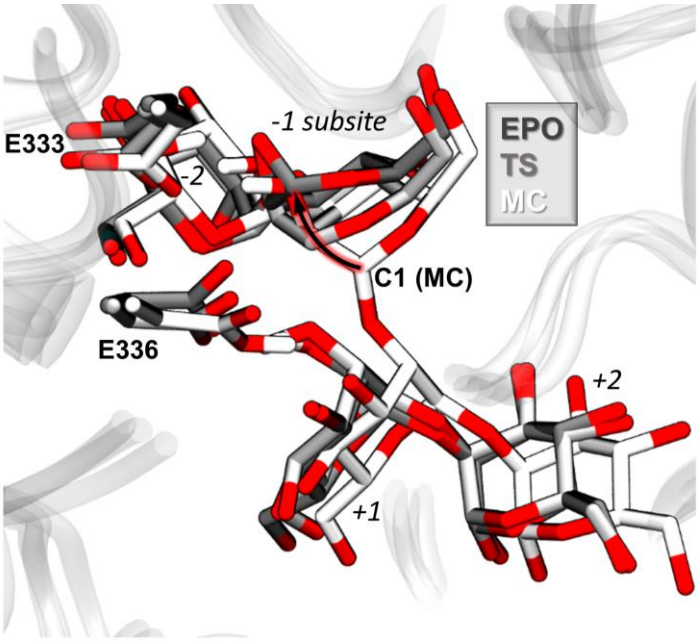

Fig. S3 | 'Electrophilic' migration of the anomeric carbon upon conversion of Michaelis complex to EPO via the transition state.
Superposition of the calculated Michaelis (MC), transition state (TS) and 1,2-anhydro sugar (EPO) complexes highlight that major atomic movements involve C2, C1, O5 and C5.

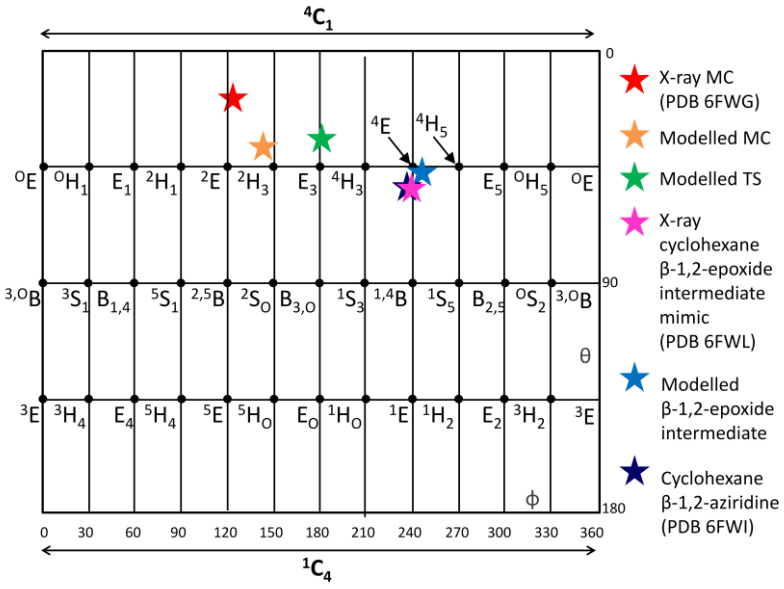

Fig. S4 | Conformational states mapped on the Cremer-Pople projection. Conformation of the –1 saccharide ring in the *Bx*GH99 *endo*-α-1,2-mannanase complexes investigated (both experiments and theory).

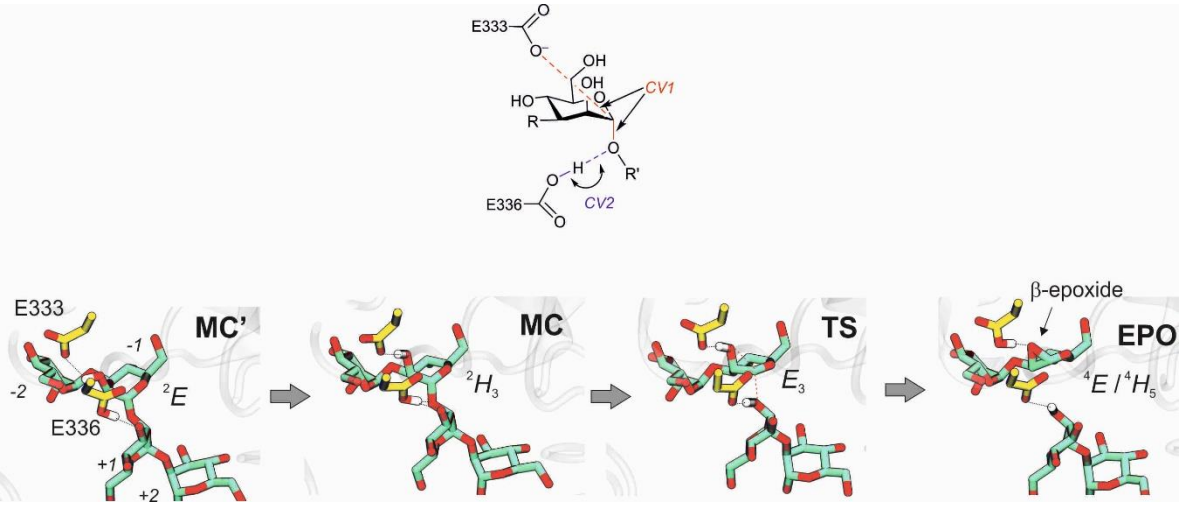

Fig. S5 | Reaction pathway obtained from QM/MM metadynamics simulation using alternative collective variables.
The first collective variable accounts for the direct nucleophilic attack of E333 onto the anomeric carbon (formation of an OE333-C1 bond), whereas the second one accounts for the protonation of the glycosidic oxygen. Specifically, CV1 = d(O_{E333}-C1)- d(C1-O1) and CV2 = d(O_{E336}-H_{E336}) – d(H_{E336}-O1). These are the CVs typically used to describe the double-displacement reaction of retaining GHs.[2]

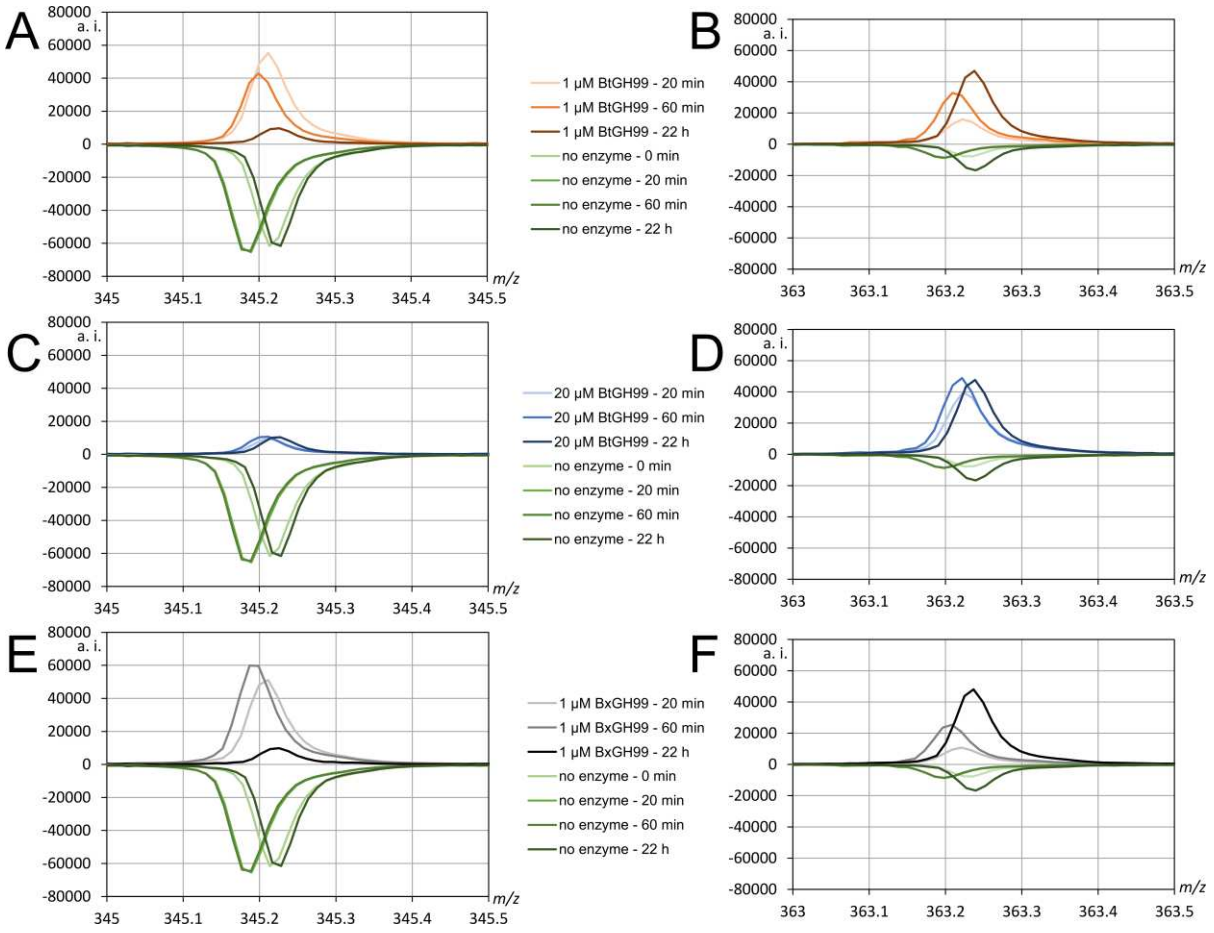

Fig. S6 | Mass spectrometry data for the β-epoxide reaction. 1 µM *Bt*GH99 was incubated with the indicated amounts of epoxide mixture and the signals corresponding to (A) epoxide substrate and (B) diol product, were monitored over time. In (C) and (D), 20 µM *Bt*GH99 was used. Note that the signal for the epoxide does not get smaller after the 20 min measurement in the case of incubation with 20 µM enzyme (C) because the total available β-epoxide was consumed within approximately 6 min. *Bx*GH99 was incubated with the indicated amounts of epoxide mixture and the signals corresponding (E) epoxide substrate and (F) diol product, were monitored over time. Values for controls (no enzyme, shades of green) were made negative for clarity. The small differences in apparent molecular mass are due to instrument recalibrations; a. i. – arbitrary intensity units. The spectra for no enzyme controls at 20 and 60 min are largely overlapping.

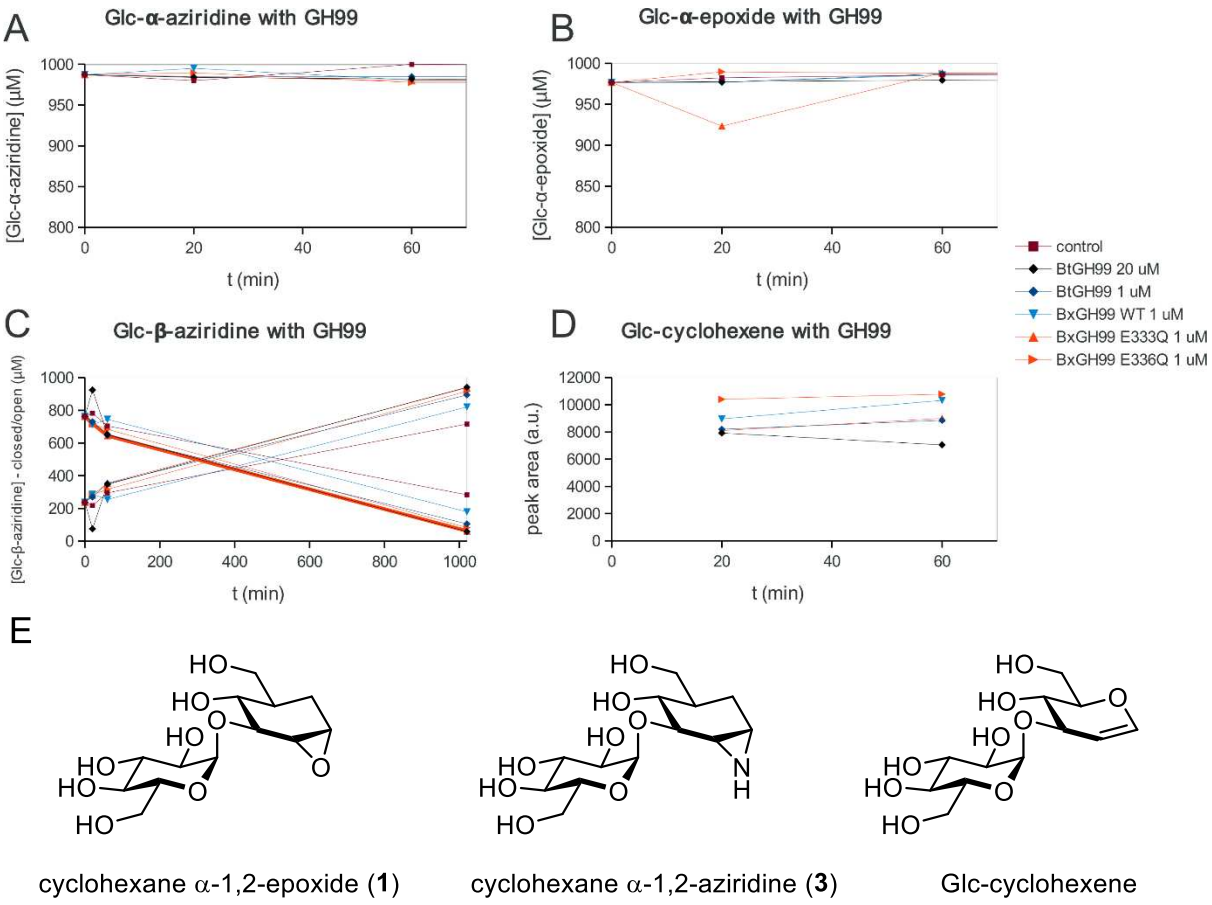

Fig. S7 | Mass spectrometry data for GH99 reactivity of Glc-α-1,2-aziridine, cyclohexane-α-1,2-epoxide, cyclohexane-β-1,2-aziridine and Glc-cyclohexene. Plots show concentrations of various substrates as a function of time when incubated with *Bt*GH99, *Bx*GH99 and *Bx*GH99 E336Q. (A) Glc-α-aziridine. (B) Glc-α-epoxide. The outstanding point at 20 min is due to a larger experimental error caused by a smaller overall concentration of ligand in this particular sample. (C) Glc-β-aziridine: falling line; hydrolysis product: rising line. The β-aziridine was unstable in solution, and its rate of hydrolysis was not altered by enzyme. (D) Area of peaks corresponding to Glc-cyclohexene.[3] This ligand is not a substrate for the enzyme. The concentration could not be estimated due to the lack of a peak corresponding to a hydrolysis product. (E) Structures of cyclohexane-α-1,2-epoxide (**1**), cyclohexane-α-1,2-aziridine (**3**), and Glc-cyclohexene.

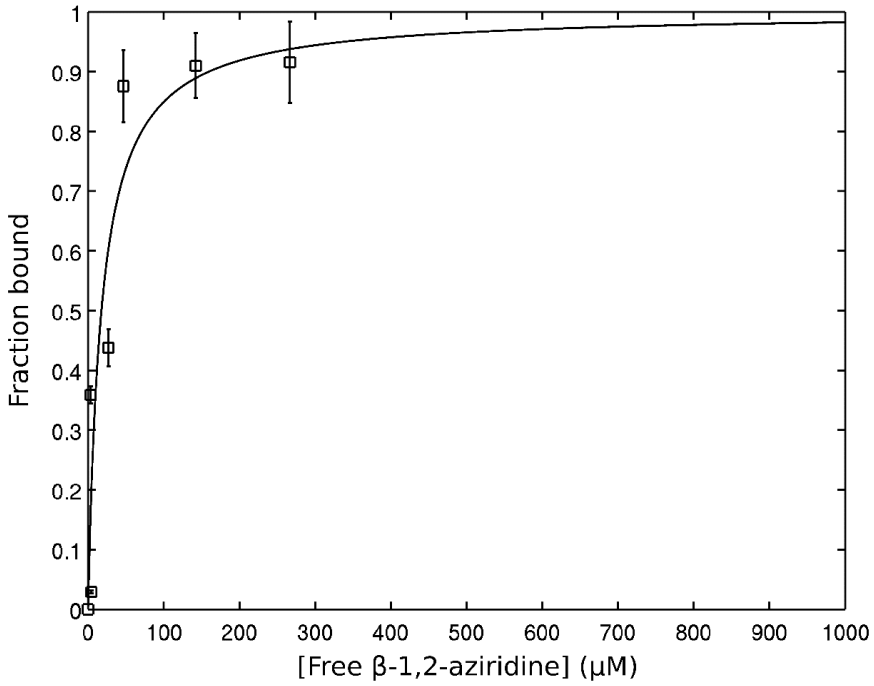

Fig. S8 | NMR titration of *Bt*GH99 with cyclohexane β-1,2-aziridine.

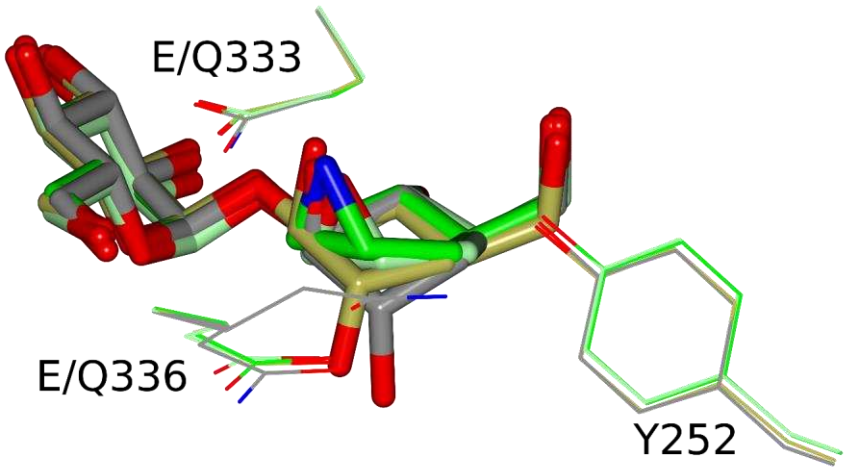

Fig. S9 | Superposition of models of *Bx*GH99 complexed with intermediate mimics. Light green: cyclohexane β-1,2-epoxide with E333Q mutant; green: cyclohexane β-1,2-aziridine with wildtype; gold: β-epoxide with wildtype; grey: β-epoxide with E336Q mutant (note the dual conformations of Q336). The models were aligned in ccp4mg[1] using the main chain atoms of residues 333 to 336.

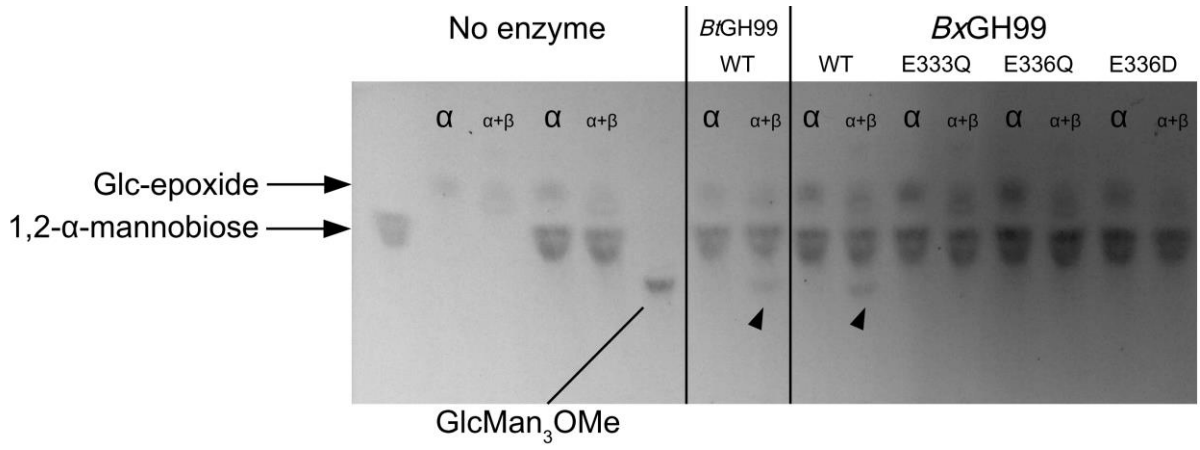

Fig. S10 | Thin layer chromatography of the GH99-mediated transglycosylation reaction. The epoxides present in the reaction mixture are labelled on the top of the lane. The acceptor (α-1,2-mannobiose) is present at the same concentration in all lanes except 2, 3 and 6. The synthesis of $GlcMan_3OMe$ will be reported elsewhere.

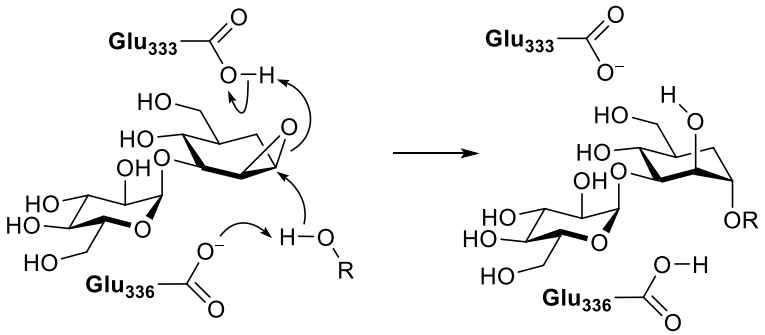

Fig. S11 | Proposed mechanism of endomannosidase-mediated pseudotetrasaccharide formation using the cyclohexane β-1,2-epoxide used as the donor. The residue numbering refers to *Bx*GH99 protein.

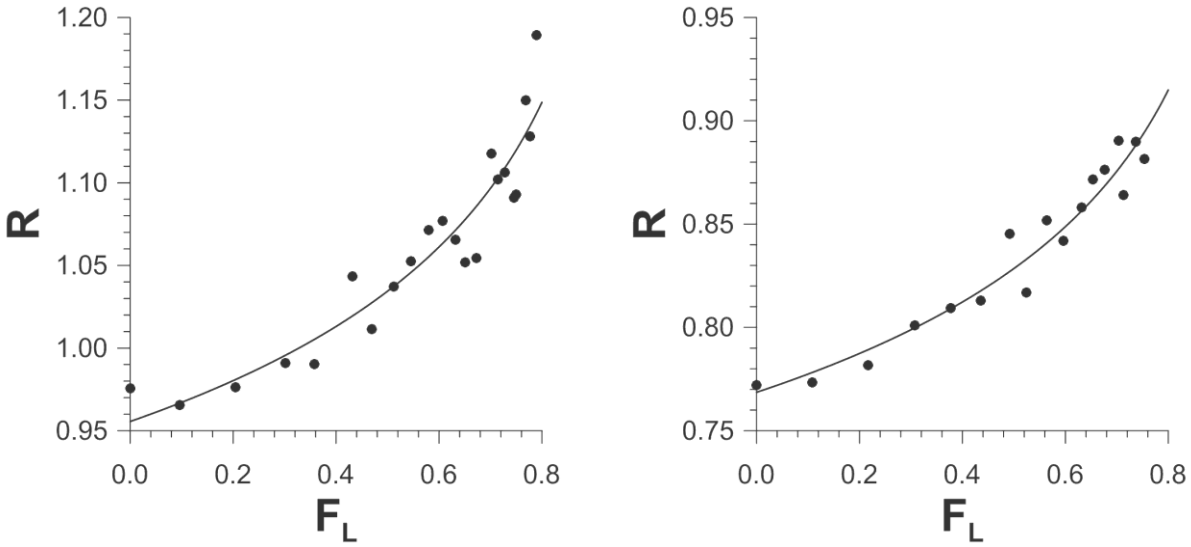

Fig. S12 | Deuterium kinetic isotope effects. Change in isotopologue ratio (R 1-^{2}H/1-^{1}H) vs. F_1 for the GH99-catalyzed hydrolysis of Man$_4$OMe. (Left) data from expt. 1; (right) data from expt. 2. Also shown is the non-linear least squares fit to eqn 1.

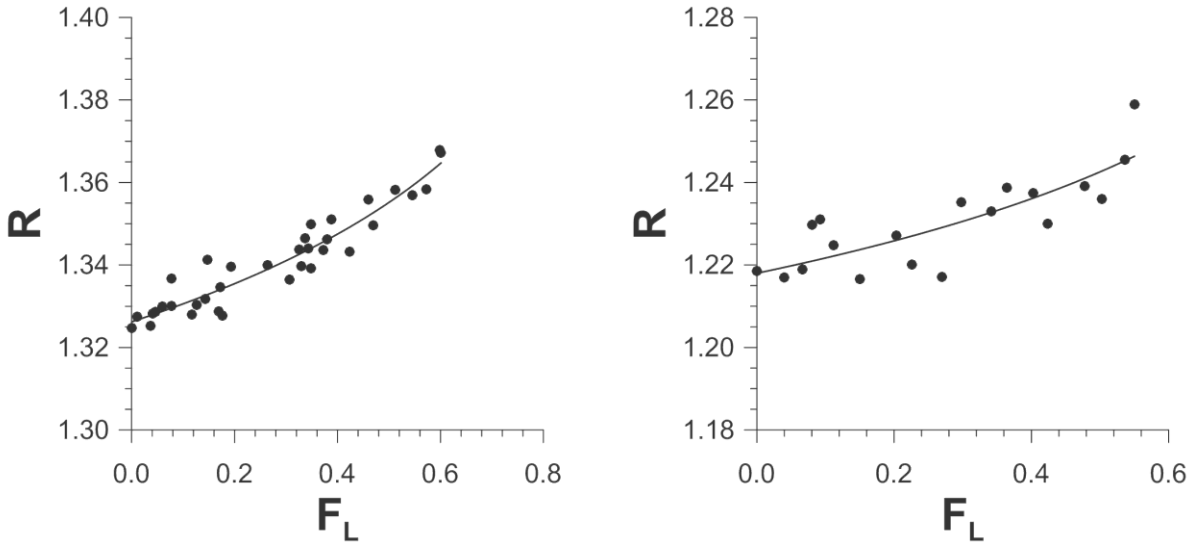

Fig. S13 | ^{13}C kinetic isotope effects. Change in isotopologue ratio R (1-^{13}C/1-^{12}C) vs. F_L for the GH99-catalyzed hydrolysis of Man_4OMe. (Left) data from expt. 1; (right) data from expt. 2. Also shown is the non-linear least squares fit to eqn 1.

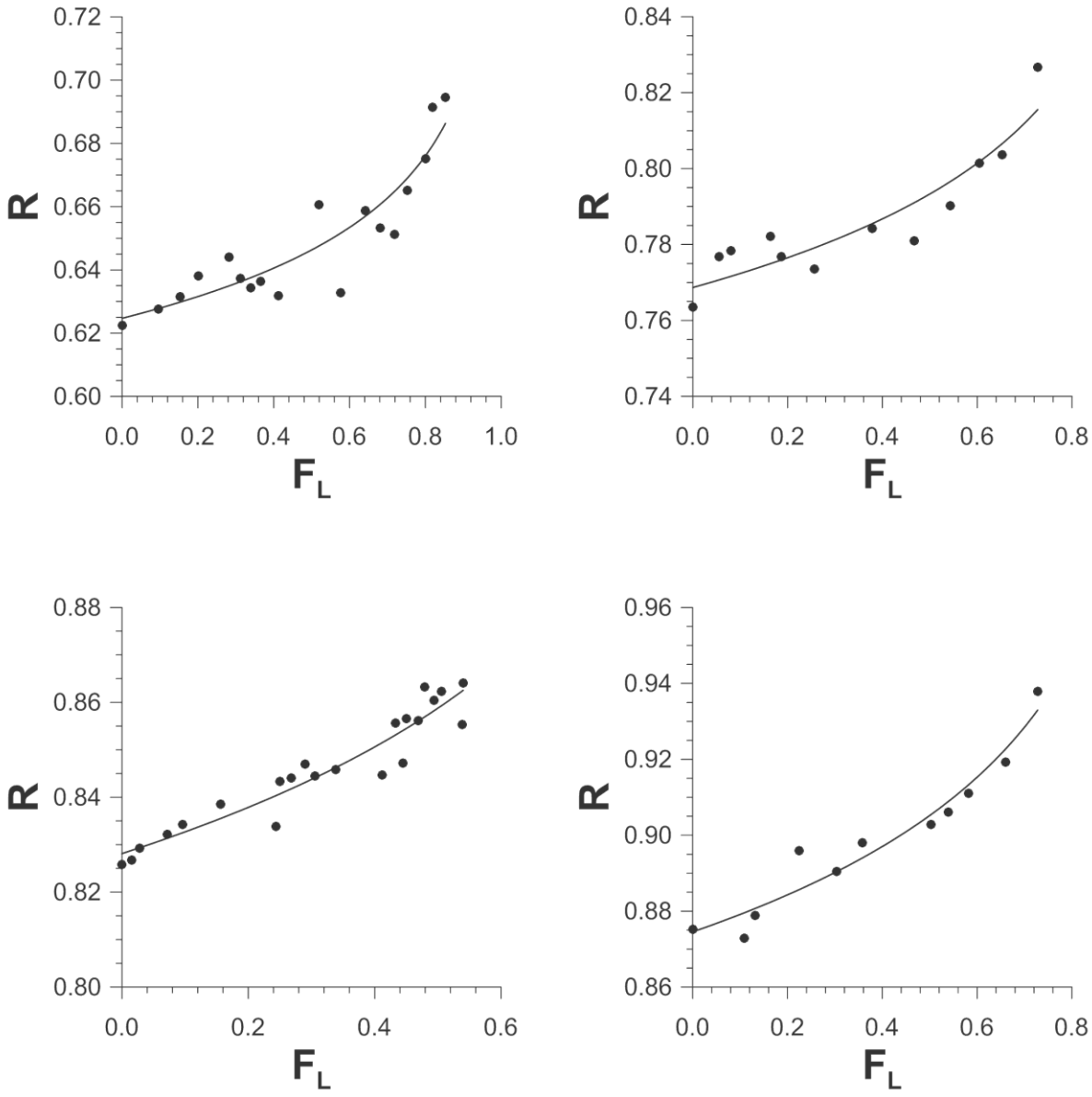

Fig. S14 | Change in isotopologue ratio R (2-^{18}O/2-^{16}O) vs. F_L for the GH99-catalyzed hydrolysis of Man$_4$OMe. (Top left) data from expt. 1; (top right) data from expt. 2; (bottom left) data from expt. 3; (bottom right) data from expt. 4. Also shown is the non-linear least squares fit to eqn 1.

Supplementary References

1. McNicholas S, Potterton E, Wilson KS, Noble MEM. Presenting your structures: the CCP4mg molecular-graphics software. *Acta Crystallogr. D* **67**, 386-394 (2011).

2. Biarnés X, Ardèvol A, Iglesias-Fernández J, Planas A, Rovira C. Catalytic Itinerary in 1,3-1,4-β-Glucanase Unraveled by QM/MM Metadynamics. Charge Is Not Yet Fully Developed at the Oxocarbenium Ion-like Transition State. *J. Am. Chem. Soc.* **133**, 20301-20309 (2011).

3. Petricevic M, Sobala LF, Fernandes P, Raich L, Thompson AJ, Bernardo-Seisdedos G, Millet O, Zhu S, Sollogoub M, Jimenez-Barbero J, Rovira C, Davies GJ, Williams SJ. Contribution of shape and charge to the inhibition of a family GH99 *endo*-α-1,2-mannanase. *J. Am. Chem. Soc.* **139**, 1089–1097 (2017).

Supplementary Methods

An epoxide intermediate in glycosidase catalysis

Contents

Safety statement

No unexpected or unusually high safety hazards were encountered in this work.

Crystal handling, X-ray crystallography and structure solution

Crystals of *Bx*GH99 were grown in 3 M sodium acetate, pH 6.4-7.4 at 19 ºC in darkness using the hanging drop vapor diffusion method. Soaking (30 min) was performed by adding a 0.5-1 µl concentrated (20-50 mM) aqueous solution of a ligand to the droplet. In the case of the structure of wild-type *Bx*GH99 with β-epoxide, the crystals were soaked for 3 min. All β-epoxide soaks were performed at pH 7.4 to minimize acid-catalyzed reactions. Data reduction was performed in xia2.[1] The data were scaled and merged using aimless.[2] Structures were solved by matching the HKL index of a dataset to that of 5M17 (PDB code) and direct refinement in REFMAC5[3] using only the polypeptide chain model. The R_{free} set was kept identical to that in PDB 5M17. In all cases, the space group was the same (I4). Coot[4] was used for model building and real-space refinement. The models were validated using Coot and edstats. Cremer-Pople parameters of sugars[5] were obtained using Privateer,[6] which was also used to validate their real space electron density correlation coefficient. Figures were made using ccp4mg.[6-7]

Computational Methods

Classical and QM/MM molecular dynamics simulations

The initial structure for the simulations was taken from the structure of *Bx*GH99-E333Q bound to αMan-1,3-αMan-1,2-αMan-1,2-αMan-OMe [$(Man)_4OMe$] reported in this work (PDB 6FWG). To simulate the wild type enzyme, the mutation of the acid residue (Q333E) was manually reverted, and the substrate was modelled as $(Man)_4OH$. The protonation states and hydrogen atom positions of all amino acid residues were taken according to their protein environment. Histidines 60, 63, 109 and 245 were considered as double protonated, His154 and His 180 were protonated at Nε and His335 was protonated at N_δ. A total number of 22.240 water molecules were added to the protein surface, within a radius of 15 Å from the protein.

Molecular dynamics (MD) simulations were performed using the Amber11 software.[10] The protein was modeled using the FF99SB force field.[11] The carbohydrate substrate and water molecules were described with the GLYCAM0611 and TIP3P12 force fields, respectively.[12-13] The MD simulation was carried out in several steps. First, the system was minimized, holding the protein and substrate fixed, followed by energy minimization on the entire system. To gradually reach the desired temperature, weak spatial constraints were initially added to the

protein and substrate, while water molecules were allowed to move freely at 100 K. The constraints were then applied only to the catalytic residues and the working temperature of 300K was reached after four more 50 K heating steps in the NVT ensemble. Afterwards, the density was converged up to water density at 300 K in the NPT ensemble and the simulation was extended to 30 ns in the NVT ensemble, releasing the restraints on the the two catalytic residues during the last 15 ns.

Analysis of the trajectory was carried out using standard tools of AMBER and VMD.[14] QM/MM MD simulations were performed using the method developed by Laio *et al.*,[15] which combines Car–Parrinello MD,[16] based on Density Functional Theory (DFT), with force-field MD methodology. In this approach, the system is partitioned into quantum mechanics (QM) and molecular mechanics (MM) fragments. The dynamics of the atoms on the QM fragment depend on the electronic density, $\rho(r)$, computed with Density Functional Theory, whereas the dynamics of the atoms on the MM fragment are ruled by an empirical force field. The QM/MM interface is modeled by the use of link-atom that saturates the QM region. The electrostatic interactions between the QM and MM regions were handled via a fully Hamiltonian coupling scheme,[15] where the short-range electrostatic interactions between the QM and the MM regions are explicitly taken into account for all atoms. An appropriately modified Coulomb potential was used to ensure that no unphysical escape of the electronic density from the QM to the MM region occurs. The electrostatic interactions with the more distant MM atoms were treated via a multipole expansion. Bonded and van der Waals interactions between the QM and the MM regions were treated with the standard AMBER force-field. Long-range electrostatic interactions between MM atoms were described with the P3M implementation,16 using a 64 x 64 x 64 mesh.

The QM region included all the atoms of the $(Man)_4OH$ substrate and the catalytic residues E333 and E336, leading a total number of 108 QM atoms (including capping hydrogens). The MM subsystem includes a total number of 72.235 MM atoms. The QM region was enclosed in an isolated supercell of size 19.4 x 17.9 x 23.7 $Å^3$. Kohn–Sham orbitals were expanded in a planewave basis set with a kinetic energy cutoff of 70 Ry. Norm-conserving Troullier–Martins ab initio pseudopotentials[17] were used for all elements. The calculations were performed using the Perdew, Burke and Ernzerhoff generalized gradient-corrected approximation (PBE).[18] This functional form has been proven to give a good performance in the description of hydrogen bonds[19] and carbohydrate conformations[20] and was already used with success in previous works on glycoside hydrolases and glycosyltransferases.[21] The fictitious electronic mass was set to 700 au and the timestep to 5 au.

QM/MM metadynamics simulations

The free energy landscape (FEL) of the reaction was explored using the metadynamics approach[22] with two collective variables (CVs). We used the metadynamics driver provided by the Plumed2 plugin.[23] The first collective variable (CV1) was defined as the difference between the O2-C1 and the C1-O1 distances. This variable accounts for the nucleophilic attack of the 2-OH to the anomeric center and the cleavage of the glycosidic bond. The second collective variable (CV2) was defined as the distance difference between the O_{E336}-H and H-O1. This variable accounts for proton transfer between the acid/base residue and the glycosidic bond. Repulsive walls were set to 2.5 and -2.5 Å for each of the variables, with a constant of 150 kcal/mol·Å^2, to restrain the exploration to the reactive event. Symmetric Gaussians of 1 kcal/mol height and 0.15 Å width were deposited every 30 fs (250 MD steps). Sampling of the FES was completed after 1049 deposited Gaussians.

An additional metadynamics simulation was performed without including the O2 atom in the collective variables definition. In this case, the nucleophilic attack (CV1) was defined as the difference between the O_{E333}-C1 and the C1-O_{Gly} distances, i.e. with E333 acting as a "classical" nucleophile in a double-displacement reaction. The same parameters as in the previous metadynamics simulation were used, adapting the wall on CV1 to the new boundaries (4.5 and -4.5 Å). The FES was completed after 805 deposited Gaussians. This simulation also conduced reactants towards the formation of the epoxide (**Supplementary Fig. 5**).

Cyclohexane β-1,2-epoxide transfer reaction and thin layer chromatography

For all reactions, freshly prepared, aqueous solutions of α-1,2-epoxide and β-1,2-epoxide were used and the buffer was 50 mM potassium phosphate pH 7.0, 185 mM KCl. Due to the difficulty of separating the cyclohexane α-1,2-epoxide and β-1,2-epoxide, a mixture of both was used (1.78:1 α/β ratio). $GlcMan_3OMe$ was used at 250 μM. The reactions contained 10 μM of each enzyme and were incubated at 37 °C for 2 h. The concentration of cyclohexane α-1,2-epoxide in the samples was 1 mM and the concentration of cyclohexane β-1,2-epoxide, in the samples which contained it, was 0.56 mM. The concentration of the acceptor, α-1,2-mannobiose, was 1 mM. The total reaction volume was 10 μl (for TLC) or 40 μl (for mass spectrometry (MS)).

The samples were transferred in 1 μl droplets onto SUPELCO silica gel on TLC Al foils (Sigma Aldrich). Each droplet was allowed to dry before adding the next droplet. A total of 5 μl for each lane was loaded onto the silica gel. TLC was performed in a preequilibrated

chamber using 50% v/v n-butanol, 25% v/v acetic acid, 25% v/v H_2O as the eluent. When the eluent reached 75% of the plate height, the plate was taken out of the chamber, dried and run a second time to allow better compound resolution. The eluent was allowed to reach 75% of the plate height, at which point the migration was terminated. After drying, the samples were visualized by applying a staining solution (3% v/v sulfuric acid, 75% v/v ethanol, 0.1% orcinol monohydrate). The spots appeared after the plate was dried and subsequently heated on a hot plate (70–100 °C).

Epoxide hydrolysis and transfer reactions and mass spectrometry

Reactions were conducted at 37 ºC in 1.25 µM HEPES pH 7.0, 5 mM NaCl. Samples were taken after 20 min, 60 min and an overnight wait: 17-22 h. Quenching was achieved by mixing 10 µl reaction mixture with 100 µl methanol. Compounds were incubated in separate reaction tubes with 1 µM of each of wild-type *Bt*GH99, wild-type *Bx*GH99, *Bx*GH99 E333Q, *Bx*GH99 E336Q; 20 µM of wild-type *Bt*GH99; or buffer only. MS were obtained using a Bruker microTOF spectrometer using electrospray ionization (ESI). All compounds were used at a starting concentration of 1 mM with correction factors from calculations applied later. The peaks corresponding to the $[M+Na]^+$ ions were integrated in Origin software (OriginLab). The concentration of the compounds was estimated as follows: the areas of the peaks corresponding to unreacted epoxide or aziridine and their ring-opened forms in each mass spectrum were added and assumed to be 1 mM. The area of each peak was divided by the total area and this was the reported concentration. In the case of the β-epoxide, extended digestion with enzyme revealed that a portion of the substrate peak was not processed by the enzyme – most likely traces of α-1,2-epoxide. This amount was subtracted from the total calculated cyclohexane β-1,2-epoxide concentration. Additionally, β-epoxide and β-aziridine were not stable. We have included the starting amount of cyclohexane-diol in our calculations of reaction rate.

For the MS of β-1,2-epoxide transfer reaction, 5 µl of the reaction mixture used in the TLC experiment was used for permethylation, during which a procedure by Ciucanu and Kerek[8] was followed. The products of the reaction were analyzed by MALDI-MS. The mass spectra are presented below.

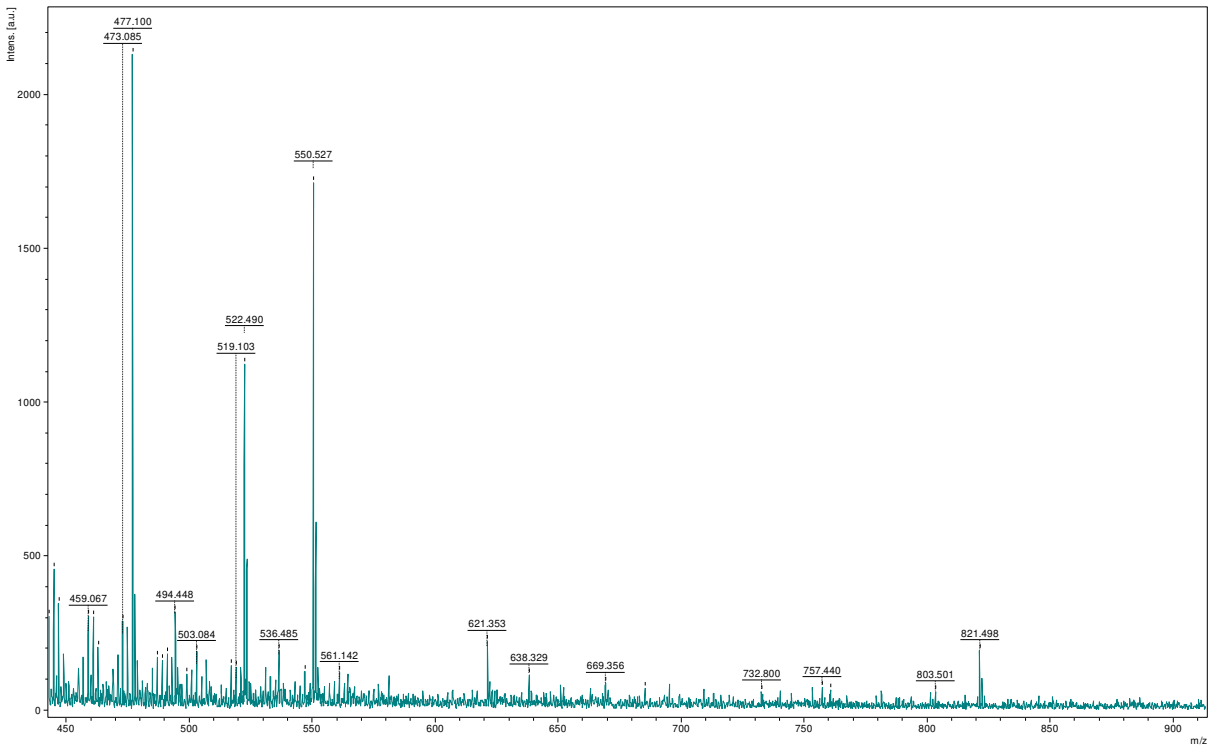

Mass spectrum of the α-1,2-epoxide incubated in presence of *Bx*GH99 and α-1,2-mannobiose.

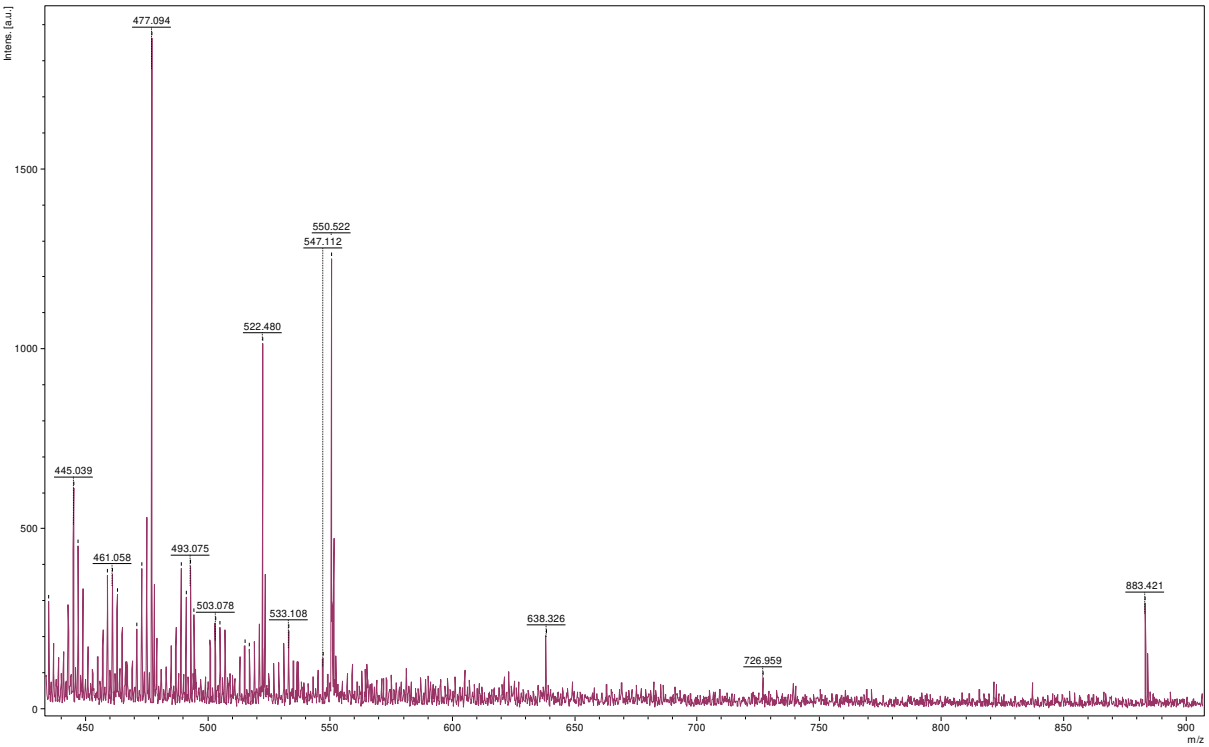

Mass spectrum of the β-1,2-epoxide incubated in presence of *Bx*GH99, α-1,2-epoxide and α-1,2-mannobiose. Note the peak at *m/z* 883.4, corresponding to a sodiated, permethylated pseudotetrasaccharide species.

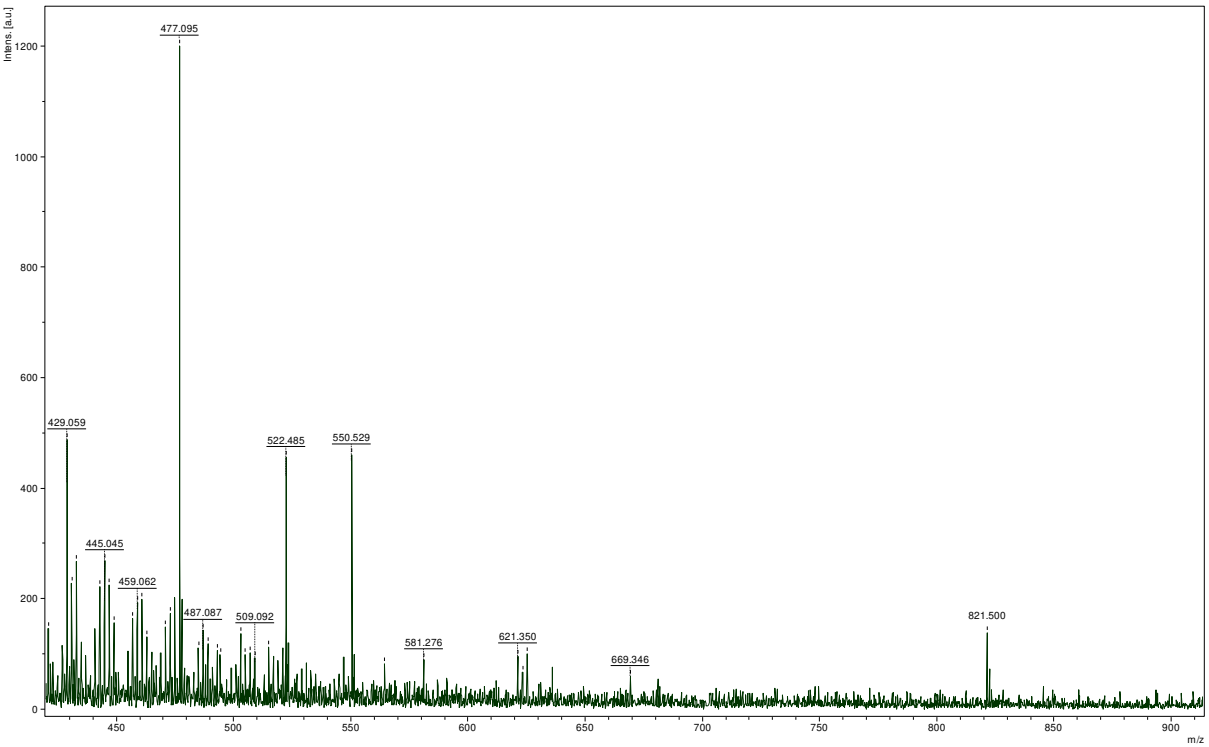

Mass spectrum of the α-1,2-epoxide incubated in presence of *Bt*GH99 and α-1,2-mannobiose.

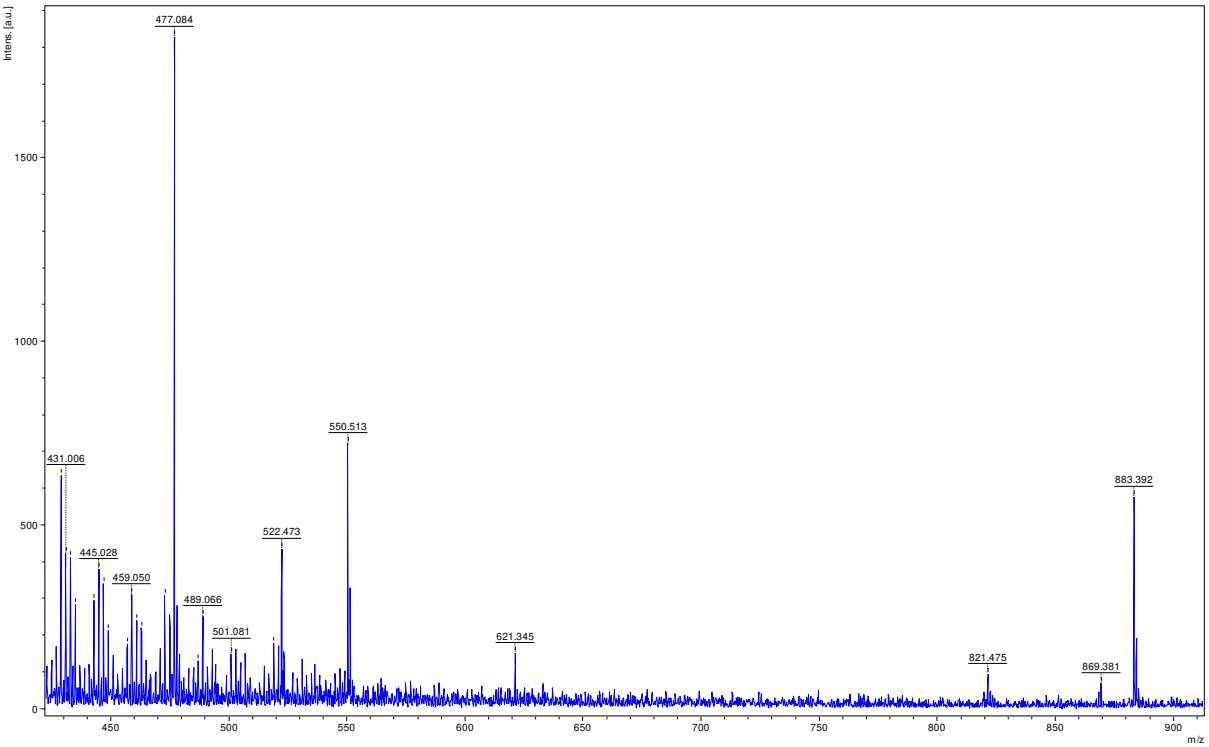

Mass spectrum of the β-1,2-epoxide incubated in presence of *Bt*GH99, α-1,2-epoxide and α-1,2-mannobiose. Note the peak at *m/z* 883.4, corresponding to a sodiated, permethylated pseudotetrasaccharide species.

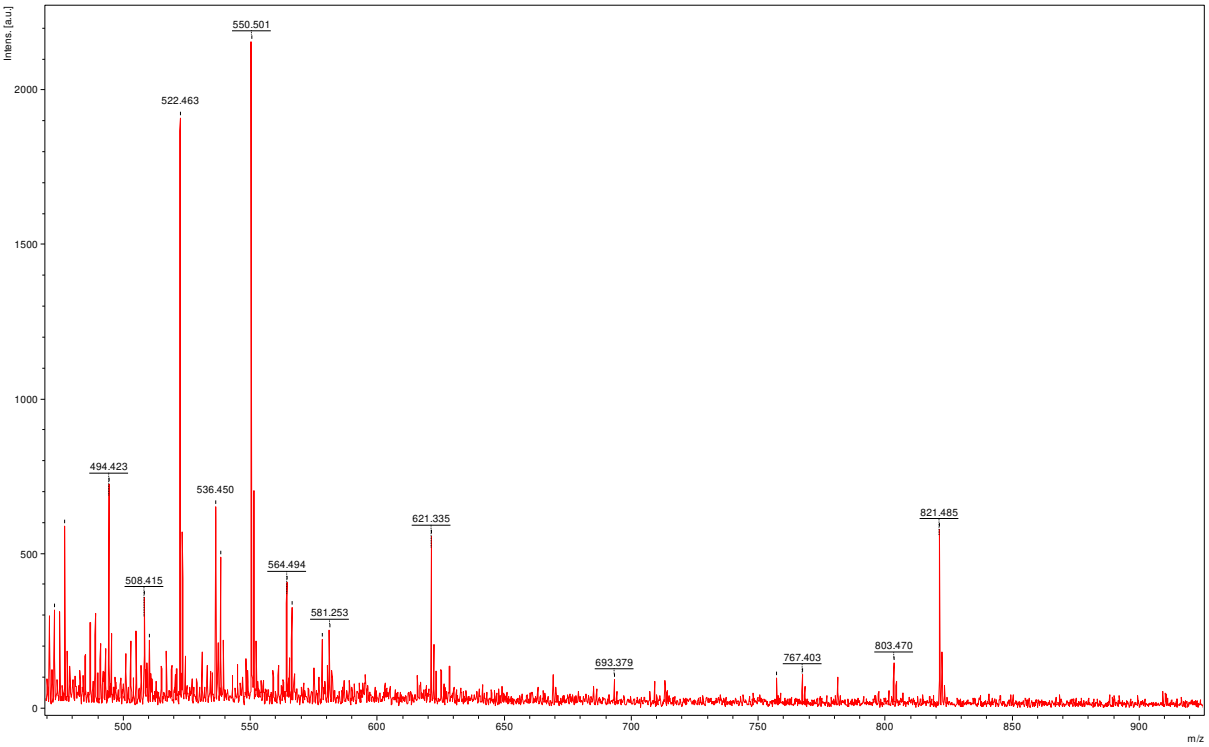

Mass spectrum of the permethylation reaction blank sample.

NMR analysis of *Bt*GH99-catalyzed hydrolysis of the β-epoxide (1).

^{1}H and ^{13}C 1-D NMR spectra of the product of the enzyme-digest of the β-1,2-epoxide were obtained on a Bruker Avance 600 MHz instrument. Binding kinetics were determined as described earlier.[9]

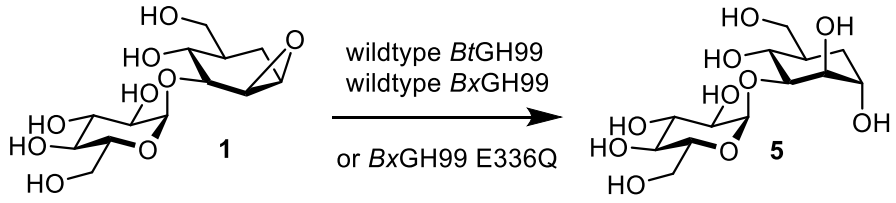

NMR data for 5: ^{1}H-NMR (600 MHz, D_2O) δ 1.81–1.77 (2 H, m, H5a,5b), 2.00 (1 H, s), 1.94 (1 H, m, H5), 3.47 (1 H, t, $J_{2',3'}$ = 9.9 Hz, H3'), 3.60 (1 H, dd, $J_{2',3'}$ = 9.9, $J_{1',2'}$ = 3.9 Hz, H2'), 3.76 (2 H, dd, $J_{a,b}$ = 7.6, 4.6 Hz, H6a',6b'), 3.80–3.86 (4 H, m, H3,5',4,6b), 3.90 (2 H, d, $J_{4',5'}$ = 11.2 Hz, H4',6a), 4.05 (1 H, m, H1), 4.16 (1 H, t, $J_{1,2}$ = 2.9, $J_{2,3}$ = 5.8 Hz, H2), 5.25 (1 H, d, $J_{1',2'}$ = 3.9 Hz, H1'). ^{13}C NMR (151-MHz, D_2O) δ), 28.0 (C5a), 38.8 (C5), 60.6 (C6), 62.4 (C6'), 69.2 (C1), 69.64 (C3), 69.57 (C5'), 71.9 (C2'), 72.3 (C4), 72.4 (C2), 73.0 (C4'), 81.4 (C3), 100.8 (C1').

KIE Measurements

1-^{2}H-KIE measurements: Competitive *V/K* KIEs were measured using ^{13}C NMR spectroscopy on a Bruker AVANCE II 600 MHz spectrometer with a 5 mm QNP cryoprobe.[24] Carbon-13 T_1 values were measured for phenyl 1-thio-β-D-(1-^{13}C)glucopyranoside (internal standard), 1-^{13}CMan$_4$OMe and 1-^{13}C,1-^{2}H-Man$_4$OMe at 25°C and pH 7.0 using a standard inversion recovery pulse sequence modified to add simultaneous ^{1}H and ^{2}H inverse gated decoupling and determined to be 1.049 s, 0.437 s and 2.533 s, respectively. In a typical experiment, a mixture of two labelled Man$_4$OMe isotopologues (~1.0 mg of each) and phenyl 1-thio-β-D-(1-^{13}C)glucopyranoside (0.25 mg) was dissolved in 590 µL buffer (25 mM HEPES, pH 7.0, 10% v/v D_2O) and transferred into a standard 5 mm glass NMR tube. Reactions were initiated by the addition of a stock solution of enzyme (10 µL of 10 mg mL^{-1}; final concentration of enzyme 3.86 µM. The magnetic field was shimmed to obtain symmetrical (as close to a Lorentzian shape as possible) peaks. ^{1}H NMR and ^{13}C NMR spectra were then acquired before sequentially acquiring more than hundred quantitative ^{13}C NMR spectra with simultaneous inverse-gated proton- and deuterium-decoupling.[25-26] FIDs were acquired for 36

scans (acquisition time per scan of 1.42 s) with a relaxation delay of 23.5 s (15 min per spectrum).

The resultant quantitative ^{13}C spectra were deconvolved by performing the following operations: i) Fourier transformation of the FIDs was performed with two-fold zero-filling and application of an exponential line broadening of 1.0 Hz; ii) spectra were manually phased and baseline corrected using MestReNova version 9; iii) spectra were fit using standard MestReNova line fitting algorithm for a generalized Lorentzian line shape; iv) to optimize the calculated fit peak positions, peak widths at half-height, peak heights and optimal combination of Lorentzian and Gaussian (L/G) shapes for each individual peak were allowed to vary; and v) the peak areas were normalized relative to that of the internal standard. Then, for each spectrum the fraction of reaction (F_L) for the lighter isotopologue and the associated R values were calculated from the respective integrals. These data were fit to equation (1) using GraphPad Prism 8.02 and a non-linear least squares regression.[27]

$$R = R_0(1 - F_L)^{(1/KIE-1)} \qquad (1)$$

2-^{18}O-KIE measurements: Carbon-13 T_1 value was measured for labelled 2-^{13}CMan$_4$OMe at 25 °C and pH 7.0 using a standard inversion recovery pulse sequence and determined to be 0.420 s. In a typical experiment, a mixture of two labelled Man$_4$OMe isotopologues, 2-^{13}CMan$_4$OMe and 2-^{13}C,2-^{18}O-Man$_4$OMe (~1.0 mg of each), and phenyl 1-thio-β-D-(1-^{13}C)glucopyranoside (0.25 mg) was dissolved in 650 µL buffer (25 mM HEPES, pH 7.0, 10% v/v D_2O) and transferred into a standard 5 mm glass NMR tube. Reactions were initiated by the addition of enzyme (4–6 µL of a 2.3 mg mL^{-1} stock solution). The magnetic field was shimmed to obtain symmetrical (as close to a Lorentzian shape as possible) peaks. A ^{1}H NMR and ^{13}C NMR spectra were then acquired before sequentially acquiring more than fifty quantitative proton-decoupled ^{13}C NMR spectra using an inverse-gated pulse sequence.[2,3] FIDs were acquired for 128 scans (acquisition time per scan of 2.99 s) with a relaxation delay of 8.5 s (24.5 min per spectrum). After the reaction had reached ~50–80% completion, which occurred after ~48–50 hours, an additional 20 µL of GH99 enzyme was added to ensure complete hydrolysis of the starting material. Subsequently, a quantitative $^{13}C\{^1H\}$ spectrum of the products and the unreactive impurity was collected by accumulating 6000 scans.

The resultant quantitative ^{13}C spectra were deconvolved by performing the following operations: i) Fourier transformation of the FIDs was performed with two-fold zero-filling and application of an exponential line broadening between 0.3–0.5 Hz; ii) Spectra were manually phased and baseline corrected using MestReNova version 10.0.2 and the chemical shift of the anomeric carbon signal of the internal standard phenyl 1-thio-β-D-(1-^{13}C)glucopyranoside was set to be 87.18 ppm; iii) Every 5 spectra were summed and the internal standard peaks were fit using standard MestReNova line fitting algorithm for a generalized Lorentzian line shape. To optimize the calculated fit peak positions, peak widths at half-height, peak heights and optimal combination of Lorentzian and Gaussian (L/G) shapes for each individual peak were allowed to vary; iv) Internal standard signal intensities, for each summed spectrum and the completely hydrolyzed final sample, were normalized and a difference spectrum was calculated. For every reaction summed spectrum obtained (see part 3) the difference spectrum was used to calculate R; v) The starting materials' peak areas were normalized relative to that of the internal standard. Then, for each spectrum the fraction of reaction (F_L) for the lighter isotopologue and the associated R values (ratio of heavy/light isotopologues) were calculated from the respective integrals. These data were then fit using GraphPad Prism 8.02 and a non-linear least squares regression to equation 1.[4]

1-^{13}C-KIE measurements: Competitive *V/K* KIEs were measured using ^{13}C NMR spectroscopy on a Bruker AVANCE III 600 MHz spectrometer with a 5 mm QCI cryoprobe.[1] Carbon-13 T_1 values were measured for phenyl 1-thio-β-D-(1-^{13}C)glucopyranoside (internal standard), 2-^{13}CMan$_4$OMe and 1,2-^{13}CMan$_4$OMe at 25 °C and pH 7.0 using standard inversion recovery pulse sequence and determined to be 0.929 s, 0.391 s and 0.379 s, respectively. In a typical experiment, a mixture of two labelled Man$_4$OMe isotopologues (~1.0 mg of each) and phenyl 1-thio-β-D-(1-^{13}C)glucopyranoside (0.25 mg) was dissolved in 650 µL buffer (25 mM HEPES, pH 7.0, 10% v/v D_2O) and transferred into a standard 5 mm glass NMR tube. Reactions were initiated by the addition of enzyme (10–15 µL of 2.3 mg mL^{-1}). The magnetic field was shimmed to obtain symmetrical (as close to a Lorentzian shape as possible) peaks. A ^1H NMR and ^{13}C NMR spectra were then acquired before sequentially acquiring more than fifty quantitative proton-decoupled ^{13}C NMR spectra using an inverse-gated pulse sequence.[2,3] FIDs were acquired for 128 scans (acquisition time per scan of 1.73 s) with a relaxation delay of 8.5 s (21.8 min per spectrum). After reaction reached 70–80% completion an additional quantity of GH99 enzyme (20 µL of 2.3 mg mL^{-1}) was added to ensure full transformation of the starting material. Then a quantitative $^{13}C\{^1H\}$ spectrum of products and the unreactive

impurities was collected by accumulating 6000 scans. All data manipulations were performed in an identical manner as described above.

General synthetic methods

Pyridine was distilled over KOH or CaH_2. Dichloromethane was freshly distilled from P_2O_5, and THF distilled from sodium/benzophenone, or alternatively were dried over alumina according to the method of Pangborn *et al.*[28] DMF was dried over molecular sieves. Reactions were monitored using TLC, performed with silica gel 60 F_{254}. Detection was effected by charring in a mixture of 5% sulfuric acid in methanol, 10% phosphomolybdic acid in EtOH, and/or visualizing with UV light. Flash chromatography was performed according to the method of Still et al.[29] using silica gel 60. $[\alpha]_D$ values are given in deg 10^{-1} cm^2 g^{-1}. NMR experiments were conducted on 400, 500 or 600 MHz instruments, with chemical shifts referenced relative to residual protiated solvent and are in δ ppm. Assignments were aided by 2D $^1H-^1H$ COSY, HSQC, HMQC, HMBC, NOESY and TOCSY experiments. High resolution mass spectra were acquired in the ESI-QTOF or ESI-FTMS modes, or using a Bruker microTOF spectrometer, using Agilent ESI-L Low Concentration Tuning-Mix as reference. For oligosaccharides, the sugar rings leading away from the reducing end are denoted ', '', and ''', respectively.

Synthesis of cycloalkene 7, and epoxides 1 and 3.

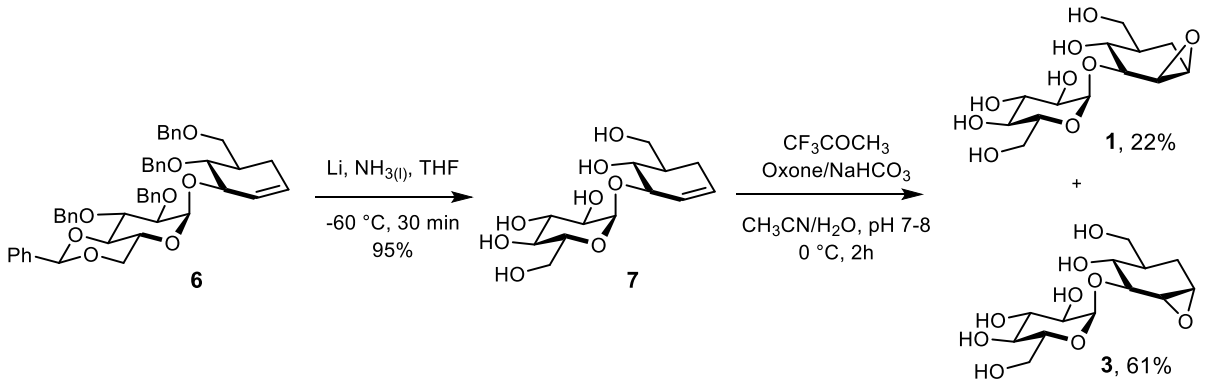

(3*R*,4*R*,5*R*)-3-α-D-Glucopyranosyloxy-4-hydroxyl-5-(hydroxymethyl) cyclohexene (7)

Ammonia (10 mL) was condensed at -60 °C. Lithium (100 mg) was added piece-wise and the mixture was stirred for about 20 min until the lithium was completely dissolved, to give a dep-blue solution. A solution of **6**[30] (97.8 mg, 0.147 mmol) in THF (5 mL) was added dropwise to the blue solution. The reaction was stirred for 30 min at -60 °C and then quenched with water (4 mL). This solution was stirred at r.t. overnight until all ammonia had evolved. Next, the solution was evaporated, then re-dissolved in water and neutralized with Amberlite IR 120/H^+.

The solution was filtered and washed with water. Product **7** (40 mg, 95%) was obtained after lyophilisation of the combined eluate as a white amorphous solid. R_f = 0.28 (CH_2Cl_2-MeOH 10:4); $[\alpha]_D^{20}$ 47.6 (c 1.0 in H_2O). ^{1}H-NMR (400 MHz, D_2O) δ = 5.97-5.87 (m, 1H, H-1), 5.76-5.66 (m, 1H, H-2), 5.29 (d, $J_{1,2}$ = 3.9 Hz, 1H, H-1'), 4.33-4.27 (m, 1H, H-3), 3.93-3.77 (m, 5H, H-6'a, H-5', H-4, H-6a, H-6'b), 3.77-3.70 (m, 2H, H-3', H-6b), 3.60 (dd, $J_{1,2}$ = 3.9 Hz, $J_{2,3}$ = 9.9 Hz, 1H, H-2'), 3.46 (t, $J_{3,4}$, $J_{4,5}$ = 9.4 Hz, 1H, H-4'), 2.36-2.24 (m, 1H, H-5aa), 2.11-1.96 (m, 2H, H-5ab, H-5). ^{13}C-NMR (100.6 MHz, D_2O) δ = 129.91 (C-1), 126.03 (C-2), 99.30 (C-1'), 81.12 (C-3), 73.01 (C-3'), 72.38 (C-4), 72.18 (C-5'), 71.57 (C-2'), 69.68 (C-4'), 62.42 (C-6), 60.61 (C-6'), 40.46 (C-5), 27.39 (C-5a). ESI-HRMS (*m/z*) calcd for $C_{13}H_{22}O_8Na$ ($M + Na^+$) 329.1207, found: 329.1204.

(1*R*,2*R*,3*R*,4*R*,5*R*)-1,2-β-Anhydro-3-α-D-glucopyranosyloxy-4-hydroxyl-5-(hydroxymethyl) cyclohexane (1) and (1*S*,2*S*,3*R*,4*R*,5*R*)-1,2-α-Anhydro-3-α-D-glucopyranosyloxy-4-hydroxyl-5-(hydroxymethyl) cyclohexane (3)

A solution of **7** (47 mg, 0.154 mmol, 1eq) in aqueous Na_2EDTA solution (4.5 mL, 4×10^{-4} M) and CH_3CN (3 mL) was cooled to 0-2 °C, followed by addition of trifluoroacetone (0.14 mL, 1.54 mmol, 10 eq) via a precooled syringe. To this solution was added a mixture of $NaHCO_3$ (100 mg, 1.19 mmol, 7.8 eq) and Oxone (236 mg, 0.76 mmol, 5 eq) portionwise over 1 h. The reaction mixture was stirred for another 1 h, and then concentrated. The resulting solid was redissolved in methanol, and centrifuged to keep the clear organic solution, which was then concentrated again. The residue was purified by silica gel column chromatography (EtOAc-iPrOH-H_2O 13:5:0.36). Product **3** (30 mg, 61%) and **1** (11 mg, 22%) were isolated and obtained as white amorphous solids.

Product **3**: R_f = 0.41 (EtOAc-iPrOH-H_2O 5:10:1); $[\alpha]_D^{20}$ 79.3 (c 0.3 in H_2O). ^{1}H-NMR (400 MHz, D_2O) δ = 5.29 (d, $J_{1,2}$ = 3.8 Hz, 1H, H-1'), 3.90-3.70 (m, 5H, H-6'a, H-5', H-3, H-6'b, H-3'), 3.69-3.64 (m, 2H, H-6a, H-6b), 3.58 (dd, $J_{1,2}$ = 3.8 Hz, $J_{2,3}$ = 9.5 Hz, 1H, H-2'), 3.51 (dd, $J_{4,5}$ = 11.5 Hz, $J_{3,4}$ = 8.2 Hz, 1H, H-4), 3.46-3.41 (m, 2H, H-4', H-1), 3.39 (d, $J_{1,2}$ = 3.8 Hz, 1H, H-2), 2.29-2.20 (m, 1H, H-5aa), 1.90-1.77 (m, 1H, H-5ab), 1.61-1.51 (m, 1H, H-5). ^{13}C-NMR (100.6 MHz, D_2O) δ = 101.05 (C-1'), 80.53 (C-3), 73.44 (C-3'), 73.13 (C-5'), 72.55 (C-4), 72.17 (C-2'), 70.20 (C-4'), 62.32 (C-6), 61.20 (C-6'), 56.27 (C-2), 54.96 (C-1), 34.93 (C-5), 26.77 (C-5a). ESI-HRMS (*m/z*) calcd for $C_{13}H_{22}O_9Na$ ($M + Na^+$) 345.1156, found: 345.1156.

Product **1:** R_f = 0.29 (EtOAc-iPrOH-H_2O 5:10:1); $[\alpha]_D^{20}$ 85.5 (c 0.1 in MeOH). ^{1}H-NMR (400 MHz, CD_3OD) δ = 5.17 (d, $J_{1,2}$ = 3.8 Hz, 1H, H-1'), 3.93 (ddd, $J_{4,5}$ = 9.9 Hz, $J_{5,6a}$ = 5.4 Hz,

$J_{5,6b}$ = 2.4 Hz, 1H, H-5'), 3.89-3.81 (m, 2H, H-6'a, H-3), 3.79-3.72 (m, 2H, H-3', H-6'b), 3.72-3.66 (m, 2H, H-6a, H-4), 3.65-3.57 (m, 2H, H-6b, H-2), 3.49 (dd, $J_{1,2}$ = 3.8 Hz, $J_{2,3}$ = 9.8 Hz, 1H, H-2'), 3.39-3.35 (1H, H-4'), 3.33 (dd, $J_{1,2}$ = 4.3 Hz, $J_{1,5a}$ = 8.9 Hz, 1H, H-1), 2.18 (dt, $J_{5aa,5ab}$ = 14.8 Hz, $J_{5,5aa}$, $J_{1,5aa}$ = 5.5 Hz, 1H, H-5aa), 1.81 (dd, $J_{5aa,5ab}$ = 14.8 Hz, $J_{5,5ab}$= 11.7 Hz, 1H, H-5ab), 1.79-1.68 (m, 1H, H-5). ^{13}C-NMR (151 MHz, CD_3OD) δ = 102.69 (C-1'), 85.53 (C-3), 75.08 (C-3'), 74.02 (C-2'), 73.93 (C-5'), 71.83 (C-4'), 71.09 (C-4), 63.78 (C-6), 62.70 (C-6'), 57.52 (C-2), 54.65 (C-1), 42.27 (C-5), 27.26 (C-5a). ESI-HRMS (*m/z*) calcd for $C_{13}H_{22}O_9Na$ ($M + Na^+$) 345.1156, found: 345.1147.

Synthesis of aziridine 2.

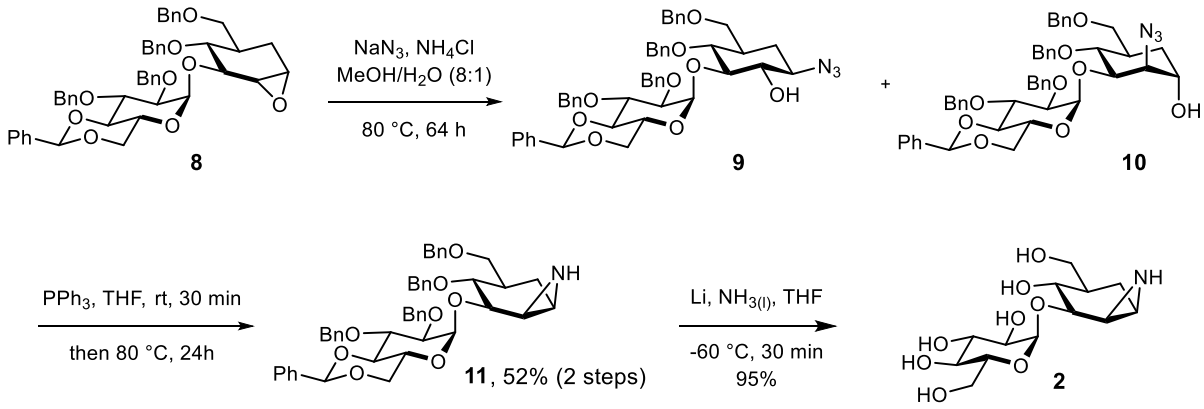

(1*R*,2*S*,3*R*,4*R*,5*R*)-1-Azido-2-hydroxyl-3-(2,3-di-*O*-benzyl-4,6-*O*-benzylidene-α-D-glucopyranosyloxy)-4-benzyloxy-5-(benzyloxymethyl) cyclohexane (9) and (1*S*,2*R*,3*R*,4*R*,5*R*)-1-Hydroxyl-2-azido-3-(2,3-di-*O*-benzyl-4,6-*O*-benzylidene-α-D-glucopyranosyloxy)-4-benzyloxy-5-(benzyloxymethyl) cyclohexane (10)

A solution of epoxide **8**[30] (75 mg, 0.097 mmol, 1 eq) in 8:1 MeOH/H_2O (9 mL) was treated with NaN_3 (120 mg, 1.85 mmol, 19 eq) and NH_4Cl (21 mg, 0.389 mmol, 4 eq). The reaction mixture was stirred at 80 °C for 72 h, diluted with ether, washed with saturated $NaHCO_3$ and brine, dried over $MgSO_4$ and concentrated to afford crude azides **9** and **10** (67 mg) for the next step without further purification.

(1*R*,2*R*,3*R*,4*R*,5*R*)-1,2-β-Aziridine-3-(2,3-di-*O*-benzyl-4,6-*O*-benzylidene-α-D-glucopyranosyloxy)-4-benzyloxy-5-(benzyloxymethyl) cyclohexane (11)

To a solution of azides **9** and **10** (67 mg) from the above step in THF (10 mL), PPh_3 (32.4 mg, 0.124 mmol) was added and the resulting solution was stirred at r.t. for 30 min, then refluxed for 24 h. The solvent was evaporated and purification by silica gel chromatography (Cyc/EtOAc 2:1) afforded β-aziridine **11** (33 mg, 52%) as a white amorphous foam. R_f = 0.26 (Cy-EtOAc 4:3); $[\alpha]_D^{20}$ 9.4 (c 0.1 in $CHCl_3$). ^{1}H-NMR (400 MHz, $CDCl_3$) δ = 7.53-7.47 (m, 2H, arom), 7.42-7.14(m, 23H, arom), 5.56 (s, 1H, PhC<u>H</u>), 5.12 (d, $J_{1,2}$ = 3.8 Hz, 1H, H-1'), 5.08, 4.45 (2d, J_{gem} = 11.5 Hz, 2H, PhC<u>H</u>$_2$), 4.93, 4.84 (2d, J_{gem} = 11.6 Hz, 2H, PhC<u>H</u>$_2$), 4.74, 4.65 (2d, J_{gem} = 12.2 Hz, 2H, PhC<u>H</u>$_2$), 4.42 (s, 2H, PhC<u>H</u>$_2$), 4.32-4.12 (m, 3H, H-5', H-3', H-6'a), 3.93 (dd, $J_{3,4}$ = 8.2 Hz, $J_{2,3}$ = 3.6 Hz, 1H, H-3), 3.71 (t, $J_{6a,6b}$, $J_{5,6b}$ = 10.2 Hz, 1H, H-6'b), 3.63 (t, $J_{3,4}$, $J_{4,5}$ = 9.4 Hz, 1H, H-4'), 3.56 (dd, $J_{1,2}$ = 3.7 Hz, $J_{2,3}$ = 9.4 Hz, 1H, H-2'), 3.58-3.47 (m, 2H, H-4, H-6a), 3.46-3.35 (m, 1H, H-6b), 2.58 (dd, $J_{2,3}$ = 3.6 Hz, $J_{1,2}$ = 6.1 Hz, 1H, H-2), 3.25 (dd, $J_{1,2}$ = 6.1 Hz, $J_{1,5a}$ = 6.3 Hz, 1H, H-1), 2.28-2.12 (m, 1H, H-5aa), 1.85-1.74 (m, 2H, H-5, H-5ab). ^{13}C-NMR (100.6 MHz, $CDCl_3$) δ = 139.47, 138.85, 138.74, 138.41, 137.66 (arom C), 129.05, 128.42, 128.39, 128.38, 128.34, 128.25, 128.19, 127.94, 127.83, 127.66, 127.54, 127.23, 126.30 (arom CH), 101.56 (Ph<u>C</u>H), 100.40 (C-1'), 84.68 (C-3), 82.68 (C-4'), 79.38 (C-2'), 78.38 (C-3'), 78.19 (C-4), 75.23 (Ph<u>C</u>H$_2$), 75.00 (Ph<u>C</u>H$_2$), 73.54 (Ph<u>C</u>H$_2$), 73.19 (Ph<u>C</u>H$_2$), 70.73 (C-6), 69.32 (C-6'), 63.06 (C-5'), 40.78 (C-5), 36.22 (C-2), 31.19 (C-1), 28.31 (C-5a). ESI-HRMS (*m/z*) calcd for $C_{48}H_{52}NO_8Na$ (M + Na^+) 770.3687, found: 770.3706.

(1*R*,2*R*,3*R*,4*R*,5*R*)-1,2-β-Aziridine-3-α-D-glucopyranosyloxy-4-hydroxyl-5-(hydroxymethyl) cyclohexane (2)

Ammonia (7 mL) was condensed at -60 °C. Lithium (50 mg) was added piece-wise and the mixture was stirred for about 20 min until the lithium was completely dissolved. A solution of **11** (10 mg, 0.130 mmol) in THF (2.5 mL) was added dropwise to the mixture. The reaction was stirred for 30 min at -60 °C and then quenched with water (2 mL). This solution was stirred at r.t. overnight until all ammonia had evolved. Next, the solution was evaporated, then re-dissolved in water and neutralized with Amberlite IR 120/H^+. The solution was filtrated and washed with water. Then, the resin was eluted with 1 M NH_4OH solution (8 mL× 4), and the filtrate was evaporated under reduced pressure. The resulting solid was re-dissolved in water and neutralized with Amberlite-NH_4^+, and then filtered and washed with water. Target product **2** (3.8 mg, 95%) was obtained after lyophilisation of the combined eluate as a white amorphous

solid. R_f = 0.38 (EtOAc-iPrOH-H_2O 5:10:6); $[\alpha]_D^{20}$ 79.0 (c 0.03 in H_2O). ^{1}H-NMR (400 MHz, D_2O) δ = 5.24 (d, $J_{1,2}$ = 3.8 Hz, 1H, H-1'), 3.99-3.93 (m, 1H, H-5'), 3.93-3.87 (m, 1H, H-3), 3.87-3.78 (m, 3H, H-3', H-6'a, H-6'b), 3.70 (dd, $J_{6a,6b}$ = 11.3 Hz, $J_{5,6a}$ = 4.1 Hz, 1H, H-6a), 3.60 (dd, $J_{1,2}$ = 3.8 Hz, $J_{2,3}$ = 9.8 Hz, 1H, H-2'), 3.59-3.50 (m, 2H, H-6b, H-4), 3.47 (t, $J_{3,4}$, $J_{4,5}$ = 9.8 Hz, 1H, H-4'), 2.74 (dd, $J_{2,3}$ = 3.8 Hz, $J_{1,2}$ = 6.0 Hz, 1H, H-2), 2.55 (t, $J_{1,2}$, $J_{1,5a}$ = 7.1 Hz, 1H, H-1), 2.25-2.16 (m, 1H, H-5aa), 1.80-1.67 (m, 1H, H-5), 1.53 (dd, $J_{5aa,5ab}$ = 14.3 Hz, $J_{5,5ab}$ = 12.5 Hz, 1H, H-5ab). ^{13}C-NMR (100.6 MHz, $CDCl_3$) δ = 100.40 (C-1'), 83.74 (C-3), 72.99 (C-3'), 72.14 (C-5'), 71.95 (C-2'), 70.60 (C-4), 69.72 (C-4'), 62.42 (C-6) 60.55 (C-6'), 40.96 (C-5), 35.16 (C-2), 30.75 (C-1), 26.09 (C-5a). ESI-HRMS (*m/z*) calcd for $C_{13}H_{24}NO_8$ ($M + H^+$) 322.1496, found: 322.1500.

Preparation of (Man)$_4$OMe isotopologues

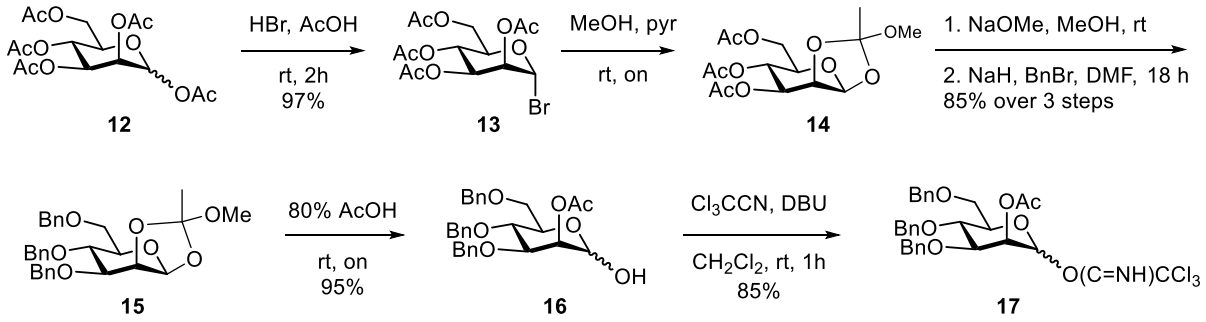

2,3,4,6-Tetra-*O*-acetyl-α-D-mannopyranosyl bromide[31] (13)

D-Mannose pentaacetate **12** (5.0 g, 12.8 mmol) was dissolved in a solution of hydrogen bromide (33% in acetic acid, 6 mL) the reaction mixture was stirred at r.t for 2 h, after which TLC analysis indicated complete consumption of the starting material. The reaction mixture was poured into ice water, and extracted with CH_2Cl_2 (3 × 75 mL). The combined organic phase was washed with brine (3 × 75 mL), sat. $NaHCO_3$ (3 × 75 mL) and again with brine. The organic phase was dried over anhydrous $MgSO_4$, filtered and evaporated *in vacuo* to afford **13** (5.00 g, 97%) as a pale yellow oil. $[\alpha]_D^{22}$ +118° (*c* 0.8, $CHCl_3$; lit.[31] +122°); ^{1}H-NMR (400 MHz, $CDCl_3$) δ 2.00, 2.06, 2.09, 2.16 (4 × 3H, s, Me), 4.13 (1H, dd, $J_{6,6a}$ =12.4, $J_{5,6a}$ = 2.1 Hz, H6a), 4.21 (1H, ddd, $J_{4,5}$ = 10.1, $J_{5,6}$ = 4.9, $J_{5,6a}$ = 2.1 Hz, H5), 4.32 (1H, dd, $J_{6,6a}$ = 12.5, $J_{5,6}$ = 4.8 Hz, H6), 5.36 (1H, app. t, $J_{3,4}$ = $J_{4,5}$ =10.1 Hz, H4), 5.43 (1H, dd, $J_{2,3}$ = 3.5, $J_{1,2}$ = 1.5 Hz, H2), 5.70 (1H, dd, $J_{3,4}$ = 10.2, $J_{2,3}$ = 3.5 Hz, H3), 6.29 (1H, d, $J_{1,2}$ = 1.5 Hz, H1); ^{13}C-NMR (101

MHz, $CDCl_3$) δ 20.5, 20.5, 20.6, 20.7 (4 × 1C, Me), 61.3 (1C, C6), 65.2 (1C, C4), 67.8 (1C, C3), 72.0 (1C, C5), 72.7 (1C, C2), 83.0 (1C, C1), 169.4, 169.6, 169.6, 170.4 (4 × 1C C=O).

3,4,6-Tri-*O*-acetyl-1,2-*O*-(methoxyethylidene)-β-D-mannopyranoside (14).

The bromide **13** (2.1 g, 5.1 mmol) was dissolved in dry pyridine (4 mL), then dry methanol (2 mL) was added and the solution was stirred overnight at room temperature. The solution was poured into ice-water (50 mL) and the aqueous phase extracted with CH_2Cl_2 (3 × 30 mL). The combined organic phase was washed with brine (50 mL), dried ($MgSO_4$), filtered and concentrated. The residue was redissolved in toluene (50 mL) and the remaining pyridine removed by azeotropic distillation *in vacuo*. The resulting solid of **14** was used for the following step without further purification, m.p. 110–112 °C. ^{1}H-NMR (400 MHz, $CDCl_3$) δ 1.74, 2.05, 2.07, 2.12 (4 × 3H, s, Me), 3.28 (3H, s, OMe), 3.68 (1H, m, H5), 4.14 (1H, dd, $J_{6,6a}$ = 11.7, $J_{5,6a}$ =1.9 Hz, H6a), 4.24 (1H, dd, $J_{6,6a}$ = 11.7, $J_{5,6}$ = 5.0 Hz, H6), 4.61 (1H, dd, $J_{2,3}$ = 3.5, $J_{1,2}$ = 2.5 Hz, H2), 5.15 (1H, dd, $J_{3,4}$ =10.0, $J_{2,3}$ = 3.5 Hz, H3), 5.30 (1H, app. t, $J_{3,4}$ = $J_{4,5}$ = 10.0 Hz, H4), 5.49 (1H, d, $J_{1,2}$ = 2.5 Hz, H1).

3,4,6-Tri-*O*-benzyl-1,2-*O*-(methoxyethylidene)-β-D-mannopyranoside (15).

A small piece of freshly cut Na metal was added to a solution of **14** (370 mg) in dry MeOH (3.5 mL), and the mixture was stirred at rt for 30 min. The solvent was evaporated and the residue redissolved in dry DMF (4 mL). The reaction was cooled to 0 °C, then NaH (60% in mineral oil, 245 mg, 6.1 mmol) was added and the mixture was stirred for 30 min. Benzyl bromide (0.55 mL, 4.59 mmol) was added dropwise and the slurry was stirred overnight. After 18 h, TLC analysis indicated complete consumption of the starting material. Ice-water was slowly added to quench the excess NaH, and the mixture was extracted with toluene (3 × 20 mL). The combined organic phase was dried ($MgSO_4$), filtered and concentrated. Flash chromatography (EtOAc:hexane:Et_3N, 25:74:1) gave **15** (430 mg, yield over two steps 85%) as an *endo/exo* mixture. Colorless needles, m.p. 76–78 °C. ^{1}H-NMR (400 MHz, $CDCl_3$) δ 1.57 (3 H, s, Me), 3.28 (3 H, s, OMe), 3.44–5.35 (13 H, m, H1,2,3,4,5,6a,6b and PhCH_2), 7.24–7.89 (15 H, m, Ar); ^{13}C-NMR (101 MHz, $CDCl_3$) δ 24.4 (1 C, Me), 49.8 (1 C, OMe), 69.0–79.0 (8C, C2-6 and Ph**C**H_2), 97.6 (1 C, C1), 124.0–138.2 (Ar).

2-*O*-Acetyl-3,4,6-tri-*O*-benzyl-D-mannopyranose (16)

A suspension of compound **15** (430 mg, 0.86 mmol) in 80% AcOH (9 mL) was stirred overnight at rt. The resulting solution was poured into a mixture of toluene (20 mL) and water (20 mL). The organic phase was washed with brine, sat. $NaHCO_3$, and water (×3), and then dried ($MgSO_4$). The residue was concentrated, yielding **16** (420 mg, 95%) as a colorless syrup, mixture of anomers. ^{1}H-NMR (400 MHz, $CDCl_3$) δ 2.14 (3 H, s, Me), 2.24 (3 H, s, Me), 3.77–3.82 (4 H, m), 3.95 (1 H, m), 4.12–4.15 (2 H, m), 4.54–4.64 (4 H, m), 4.68–4.71 (1 H, m), 4.78–4.81 (1 H, m), 4.94–4.97 (1 H, m), 5.30 (1 H, s, H1β), 5.46 (1 H, s, H1α), 7.24–7.43 (15 H, m, Ar); ^{13}C-NMR (101 MHz, $CDCl_3$) δ 21.1 (1 C, Me), 69.1, 69.2, 70.9, 71.7, 73.3, 74.6, 75.0, 77.6 (8 × C, C2-6 and Ph**C**H_2), 92.4 (1 C, C1), 127.7, 127.8, 128.0, 128.1, 128.3, 128.4, 137.7, 137.9, 138.2 (18 C, Ar), 170.5 (1 C, C=O); HRMS (ESI)$^+$ *m/z* 515.2049 [$C_{29}H_{32}NaO_7$ $(M + Na)^+$ requires 515.2046].

2-*O*-Acetyl-3,4,6-tri-*O*-benzyl-D-mannopyranosyl trichloroacetimidate (17)

The hemiacetal **16** (472 mg, 0.960 mmol) was dissolved in dry CH_2Cl_2 (20 mL) and cooled to 0 °C. Trichloroacetonitrile (479 µL, 4.79 mmol) and DBU (7 µL, 0.05 mmol) were added and the resulting solution was stirred for 1 h at r.t. The solvent was evaporated under reduced pressure and the residue was purified by flash chromatography (EtOAc:hexane:Et_3N, 2:8:0.1) to yield **16** (0.520 g, 85%) as a white foam. ^{1}H-NMR (400 MHz, $CDCl_3$) δ 2.19 (3 H, s, Me), 3.70–3.73 (1 H, m), 3.83–3.86 (1 H, m), 3.99–4.05 (4 H, m), 4.49–4.60 (4 H, m), 4.67–4.75 (2 H, m), 4.86–4.88 (1 H, m), 5.50 (1 H, s), 6.30 (1 H, d, H1α), 7.26–7.34 (15 H, m, Ar), 8.68 (1 H, s, NH); ^{13}C-NMR (101 MHz, $CDCl_3$) δ 20.8, 67.1, 68.2, 71.9, 73.4, 73.5, 74.2, 75.3, 95.3, 108.2, 127.6, 127.8, 128.3, 137.8, 143.5, 170.0.

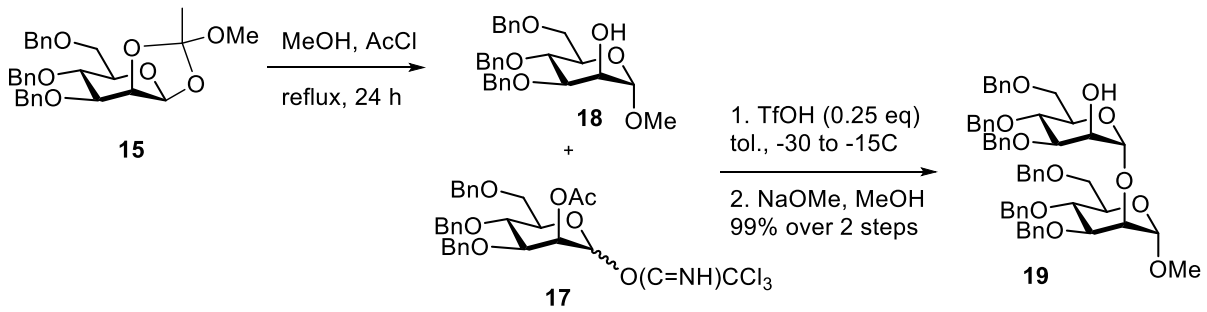

Methyl 3,4,6-tri-*O*-benzyl-α-D-mannopyranoside[32] (18)

The orthoester **15** (200 mg, 0.39 mmol) was dissolved in dry MeOH (4 mL) and heated to reflux. Acetyl chloride (0.12 mL, 0.11 mmol) was then dropwise added. The solution was stirred for one day, then was concentrated under reduced pressure. The residue was dissolved in EtOAc (15 mL), and washed with sat. $NaHCO_3$ (3 × 20 mL), then dried ($MgSO_4$), filtered and concentrated. The crude residue was purified by flash chromatography (EtOAc:toluene, 6:4), yielding **18** (180 mg, 99%) as a colourless oil. $[\alpha]_D^{20}$ +49° (*c* 1.0, $CHCl_3$; lit.[32] +50.7°); ^{1}H-NMR (400 MHz, $CDCl_3$) δ 2.41 (1 H, d, $J_{2,OH}$ = 3.5 Hz , OH), 3.35 (3 H, s, OMe), 3.69–3.76 (3 H, m, H5,6a,6b), 3.79–3.87 (2 H, m, H3,4), 4.00–4.02 (1 H, m, H2), 4.50, 4.53, 4.64, 4.66, 4.69, 4.81 (6 × 1 H, m, PhC**H**$_2$), 4.78 (1 H, d, $J_{1,2}$ = 1.5 Hz, H1), 7.15–7.34 (15 H, m, Ar); ^{13}C-NMR (101 MHz, $CDCl_3$) δ 54.8 (1 C, OMe), 68.3 (1 C, C2), 69.0 (1 C, C6), 71.0, 74.3 (2 C, C2,4), 72.0, 73.5, 75.0 (3 C, 3 × Ph**C**H$_2$), 80.2 (1 C, C3), 100.3 (1 C, C1), 127.5, 127.6, 127.81, 127.84, 127.9, 128.3, 128.5, 138.0, 138.3, 138.4 (18 C, Ph); HRMS (ESI)$^+$ *m/z* 487.2090 [$C_{28}H_{32}NaO_6$ (M + Na)$^+$ requires 487.2097].

Methyl 3,4,6-tri-*O*-benzyl-2-*O*-(3,4,6-tri-*O*-benzyl-α-D-mannopyranosyl)-α-D-mannopyranoside[33] (19)

A solution of **18** (250 mg, 0.54 mmol) and **17** (450 mg, 0.71 mmol) in dry toluene (20 mL) was stirred with freshly activated 4 Å molecular sieves for 1 h. The mixture was cooled to -30 °C and triflic acid (13 μL, 0.14 mmol) was added. The mixture was stirred for 60 min at -30 °C, then temperature was raised to -15°C. After 15 min, the reaction was quenched with Et_3N (0.1 mL), allowed to warm up to room temperature, filtered and the solvent evaporated under reduced pressure. The crude residue was purified by flash chromatography (EtOAc:hexane (1:19→3:7)), yielding a colourless oil (500 mg, 98%). The crude was dissolved in CH_2Cl_2:MeOH (20 mL), and a solution of MeONa (1 M in MeOH, 50 μL) was added. The solution was stirred for 30 min, after which TLC indicated completion of the reaction. The solution was neutralized with Amberlite 120R resin (H^+ form) and the mixture filtered. The filtrate was concentrated under reduced pressure and purified by flash chromatography (EtOAc:hexane (1:19→3:7)), giving **19** (485 mg, 99%) as a colourless oil. $[\alpha]_D^{22}$ +24° (*c* 1.0, $CHCl_3$; lit.[33] +24.3°); ^{1}H-NMR (400 MHz, $CDCl_3$) δ 2.44 (1 H, d, $J_{2,OH}$ = 1.7 Hz, OH), 3.25 (3 H, s, OMe), 3.71–4.00 (11 H, m), 4.02 (1 H, m), 4.11 (1 H, m), 4.52–4.60 (5 H, m), 4.64–4.71 (4 H, m), 4.75 (1 H, m), 4.79–4.94 (3 H, m), 5.16 (s, 1 H, H1′), 7.4 (30 H, m, Ar); ^{13}C-NMR (101 MHz, $CDCl_3$) δ 54.8, 68.6, 69.3, 69.4, 71.7, 71.8, 72.2, 72.3, 73.4, 73.5, 74.5, 74.8, 74.9,

75.1, 75.2, 79.9, 80.1, 99.9, 101.2, 127.50, 127.56, 127.6, 127.7, 127.7, 127.8, 127.8, 127.8, 127.9, 127.9, 127.9, 127.9, 127.9, 127.9, 128.0, 128.0, 128.0, 128.0, 128.0, 128.4, 128.4, 128.4, 128.4, 128.4, 128.6, 138.1, 138.3, 138.4, 138.5, 138.6, 138.7; HRMS $(ESI)^+$ *m/z* 897.4210 [$C_{55}H_{61}O_{11}$ $(M + H)^+$ requires 897.4208].

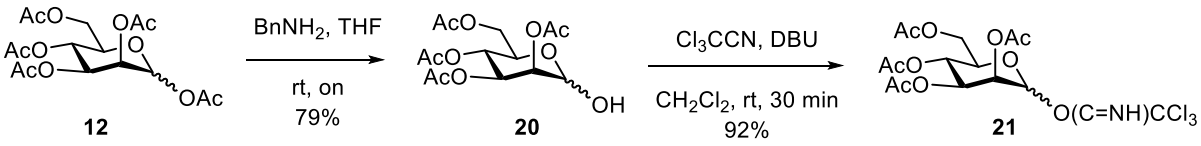

2,3,4,6-Tetra-*O*-acetyl-D-mannopyranose (20)

A solution of mannose pentaacetate **12** (1.0 g, 2.8 mmol) and benzylamine (416 μL, 3.8 mmol) in dry THF (6 mL) was stirred overnight at room temperature. The mixture was diluted with cold water and extracted with CH_2CI_2 (3 × 10 mL). The combined organic phase was then washed with 0.37 M HCI, saturated $NaHCO_3$ and brine, dried ($MgSO_4$), and concentrated. The crude was purified by flash chromatography (EtOAc:hexane, 2:3) to give **20** (0.73 g, 79%) as a mixture of anomers. ^{1}H-NMR for the α-anomer (400 MHz, $CDCl_3$) δ 2.00, 2.05, 2.11, 2.17 (4 × 3 H, s, Me), 3.16 (1 H, d, $J_{OH,1}$ = 4.0, OH), 4.13 (1 H, dd, 1 H, $J_{6,6a}$ = 8.0, $J_{5,6}$ = 5.0 Hz, H6a), 4.24 (2 H, m, $J_{5,6}$ = 5.0, $J_{5,6a}$ = 2.5 Hz, H5 and H6), 5.25 (1 H, dd, $J_{OH,1}$ = 4.0, $J_{1,2}$ = 1.8 Hz, H1), 5.28 (1 H, dd, $J_{2,3}$ = 3.2, $J_{1,2}$ = 1.8 Hz, H2), 5.31 (1 H, app. t, $J_{4,5}$ = $J_{3,4}$ = 9.5 Hz, H4), 5.43 (1 H, dd, $J_{3,4}$ = 10.0,$J_{2,3}$ = 3.2 Hz, H3); ^{13}C NMR for the α-anomer (101 MHz,$CDCl_3$) δ 20.9, 21.0, 21.0, 21.1 (4 C, Me), 62.8 (1 C, C6), 66.4, 68.7, 69.0, 70.3 (4 C, C2,3,4,5), 92.4 (1 C, C1), 170.1, 170.4, 170.5, 171.2 (4 C, C=O).

2,3,4,6-Tetra-*O*-acetyl-D-mannopyranosyl trichloroacetimidate (21)

The hemiacetal **20** (1.00 g, 2.80 mmol) was dissolved in dry CH_2Cl_2 (50 mL), then $CNCCl_3$ (1.43 mL, 14.35 mmol) was added and the solution cooled to 0 °C. After 5 min, a catalytic amount of DBU (20 μL, 0.14 mmol) was added and the reaction warmed to room temperature. After 30 min, TLC analysis shown complete conversion of the starting material. The reaction was concentrated and the residue purified by flash chromatography (EtOAc:hexane:Et_3N, (6:4:0.1)) to yield **21** (1.3 g, 92%) as a mixture of anomers, colourless oil. ^{1}H-NMR for the α-anomer (400 MHz, $CDCl_3$) δ 2.01, 2.07, 2.08, 2.20 (4 × 3 H, s, Me), 4.20 (3 H, m, H5,6,6a), 5.40 (2 H, m, H3,4), 5.43 (1 H, m, H2), 6.28 (1 H, d, $J_{1,2}$ = 1.8 Hz, H1), 8.79 (1 H, s, NH); ^{13}C NMR for the α-anomer (101 MHz,$CDCl_3$) δ 20.8, 20.9, 20.9, 21.0 (4 × 1C, Me), 62.3 (1 C,

C6), 65.6, 68.1, 69.0, 71.5 (4 × 1C, C2,3,4,5), 94.8 (1 C, C1), 160.0 (s, CNH), 169.9, 170.0, 170.1, 170.8 (4 × 1C, C=O).

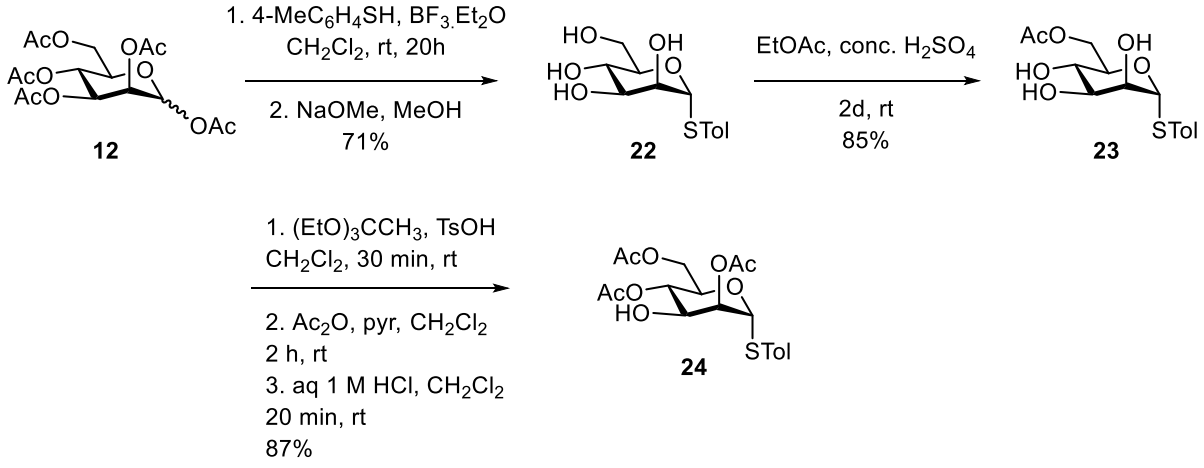

4-Methylphenyl 1-thio-α-D-mannopyranoside[34] (22).

Mannose pentaacetate **12** (1.0 g, 2.6 mmol) and thiocresol (0.35 g, 2.8 mmol) were dissolved in dry CH_2Cl_2 (20 mL) and the solution cooled to 0 °C. $BF_3 \cdot OEt_2$ (0.32 ml, 2.6 mmol) was then added dropwise. The solution was allowed to warm to rt and was left to stir under N_2 atmosphere for 20 h. Sat. $NaHCO_3$ was added and the mixture was diluted with CH_2Cl_2 and washed with sat. $NaHCO_3$ (4 × 15 ml) and brine (15 ml). The organic phase was dried over anhydrous $MgSO_4$, filtered and evaporated to afford the crude tetraacetate (1.58 g), which was used directly in the next step. The residue was dissolved in MeOH (45 mL), then a solution of NaOMe (1 M in MeOH, 1 mL) was added. The reaction was stirred for 1 h at rt, when TLC analysis indicated complete consumption of the starting material. Amberlite IR-120 resin (H^+ form) was added to neutralise the solution and, following filtration, the solvent was evaporated to give a pale yellow solid. The residue was recrystallised from EtOAc:MeOH to afford the tetraol **22** (0.518 g, 71% over two steps) as white crystals, m.p. 138-139 °C. $[\alpha]_D^{22}$ +270° (*c* 0.1, MeOH, lit.[34] +279°); ^{1}H-NMR (500 MHz, d_6-DMSO) δ 2.25 (3 H, s, CH3), 3.44–3.52 (3 H, m, H3, H4 and H5), 3.64 (1 H, ddd, $J_{6,6a}$ = 11.5, $J_{5,6}$ = 4.0 Hz, H6), 3.77 (1 H, ddd, $J_{6,6a}$ = 11.5, $J_{5,6a}$ = 2.0 Hz, H6a), 3.86 (1 H, broad s, H2), 4.47 (1 H, dd, $J_{6,OH}$ = 6.0, $J_{6a,OH}$ 6.0 Hz, 6-OH), 4.75 (1 H, d, *J* = 5.5 Hz, OH), 4.85 (1 H, d, *J* = 5.5 Hz, OH), 5.07 (1 H, d, *J* = 4.0 Hz, OH), 5.24 (1 H, d, $J_{1,2}$ = 1.0 Hz, H1), 7.15 (2 H, app. d, Ar), 7.38 (2 H, app. d, Ar); ^{13}C-NMR (125 MHz, d_6-DMSO) δ 21.1 (1 C, Me), 61.4, 67.5, 72.0, 72.4, 75.7 (5C, C2,3,4,5,6), 89.7 (1 C, C1), 130.1, 131.5, 132.6, 137.3 (6C, Ar); HRMS $(ESI)^+$ *m/z* 287.0949 [$C_{13}H_{19}O_5S$ $(M + H)^+$ requires 287.0948]

4-Methylphenyl 6-*O*-acetyl-1-thio-α-D-mannopyranoside (23)

The tetraol **22** (100 mg, 0.34 mmol) was suspended in EtOAc (10 mL), then conc. H_2SO_4 (2 drops) were added and the mixture stirred for two days. The reaction was then poured into sat. $NaHCO_3$ (20 mL), and the aqueous phase extracted with EtOAc (3 × 10 mL). The combined organic phase was dried over $MgSO_4$, filtered and the solvent evaporated. The residue was purified by flash chromatography (EtOAc:MeOH:H_2O, 17:2:1), giving **23** as a colourless oil that crystallized upon standing, m.p. 139-140°C. $[\alpha]_D^{24}$ +221° (*c* 0.8, MeOH); ^{1}H-NMR (500 MHz, *d*$_6$-DMSO) δ 1.95 (3 H, s, Me), 2.27 (3 H, s, PhMe), 3.47 (2 H, m, H3 and H4), 3.86 (1 H, broad s, H2), 4.02 (1 H, m, H5), 4.05 (1 H, dd, $J_{6,6a}$ = 11.0, $J_{5,6}$ = 7.5 Hz, H6), 4.27 (1 H, dd, $J_{6,6a}$ = 11.0, $J_{5,6a}$ = 1.0 Hz, H6a), 4.89 (1 H, d, J_{OH} = 4.0 Hz, OH), 5.13 (1 H, d, J_{OH} = 5.0 Hz, OH), 5.19 (1 H, broad s, OH), 5.23 (1 H, d, $J_{1,2}$ = 1.5 Hz, H1), 7.15 (2 H, app. d, Ar), 7.35 (2 H, app. d, Ar); ^{13}C-NMR (125 MHz, *d*$_6$-DMSO) δ 20.6 (1 C, Me), 21.3 (1 C, PhMe), 63.6, 67.1, 71.3, 71.6, 71.8 (5 × 1C, C2,3,4,5,6), 88.7 (1 C, C1), 129.7, 130.3, 132.0, 137.1 (6C, Ar), 170.2 (1 C, C=O); HRMS (ESI)$^+$ *m/z* 351.0872 [$C_{15}H_{20}O_6SNa$ $(M+Na)^+$ requires 351.0873].

4-Methylphenyl 2,4,6-tri-*O*-acetyl-1-thio-α-D-mannopyranoside (23)

The triol **23** (186 mg, 0.56 mmol) was dissolved in dry CH_2Cl_2 (4.5 mL). Triethyl orthoacetate (0.37 mL, 2.24 mmol) and *p*-toluenesulfonic acid monohydrate (14 mg, 0.074 mmol) were added. The reaction was left to stir for 30 min, when TLC analysis indicated complete consumption of the starting material. The reaction was stopped by the addition of TEA (100 μL), diluted with $CHCl_3$ (10 mL) and washed with water (2 × 20 mL) and brine (20 mL). The organic phase was dried ($MgSO_4$), filtered and rotary evaporated. The residue was redissolved in dry CH_2Cl_2 (10.0 mL) and dry pyridine (3 mL). Acetic anhydride (1 mL) was then added, and the reaction stirred for 2 h. The reaction was then diluted with CH_2Cl_2 (10.0 mL) and washed with water (2 × 20 mL) and brine (20 mL). The organic phase was dried over $MgSO_4$, filtered and concentrated. The remaining pyridine was removed by azeotropic distillation with toluene (2 × 30 mL), and the residue dissolved in CH_2Cl_2 (8.75 mL). A 1M solution of HCl was added (3.75 mL) and the biphasic solution vigorously stirred for 20 min. The acqueous phase was separated and the organic layer diluted with CH_2Cl_2 (15 mL) and washed with water (2 × 20 mL), sat. $NaHCO_3$ (20 mL) and brine (20 mL). The crude was purified by flash chromatography (EtOAc:hexane, (1:9→6:4)), yielding **24** (203 mg, 87% over three steps) as a thick oil that crystallized upon standing. $[\alpha]_D^{22}$ +115° (*c* 0.1, $CHCl_3$); ^{1}H-NMR (400 MHz, $CDCl_3$) δ 2.06 (3 H, s, Me), 2.16 (2 × 3 H, s, Me), 2.24 (1 H, d, $J_{3,OH}$ = 8.4 Hz, OH), 2.33 (3 H,

s, PhMe), 4.07 (1 H, ddd, $J_{3,4}$ = 9.9, $J_{3,OH}$ = 8.4, $J_{2,3}$ = 3.4 Hz, H3), 4.13 (1 H, dd, $J_{6,6a}$ = 12.0, $J_{5,6a}$ = 2.0, H6a), 4.31 (1 H, dd, $J_{6,6a}$ =12.2, $J_{5,6}$ = 5.9 Hz, H6), 4.51 (1 H, ddd, $J_{3,4}$ = 9.9, $J_{5,6}$ = 5.8, $J_{5,6a}$ = 2.2 Hz, H5), 5.11 (1 H, t, $J_{3,4}$ = $J_{4,5}$ = 9.9 Hz, H4), 5.32 (1 H, dd, $J_{2,3}$ = 3.5, $J_{1,2}$ = 1.4 Hz, H2), 5.49 (1 H, d, $J_{1,2}$ = 1.4 Hz, H1), 7.12 (2 H, app. d, J = 8.3 Hz, Ar), 7.37 (2 H, d, J = 8.2 Hz, Ar); ^{13}C-NMR (101 MHz, $CDCl_3$) δ 20.5, 20.6, 20.7 (3 × 1C, Me), 21.3 (1 C, PhMe), 62.4, 68.8, 69.0, 69.4, 73.5 (5 × 1C, C2,3,4,5,6), 85.5 (1 C, C1), 127.8, 129.0, 132.6, 137.8 (6C, PhMe), 170.3, 170.5, 170.6 (3 × 1C, C=O); HRMS (ESI)$^+$ *m/z* 413.1265 [$C_{19}H_{25}O_8S$ $(M+H)^+$ requires 413.1265].

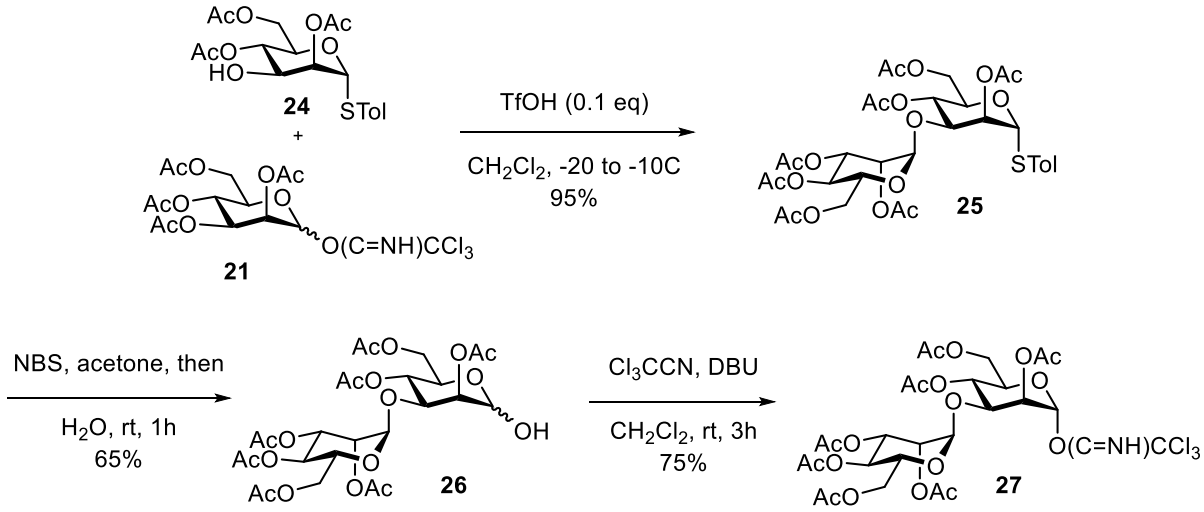

4-Methylphenyl 3-*O*-(2,3,4,6-tetra-*O*-acetyl-α-D-mannopyranoside)-2,4,6-tri-*O*-acetyl-1-thio-α-D-mannopyranoside (25)

A solution of alcohol **24** (50 mg, 0.12 mmol) and trichloroacetimidate **21** (60 mg, 0.12 mmol) in dry CH_2Cl_2 (1.5 mL) was stirred with freshly activated 3 Å molecular sieves for 45 min. The mixture was cooled to -20 °C and triflic acid (1 μL, 0.01 mmol) was added. The mixture was stirred for 15 min at -20 °C, then temperature was raised to -10°C. After 5 min, the reaction was quenched with Et_3N (0.1 mL), allowed to warm to room temperature, filtered and the solvent evaporated under reduced pressure. The crude residue was purified by flash chromatography (EtOAc:hexane (1:19→3:7)), yielding **25** (90 mg, 95%) as a colourless oil. $[\alpha]_D^{23}$ +76° (*c* 0.4, $CHCl_3$); ^{1}H-NMR (500 MHz, $CDCl_3$) δ 2.00, 2.06, 2.06, 2.15, 2.15, 2.18, 2.20 (7 × 3 H, s, Me), 2.33 (3 H, s, PhMe), 4.12–4.06 (3 H, m, H6a, H5' and H6a'), 4.16 (1 H, dd, $J_{3,4}$ = 9.8, $J_{2,3}$ = 3.4 Hz, H3), 4.23 (1 H, dd, $J_{6',6a'}$ = 12.5, $J_{5',6'}$ = 6.3 Hz, H6'), 4.27 (1 H, dd, $J_{6,6a}$ = 12.5, $J_{5,6}$ = 6.3 Hz, H6), 4.46 (ddd, $J_{3,4}$ = 9.7, $J_{5,6}$ = 6.3, $J_{5,6a}$ = 2.4 Hz, H5), 5.03 (1 H, s,

H1' and H2'), 5.22 (1 H, dd, $J_{3',4'}$ = 10.3, $J_{2',3'}$ = 2.9 Hz, H3'), 5.25 (1 H, app. t, $J_{3',4'} = J_{4',5'}$ = 10.3 Hz, H4'), 5.34 (1 H, dd, $J_{3,4} = J_{4,5}$ = 9.8 Hz, H4), 5.44 (1 H, d, $J_{1,2}$ = 1.2 Hz, H1), 5.49 (1 H, dd, $J_{2,3}$ = 3.4, $J_{1,2}$ = 1.5 Hz, H2), 7.12 (2 H, app. d, J = 7.9, Ar),7.34 (2 H, app. d, J = 7.9, Ar); ^{13}C-NMR (125 MHz, $CDCl_3$) δ 20.77, 20.78, 20.8, 20.9, 20.97, 20.99, 21.05 (7 × 1C, Me), 21.3 (1 C, PhMe), 62.7, 62.8 (2 C, C6 and C6'), 66.1 (1 C, C4'), 68.2 (1 C, C4), 68.3 (1 C, C3'), 69.67 (1 C, C5'), 69.71 (1 C, C5), 70.1 (1 C, C2'), 72.4 (1 C, C2), 75.1 (1 C, C3), 86.2 (1 C, C1), 99.0 (1 C, C1'), 128.8, 130.1, 132.7, 138.7 (6C, Ar), 169.7, 169.97, 170.00, 170.2, 170.4, 170.7, 170.9 (7 × 1C, C=O); HRMS (ESI)$^+$ *m/z* 743.2220 [$C_{33}H_{43}O_{17}S$ $(M+H)^+$ requires 743.2215].

2,3,4,6-Tetra-*O*-acetyl-α-D-mannopyranosyl-(1,3)-2,4,6-tri-*O*-acetyl-α,β-D-mannopyranose (26)

Thioglycoside **25** (60 mg, 0.08 mmol) was dissolved in acetone (3 mL), and the solution cooled to -10°C. Crystalline NBS (34 mg, 0.19 mmol) was added and the reaction stirred for 30 min. Water (50 μL) was added and the reaction stirred for an additional 30 min. TLC analysis shown completion of the reaction, and the mixture quenched with solid NH_4Cl (20 mg, 0.37 mmol) and stirred for 10 min. The reaction was diluted with EtOAc (15 mL) and the acetone removed under reduced pressure. The solution was washed with brine (2 × 20 mL), and the combined aqueous layers extracted with EtOAc (2 × 20 mL). The combined organic phase was dried over anhydrous $MgSO_4$, filtered and concentrated. Flash chromatography (EtOAc:hexane, (2:3→1:1)) afforded the hemiacetal **26** (0.305 g, 65%) as a colourless oil. ^{1}H-NMR for the α-anomer (400 MHz, $CDCl_3$) δ 1.99–2.21 (7 × 3 H, s, Ac), 3.25 (1 H, d, $J_{1,OH}$ = 4.0 Hz, OH), 4.05–4.29 (7 H, m, H3',5,6a,6,5',6',6a'), 5.00 (1 H, d, $J_{1',2'}$ = 1.5 Hz, H1'), 5.02 (1 H, d, $J_{2',3'}$ = 3.0, $J_{1',2'}$ = 2.0 Hz, H2'), 5.22 (1 H, t, $J_{2,3}$ = 3.0 Hz, H3), 5.25 (1 H, dd, $J_{1,OH}$ = 3.0, $J_{1,2}$ = 2.0 Hz, H1), 5.27 (1 H, dd, $J_{2,3}$ = 3.0, $J_{1,2}$ = 2.0 Hz, H2), 5.29, 5.32 (2 H, m, H4 and H4'); ^{13}C-NMR for the α-anomer (125 MHz, $CDCl_3$) δ 20.6–21.0 (7 C, Me), 62.5, 62.7 (2 C, C6,6'), 66.0, 67.9, 68.3, 68.5, 69.3, 70.0, 71.5, 74.2 (8 C, C2,3,4,5,C2',3',4',5'), 92.1 (1 C, C1), 98.8 (1 C, C1'), 169.7, 169.97, 170.01, 170.1, 170.6, 170.9, 171.0 (7 C, C=O); HRMS (ESI)$^+$ *m/z* 659.1793 [$C_{26}H_{36}O_{18}Na$ $(M+Na)^+$ requires 659.1794].

2,3,4,6-Tetra-*O*-acetyl-α-D-mannopyranosyl-(1,3)-2,4,6-tri-*O*-acetyl-α-D-mannopyranosyl trichloroacetimidate (27)

DBU (0.600 µL, 3.94 µmol) was added to a mixture of the hemiacetal **26** (0.126 g, 0.197 mmol) and trichloroacetonitrile (90.0 µL, 0.887 mmol) in dichloromethane (2 mL) at 0 ºC under N_2. The mixture was warmed to r.t. and stirred for 3 h and then concentrated under reduced pressure to give a light yellow residue, which was purified by flash chromatography (EtOAc:hexane:Et_3N, (2:3:0.1→1:1:0.1)) to afford the trichloroacetimidate **27** (0.115 g, 75%) as a colourless oil. ^{1}H-NMR (400 MHz, $CDCl_3$) δ 1.97–2.22 (7 × 3 H, s, Ac), 3.99–4.25 (7 H, m, H6,6a,3',5',6',6a'), 5.00 (2 H, m, H1',2'), 5.18 (1 H, dd, $J_{3',4'}$ = 10, $J_{2',3'}$ = 3.5 Hz, H3'), 5.26 (1 H, app. t, $J_{3',4'} = J_{4',5'}$ = 10 Hz, H4'), 5.37 (1 H, t, $J_{3,4} = J_{4,5}$ = 10 Hz, H4), 5.38 (1 H, m, H2), 6.27 (1 H, d, $J_{1,2}$ = 1.0 Hz, H1), 8.80 (1 H, s, NH); ^{13}C-NMR (125 MHz, $CDCl_3$) δ 20.7–20.9 (7 C, Me), 62.18, 62.23 (2 C, C6,C6'), 65.7, 67.0, 68.2, 69.4, 69.6, 69.9, 71.4, 74.7 (8 C, C2,3,4,5,2',3',4',5'), 90.6 (1 C, CCl_3), 94.4 (1 C, C1'), 99.2 (1 C, C1), 159.6 (1 C, C=NH), 169.7, 169.8, 170.1, 171.1, 170.62, 170.65 (7 C, C=O).

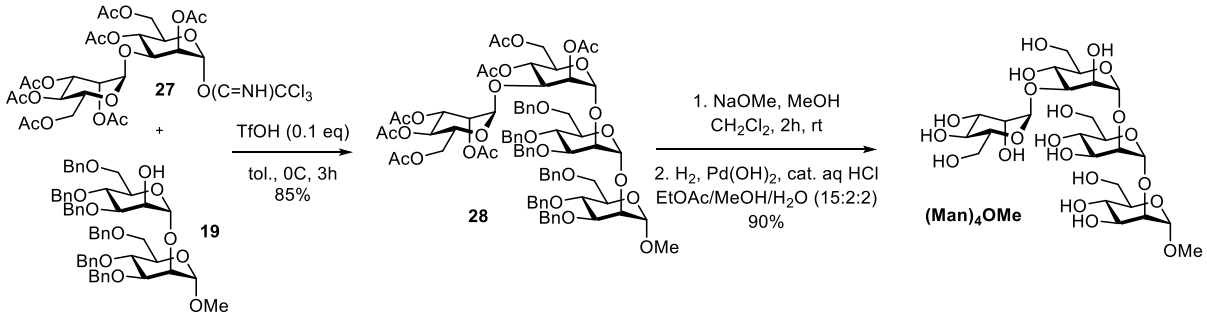

Methyl 2,3,4,6-tetra-*O*-acetyl-α-D-mannopyranosyl-(1,3)-2,4,6-tri-*O*-acetyl-α-D-mannopyranosyl-(1,2)-3,4,6-tri-*O*-benzyl-α-D-mannopyranosyl-(1,2)-3,4,6-tri-*O*-benzyl-α-D-mannopyranoside (28)

A solution of TfOH in toluene (1% v/v, 65 µL, 0.0074 mmol) was added to a mixture of the trichloroacetimidate **27** (58.0 mg, 0.074 mmol), alcohol **19** (51.0 mg, 0.057 mmol) and freshly activated 4 Å molecular sieves in dry toluene (5 mL) at 0 ˚C under N_2. The mixture was stirred for 3 h, then was quenched with Et_3N (0.1 mL), filtered through Celite, washed with dichloromethane and concentrated. The residue was purified by flash chromatography (EtOAc:hexane, (1:9→1:4)) to afford the fully protected tetrasaccharide **28** (68.8 mg, 85%) as a colourless oil. $[\alpha]_D^{22}$ +24° (*c* 0.1, $CHCl_3$); ^{1}H-NMR (400 MHz, $CDCl_3$) δ 1.99, 2.00, 2.03, 2.05, 2.06, 2.13, 2.21 (7 × 3 H, s, Ac), 3.22 (3 H, s, OMe), 3.68–4.06 (17 H, m), 4.18 (1 H, dd,

J = 3.6, 10 Hz), 4.27 (1 H, dd, J = 12.5, 4.0 Hz), 4.48–4.69 (10 H, m), 4.78 (1 H, d, $J_{1,2}$ = 1.2 Hz, H1), 4.80–4.84 (2 H, m), 4.91 (1 H, d, $J_{1,2}$ = 1.2 Hz, H1), 4.99 (1 H, d, $J_{1,2}$ = 1.6 Hz, H1), 5.05 (1 H, dd, $J_{2,3}$ = 3.2, $J_{1,2}$ = 1.6 Hz, H2), 5.22 (1 H, d, $J_{1,2}$ = 2.0 Hz, H1), 5.20-5.34 (4 H, m), 7.20–7.36 (30 H, m, Ar); ^{13}C-NMR (125 MHz, $CDCl_3$) δ 20.8–21.2 (7 C, Me), 54.8 (1 C, OMe), 68.6–77.4 (26 C, C2,3,4,5,6,2',3',4',5',6',2'',3'',4'',5'',6'',2''',3''',4''',5''',6''',Ph**C**H_2), 99.1 (1 C, C1''), 99.2, 99.8, 100.5 (3 × 1C, C1,1',1'''), 127.6–138.6 (30 C, Ar), 169.8–170.8 (7 C, C=O); HRMS (ESI)$^+$ *m/z* 1537.5830 [$C_{81}H_{94}O_{28}Na$ $(M+Na)^+$ requires 1537.5824].

Methyl α-D-mannopyranosyl-(1,3)-α-D-mannopyranosyl-(1,2)-α-D-mannopyranosyl-(1,2)-α-D-mannopyranoside ((Man)$_4$OMe)

Sodium methoxide in methanol (1 M, 12.0 µL, 0.011 mmol) was added to a solution of the tetrasaccharide **28** (43.0 mg, 0.028 mmol) in MeOH/CH_2Cl_2 (3:1, 4 mL) and the mixture was stirred for 2 h. After neutralization with Dowex-50 resin (H^+ form), the mixture was filtered and concentrated. The crude residue was dissolved in a mixture of EtOAc/MeOH/H_2O (15:2:2, 17 mL) and aq 0.5 M HCl (0.1 mL), 20% $Pd(OH)_2$/C (20 mg) was added, and the mixture was stirred under an atmosphere of hydrogen for 18 h. The reaction mixture was filtered through a layer of Celite, and washed thoroughly with MeOH:H_2O (2:1), and concentrated under reduced pressure. The residue was purified by flash chromatography (EtOAc:MeOH:H_2O (4:2:1)), and then by C_{18} reversed phase chromatography (CH_3CN:H_2O, 95:5), to afford the tetrasaccharide **(Man)$_4$OMe** (17.7 mg, 90%) as a colourless oil. ^{1}H-NMR (500 MHz, D_2O) δ 3.42 (3 H, s, OMe), 3.42–3.95 (20 H, m, H3,4,5,6a,6b,3',4',5',6a',6b', 3'',4'',5'',6a'',6b'', 3''',4''',5''',6a''',6b'''), 3.97 (1 H, dd, $J_{2,3}$ = 5.5, $J_{1,2}$ = 3.0 Hz, H2'), 4.08 (1 H, dd, $J_{2,3}$ = 5.5, $J_{1,2}$ = 3.0 Hz, H2'''), 4.12 (1 H, dd, $J_{2,3}$ = 5.5, $J_{1,2}$ = 3.0 Hz, H2''), 4.24 (1 H, dd, $J_{2,3}$ = 5.5, $J_{1,2}$ = 3.0 Hz, H2), 5.00 (1 H, d, $J_{1,2}$ = 1.5 Hz, H1''), 5.05 (1 H, d, $J_{1,2}$ = 1.5 Hz, H1), 5.16 (1 H, d, $J_{1,2}$ = 1.5 Hz, H1'''), 5.00 (1 H, d, $J_{1,2}$ = 1.5 Hz, H1''); ^{13}C-NMR (125 MHz, D_2O) δ 54.8 (1 C, OMe), 60.8, 60.9, 61.0, 61.1, 66.2, 66.8, 67.0, 69.50, 69.54, 69.9, 70.0, 70.2, 72.5, 73.2, 77.8, 78.4, 78.6, 78.7 (20 C, C2,3,4,5,6,2',3',4',5',6',2'',3'',4'',5'',6'',2''',3''',4''',5''',6'''), 99.2 (1 C, C1''), 100.6 (1 C, C1'), 102.1 (1 C, C1'''), 102.2 (1 C, C1); HRMS (ESI)$^+$ *m/z* 703.2264 [$C_{25}H_{44}O_{21}Na$ $(M + Na)^+$ requires 703.2267].

Labelled tetramannosides $(Man)_4OMe$ were synthesized accordingly to the above described procedure starting from individually isotope-labelled 1-^{13}C-, 1-^{13}C,1-^{2}H-, 2-^{13}C-, 2-^{13}C,2-^{18}O- and 1,2-$^{13}C_2$-D-mannoses (Omicron Biochemicals, USA).

$(Man)_4OMe$ isotopologue	**Label (%)**	**Characteristic NMR shifts (500 MHz, D_2O)**
[1-^{13}C]	1-^{13}C: 99	^{1}H NMR: 4.92 (1 H, dd, $J_{C,H}$ = 143.2, $J_{1,2}$ = 1.5 Hz, H1). ^{13}C NMR: 102.05 (1 C, C1).
[1-^{13}C, 1-^{2}H]	1-^{13}C: 99 1-^{2}H: 99	^{1}H NMR: H1 is ^{2}H, no signal. ^{13}C NMR: 102.0 (1 C, C1)
[2-^{13}C]	2-^{13}C: 99	^{1}H NMR: 4.08 (1 H, m, $J_{C,H}$ = 151.1 Hz, H2) ^{13}C NMR: 69.49 (1 C, C2).
[2-^{13}C, 2-^{18}O]	2-^{13}C: 99 2-^{18}O: 90	^{1}H NMR: 4.08 (1 H, m, $J_{C,H}$ = 151.1 Hz, H2) ^{13}C NMR: 69.50 (1 C, C2).
[1,2-$^{13}C_2$]	1-^{13}C: 99 2-^{13}C: 99	^{1}H NMR: 4.08 (1 H, m, $J_{C,H}$ = 151.1 Hz, H2), 4.92 (1 H, dd, $J_{C,H}$ = 143.2, $J_{1,2}$ = 1.5 Hz, H1). ^{13}C NMR: 69.49 (1 C, d, $J_{1,2}$ = 46.9 Hz, C2), 102.05 (1 C, d, $J_{1,2}$ = 46.9 Hz, C1).

References

(1) Winter, G., xia2: an expert system for macromolecular crystallography data reduction, *J. Appl. Crystallogr.* **2010,** *43*, 186-190.

(2) Evans, P. R.; Murshudov, G. N., How good are my data and what is the resolution?, *Acta Crystallogr. Sect. D* **2013,** *69*, 1204-1214.

(3) Murshudov, G. N.; Skubak, P.; Lebedev, A. A.; Pannu, N. S.; Steiner, R. A.; Nicholls, R. A.; Winn, M. D.; Long, F.; Vagin, A. A., REFMAC5 for the refinement of macromolecular crystal structures, *Acta Crystallogr. D* **2011,** *67*, 355-367.

(4) Emsley, P.; Lohkamp, B.; Scott, W. G.; Cowtan, K., Features and development of Coot, *Acta Crystallogr. Sect. D* **2010,** *66*, 486-501.

(5) Cremer, D.; Pople, J. A., General definition of ring puckering coordinates, *J. Am. Chem. Soc.* **1975,** *97*, 1354-1358.

(6) Agirre, J.; Iglesias-Fernandez, J.; Rovira, C.; Davies, G. J.; Wilson, K. S.; Cowtan, K. D., Privateer: software for the conformational validation of carbohydrate structures, *Nat. Struct. Mol. Biol.* **2015,** *22*, 833-4.

(7) McNicholas, S.; Potterton, E.; Wilson, K. S.; Noble, M. E. M., Presenting your structures: the CCP4mg molecular-graphics software, *Acta Crystallogr. D* **2011,** *67*, 386-394.

(8) Ciucanu, I.; Kerek, F., A simple and rapid method for the permethylation of carbohydrates, *Carbohydr. Res.* **1984,** *131*, 209-217.

(9) Petricevic, M.; Sobala, L. F.; Fernandes, P.; Raich, L.; Thompson, A. J.; Bernardo-Seisdedos, G.; Millet, O.; Zhu, S.; Sollogoub, M.; Jimenez-Barbero, J.; Rovira, C.; Davies, G. J.; Williams, S. J., Contribution of shape and charge to the inhibition of a family GH99 *endo*-α-1,2-mannanase, *J. Am. Chem. Soc.* **2017,** *139*, 1089–1097.

(10) Case, D. A.; Darden, T. A.; Cheatham, T. E.; Simmerling, J. W. C.; Duke, R.; Luo, R.; Crowley, M. F.; Walker, R.; Zhang, W.; Merz, K. M.; Wang, B.; Hayik, S.; Roitberg, A. E.; Seabra, G.; Kolossváry, I.; Wong, K. F.; Paesani, F.; Vanicek, J.; Wu, X.; Brozell, S.; Steinbrecher, T.; Gohlke, H.; Yang, L.; Tan, C.; Mongan, J.; Hornak, V.; Cui, G.; Mathews, D. H.; Seetin, M. G.; Sagui, C.; Babin, V.; Kollman, P. *AMBER 11*, University of California, San Francisco: 2010.

(11) Hornak, V.; Abel, R.; Okur, A.; Strockbine, B.; Roitberg, A.; Simmerling, C., Comparison of multiple Amber force fields and development of improved protein backbone parameters, *Proteins: Struct., Funct., Bioinf.* **2006,** *65*, 712-725.

(12) Kirschner, K. N.; Yongye, A. B.; Tschampel, S. M.; González-Outeiriño, J.; Daniels, C. R.; Foley, B. L.; Woods, R. J., GLYCAM06: A generalizable biomolecular force field. Carbohydrates, *J. Comput. Chem.* **2008,** *29*, 622-655.

(13) Jorgensen, W. L.; Chandrasekhar, J.; Madura, J. D.; Impey, R. W.; Klein, M. L., Comparison of simple potential functions for simulating liquid water, *J. Chem. Phys.* **1983,** *79*, 926-935.

(14) Humphrey, W.; Dalke, A.; Schulten, K., VMD: Visual molecular dynamics, *J. Mol. Graph.* **1996,** *14*, 33-38.

(15) Laio, A.; VandeVondele, J.; Rothlisberger, U., A Hamiltonian electrostatic coupling scheme for hybrid Car–Parrinello molecular dynamics simulations, *J. Chem. Phys.* **2002,** *116*, 6941-6947.

(16) Car, R.; Parrinello, M., Unified Approach for Molecular Dynamics and Density-Functional Theory, *Phys. Rev. Lett.* **1985,** *55*, 2471-2474.

(17) Troullier, N.; Martins, J. L., Efficient pseudopotentials for plane-wave calculations, *Phys. Rev. B* **1991,** *43*, 1993-2006.

(18) Perdew, J. P.; Burke, K.; Ernzerhof, M., Generalized Gradient Approximation Made Simple, *Phys. Rev. Lett.* **1996,** *77*, 3865-3868.

(19) Ireta, J.; Neugebauer, J.; Scheffler, M., On the Accuracy of DFT for Describing Hydrogen Bonds: Dependence on the Bond Directionality, *J. Phys. Chem. A* **2004,** *108*, 5692-5698.

(20) Marianski, M.; Supady, A.; Ingram, T.; Schneider, M.; Baldauf, C., Assessing the Accuracy of Across-the-Scale Methods for Predicting Carbohydrate Conformational Energies for the Examples of Glucose and α-Maltose, *J. Chem. Theory Comput.* **2016,** *12*, 6157-6168.

(21) Ardèvol, A.; Rovira, C., Reaction Mechanisms in Carbohydrate-Active Enzymes: Glycoside Hydrolases and Glycosyltransferases. Insights from ab Initio Quantum Mechanics/Molecular Mechanics Dynamic Simulations, *J. Am. Chem. Soc.* **2015,** *137*, 7528-7547.

(22) Laio, A.; Parrinello, M., Escaping free-energy minima, *Proc. Natl. Acad. Sci. USA* **2002,** *99*, 12562-12566.

(23) Tribello, G. A.; Bonomi, M.; Branduardi, D.; Camilloni, C.; Bussi, G., PLUMED 2: New feathers for an old bird, *Comput. Phys. Commun.* **2014,** *185*, 604-613.

(24) Chan, J.; Lewis, A. R.; Gilbert, M.; Karwaski, M. F.; Bennet, A. J., A direct NMR method for the measurement of competitive kinetic isotope effects, *Nat. Chem. Biol.* **2010,** *6*, 405-7.

(25) Claridge, T. D. W., *High-resolution NMR techniques in organic chemistry*. Elsevier: 2009.

(26) Pauli, G. F.; Jaki, B. U.; Lankin, D. C., Quantitative ^{1}H NMR: Development and Potential of a Method for Natural Products Analysis, *J. Nat. Prod.* **2005,** *68*, 133-149.

(27) Melander, L. C. S.; Saunders, W. H., *Reaction rates of isotopic molecules*. Wiley: 1980.

(28) Pangborn, A. B.; Giardello, M. A.; Grubbs, R. H.; Rosen, R. K.; Timmers, F. J., Safe and Convenient Procedure for Solvent Purification, *Organometallics* **1996,** *15*, 1518-1520.

(29) Still, W. C.; Kahn, M.; Mitra, A. M., Rapid Chromatographic Technique for Preparative Separations with Moderate Resolution, *J. Org. Chem.* **1978,** *43*, 2923-2925.

(30) Lu, D.; Zhu, S.; Sobala, L. F.; Bernardo-Seisdedos, G.; Millet, O.; Zhang, Y.; Jiménez-Barbero, J.; Davies, G. J.; Sollogoub, M., From 1,4-Disaccharide to 1,3-Glycosyl Carbasugar: Synthesis of a Bespoke Inhibitor of Family GH99 Endo-α-mannosidase, *Org. Lett.* **2018,** *20*, 7488-7492.

(31) Floyd, N.; Vijayakrishnan, B.; Koeppe, J. R.; Davis, B. G., Thiyl Glycosylation of Olefinic Proteins: S-Linked Glycoconjugate Synthesis, *Angew. Chem. Int. Ed.* **2009,** *48*, 7798-7802.

(32) Beignet, J.; Tiernan, J.; Woo, C. H.; Kariuki, B. M.; Cox, L. R., Stereoselective Synthesis of Allyl-C-mannosyl Compounds: Use of a Temporary Silicon Connection in Intramolecular Allylation Strategies with Allylsilanes, *J. Org. Chem.* **2004,** *69*, 6341-6356.

(33) Ito, Y.; Hagihara, S.; Arai, M. A.; Matsuo, I.; Takatani, M., Synthesis of fluorine substituted oligosaccharide analogues of monoglucosylated glycan chain, a proposed ligand of lectin-chaperone calreticulin and calnexin, *Glycoconj. J.* **2004,** *21*, 257-66.

(34) Watt, J. A.; Williams, S. J., Rapid, iterative assembly of octyl α-1,6-oligomannosides and their 6-deoxy equivalents, *Org. Biomol. Chem.* **2005,** *3*, 1982-1992.

^{1}H NMR (600 MHz) spectrum of **5**

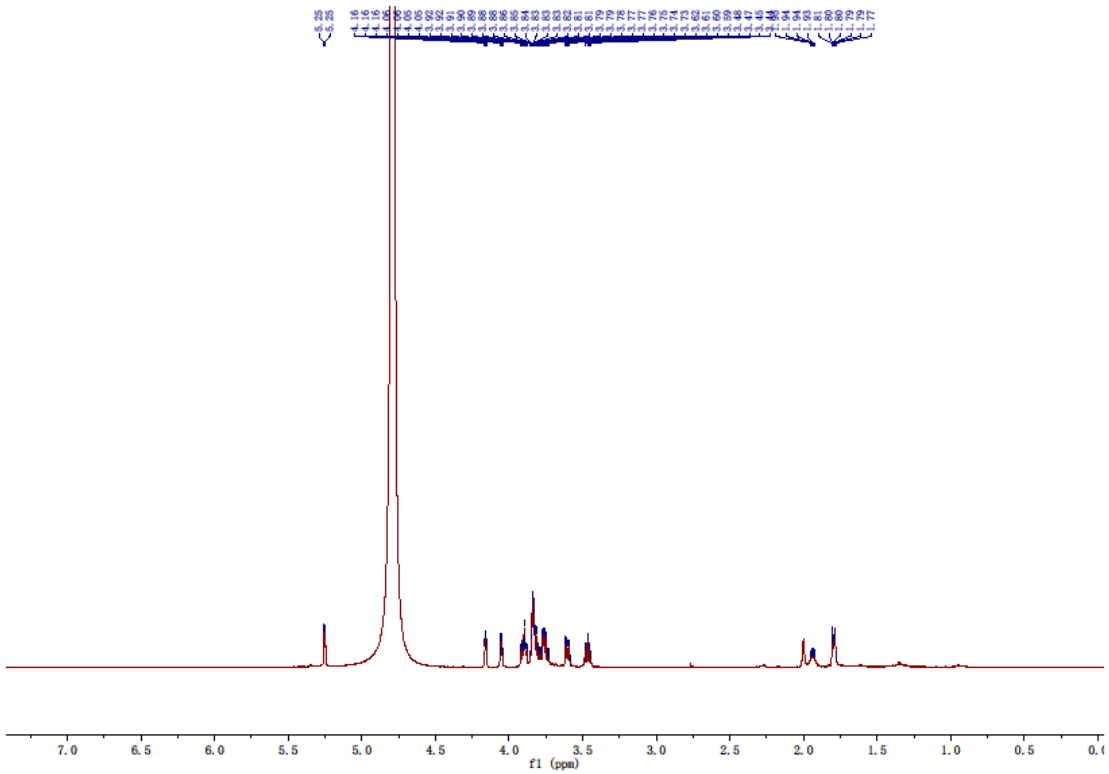

^{13}C NMR (151 MHz) spectrum of **5**

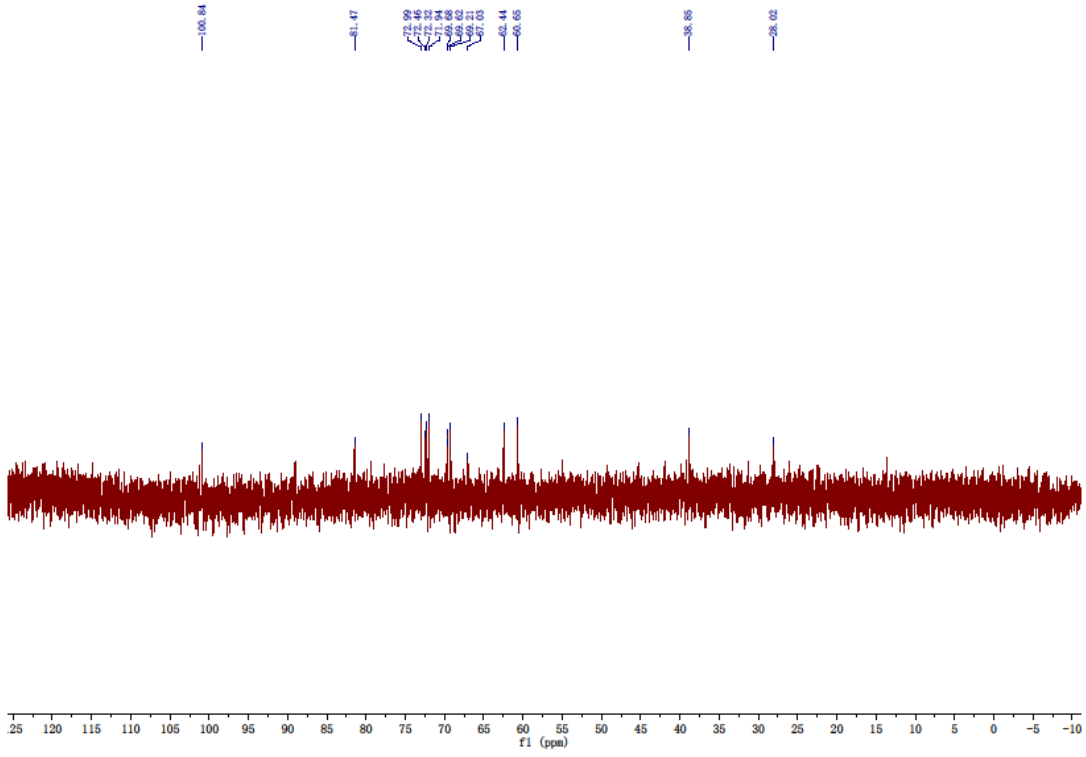

^{13}C DEPT135 spectrum of **5**

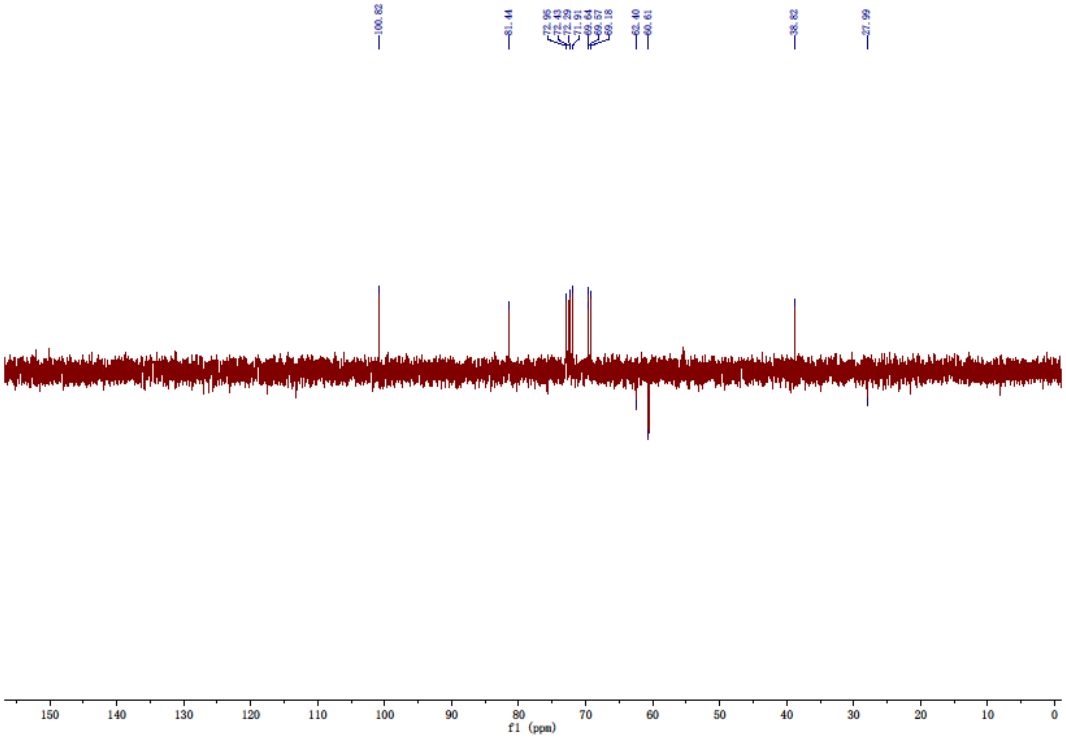

^{1}H NMR spectrum of compound **7** (400 MHz, D_2O)

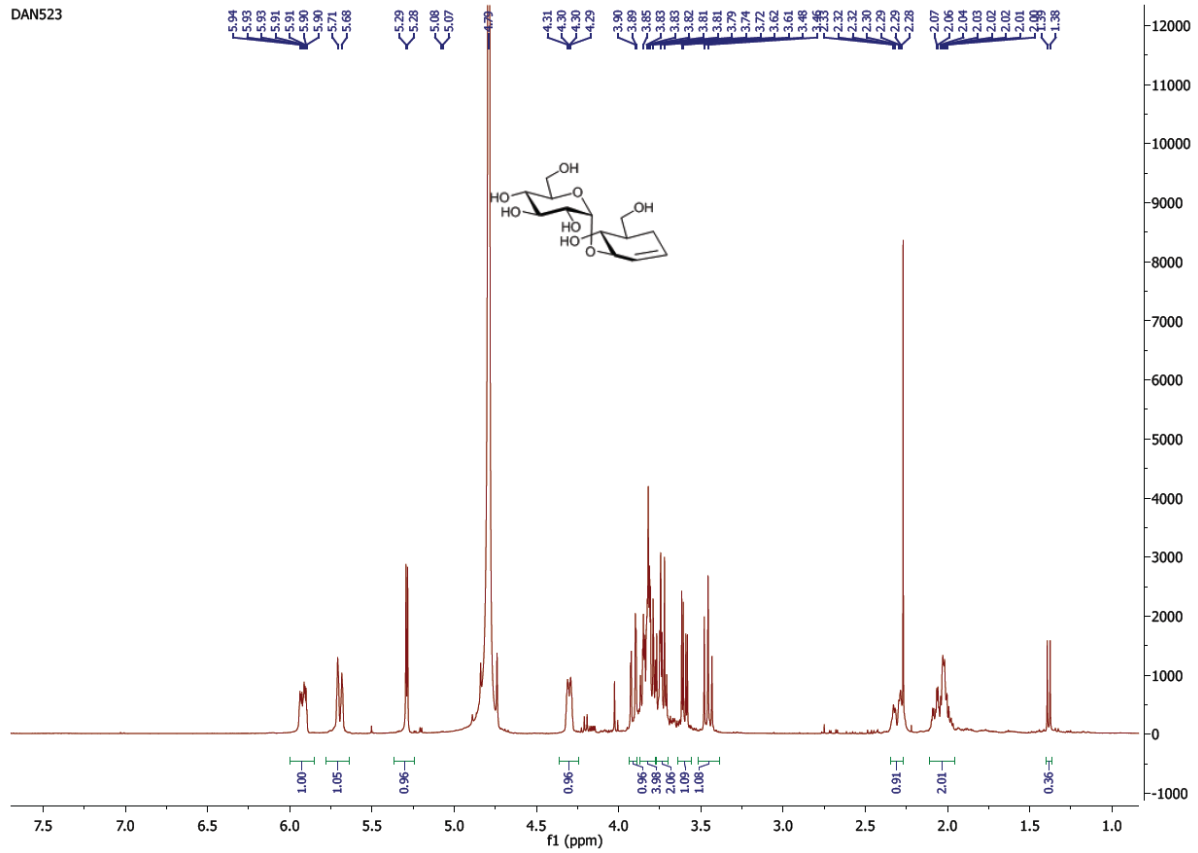

^{13}C NMR spectrum of compound **7** (100.6 MHz, D_2O)

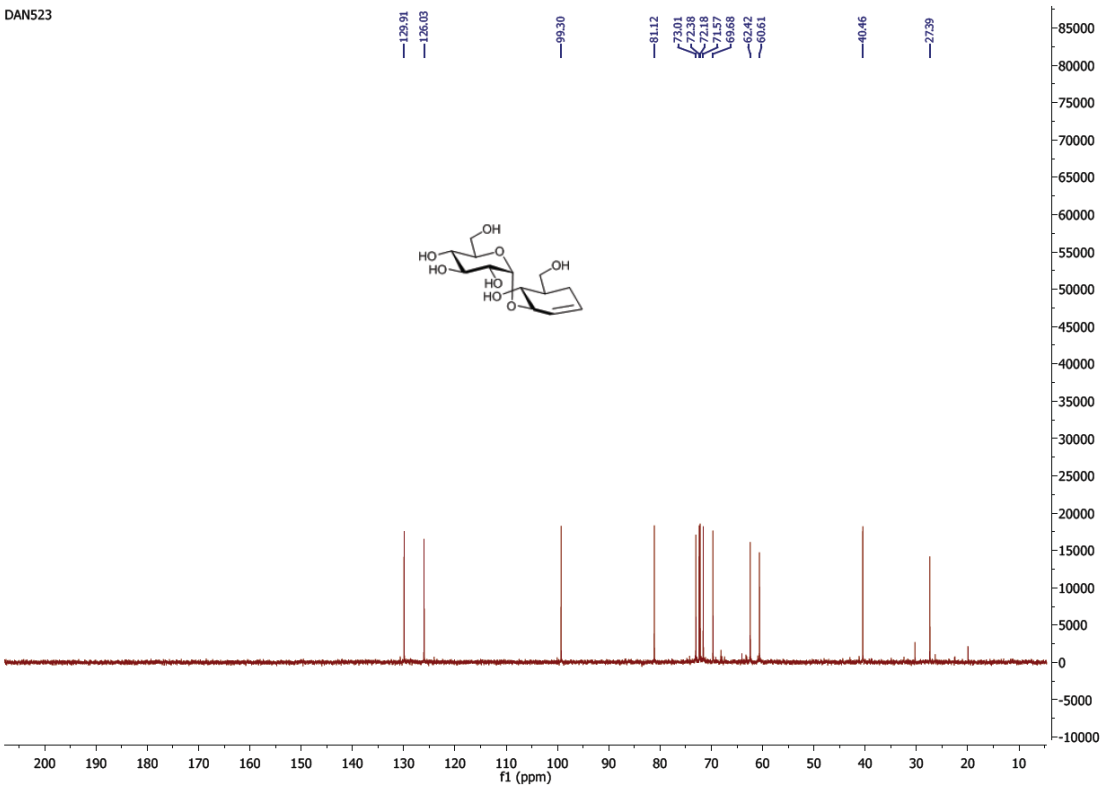

^{1}H NMR spectrum of compound **3** (400 MHz, D_2O)

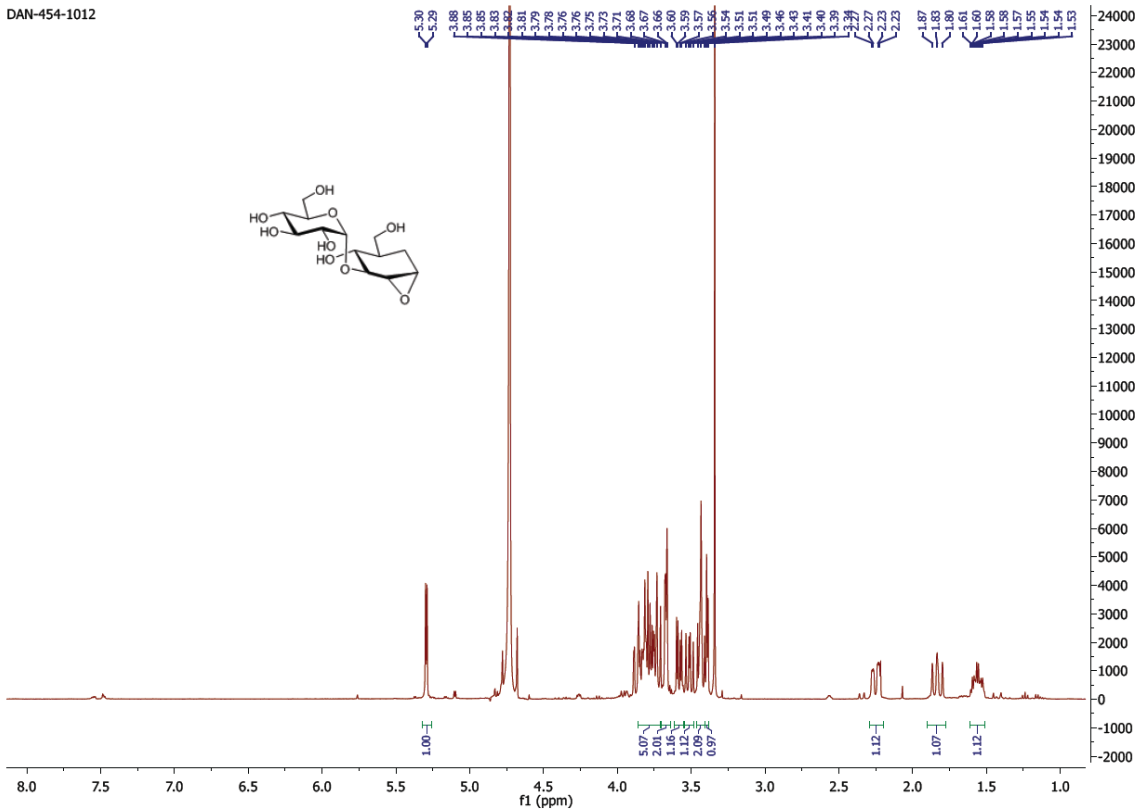

^{13}C NMR spectrum of compound 3 **(100.6 MHz, D_2O)**

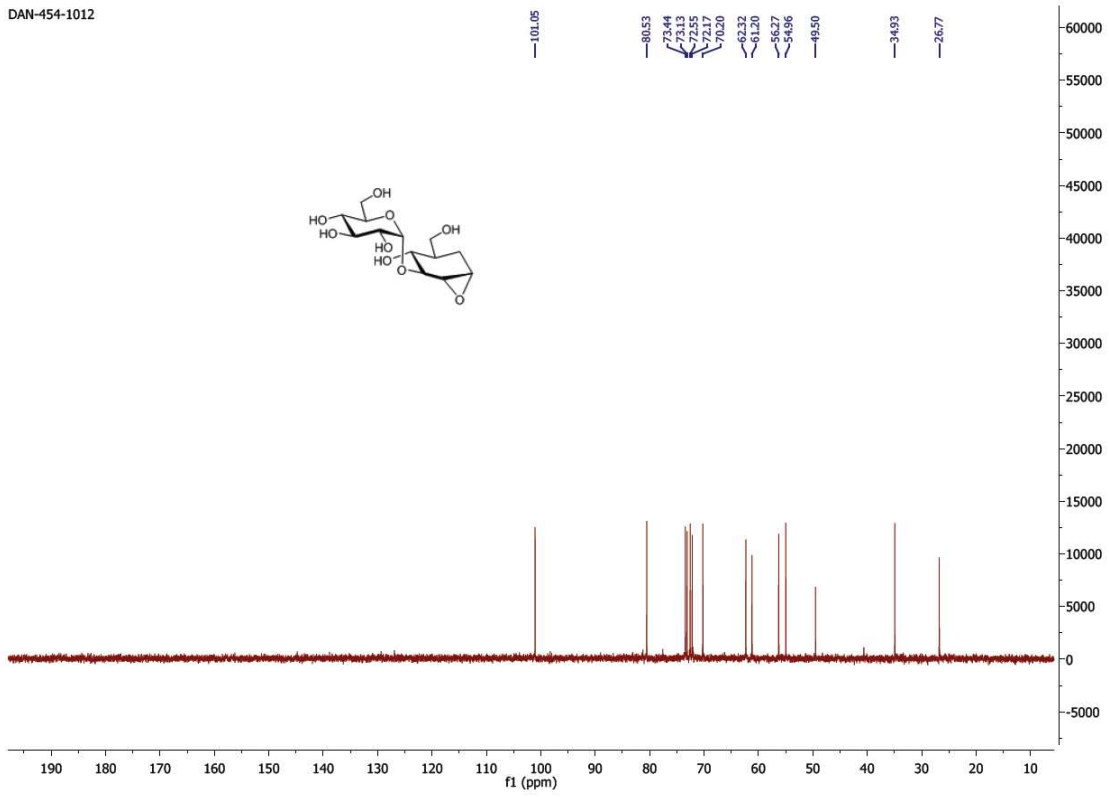

^{1}H NMR spectrum of compound **1** (400 MHz, CD_3OD)

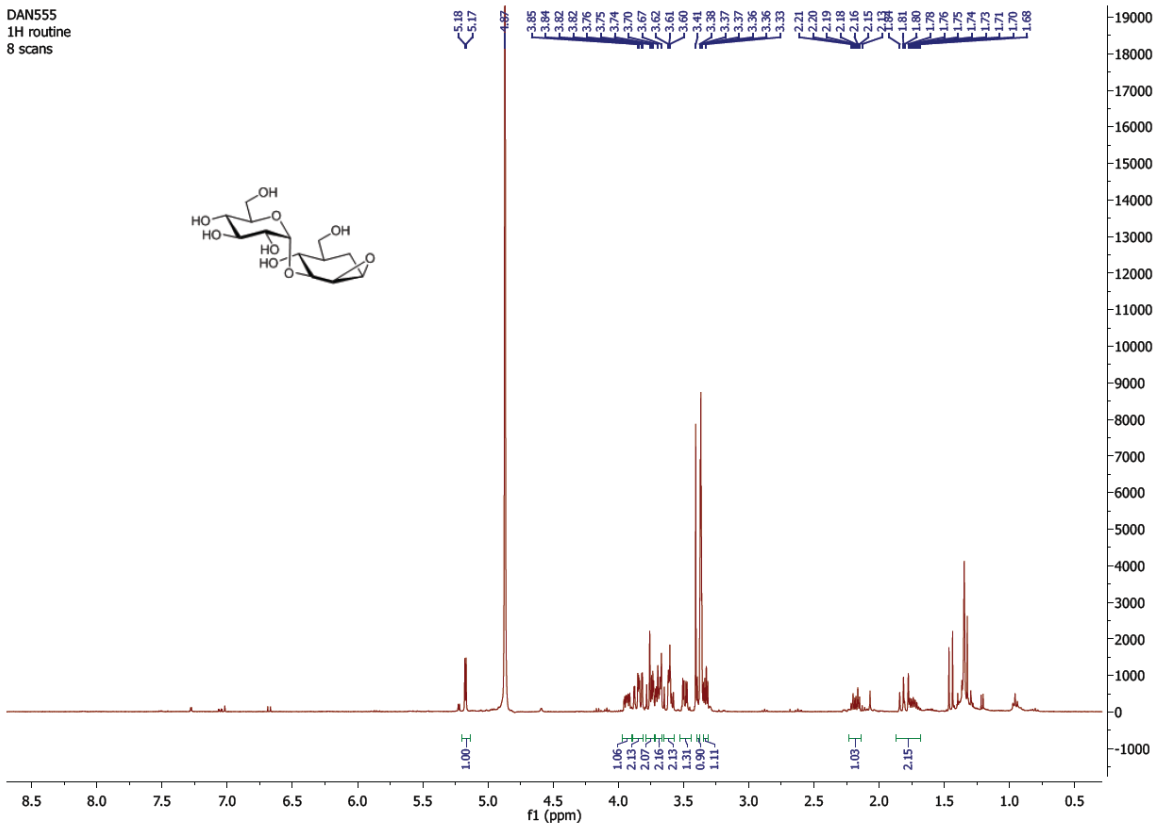

^{13}C NMR spectrum of compound **1** (100.6 MHz, CD_3OD)

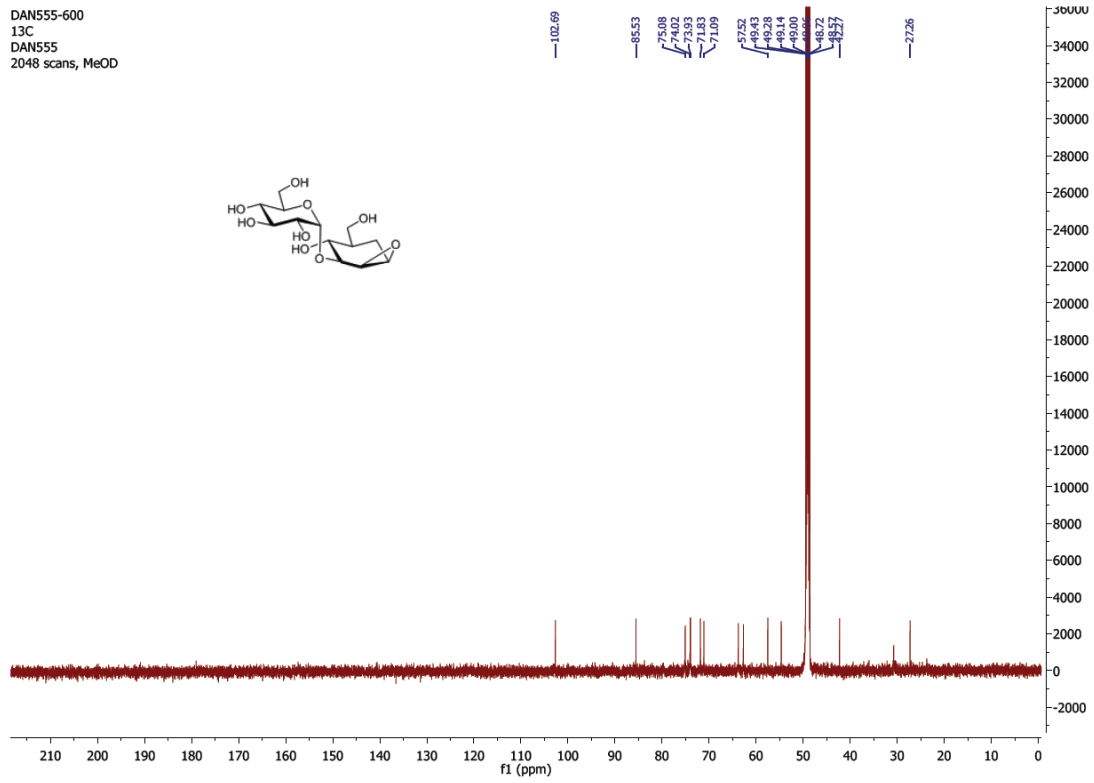

^{1}H NMR spectrum of compound **11** (400 MHz, $CDCl_3$)

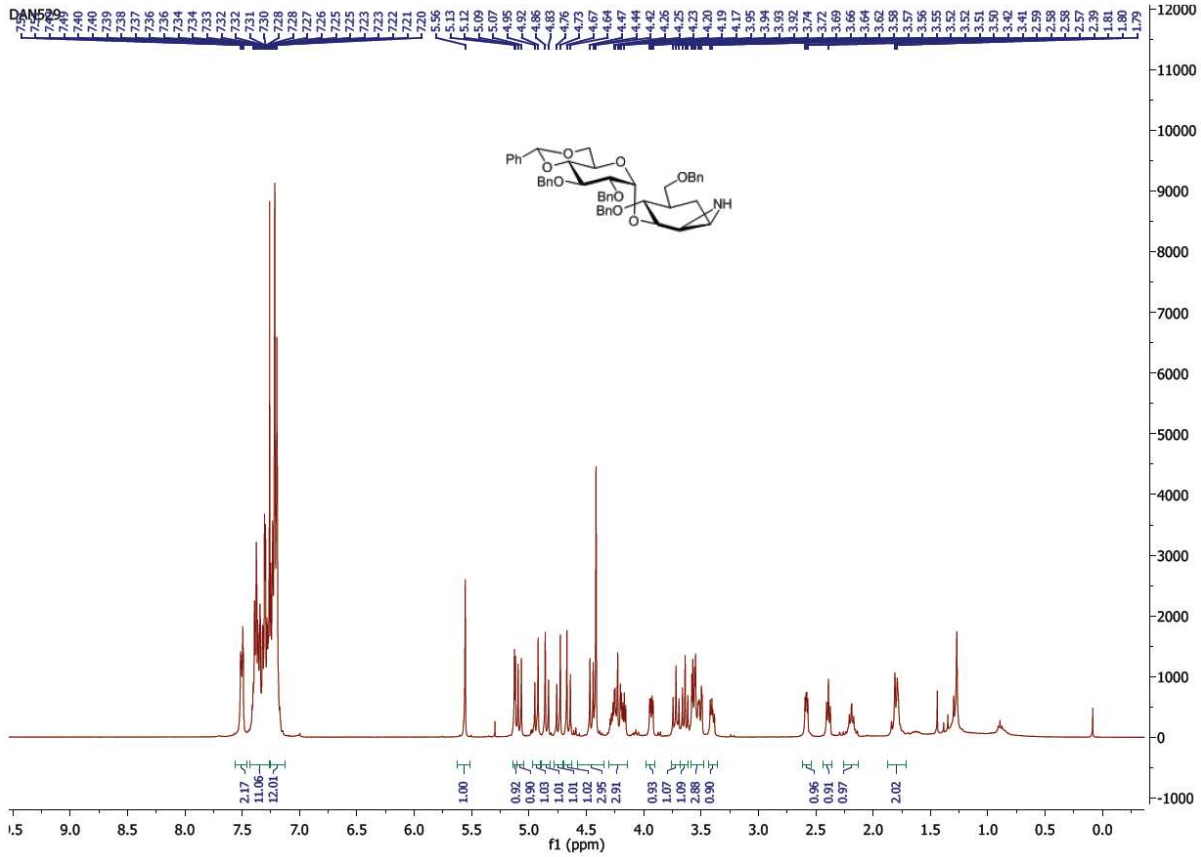

^{13}C NMR spectrum of compound **11** (100.6 MHz, $CDCl_3$)

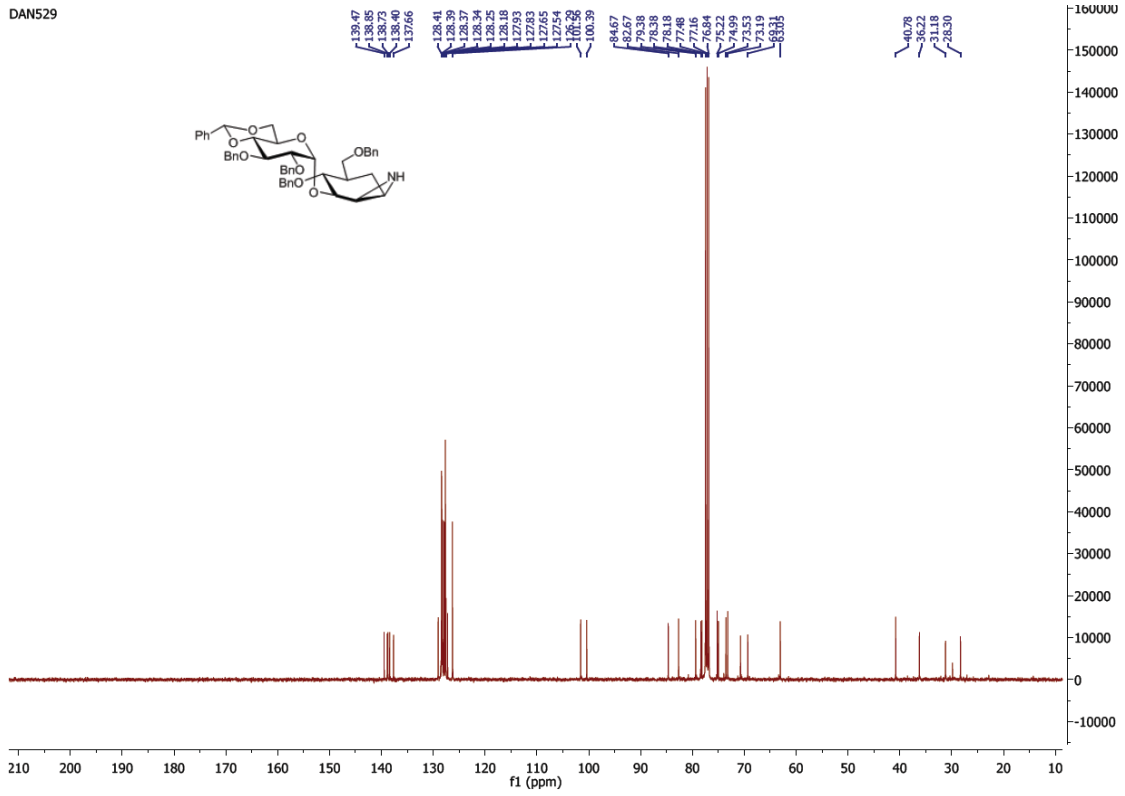

^{1}H NMR spectrum of compound **2** (400 MHz, D_2O)

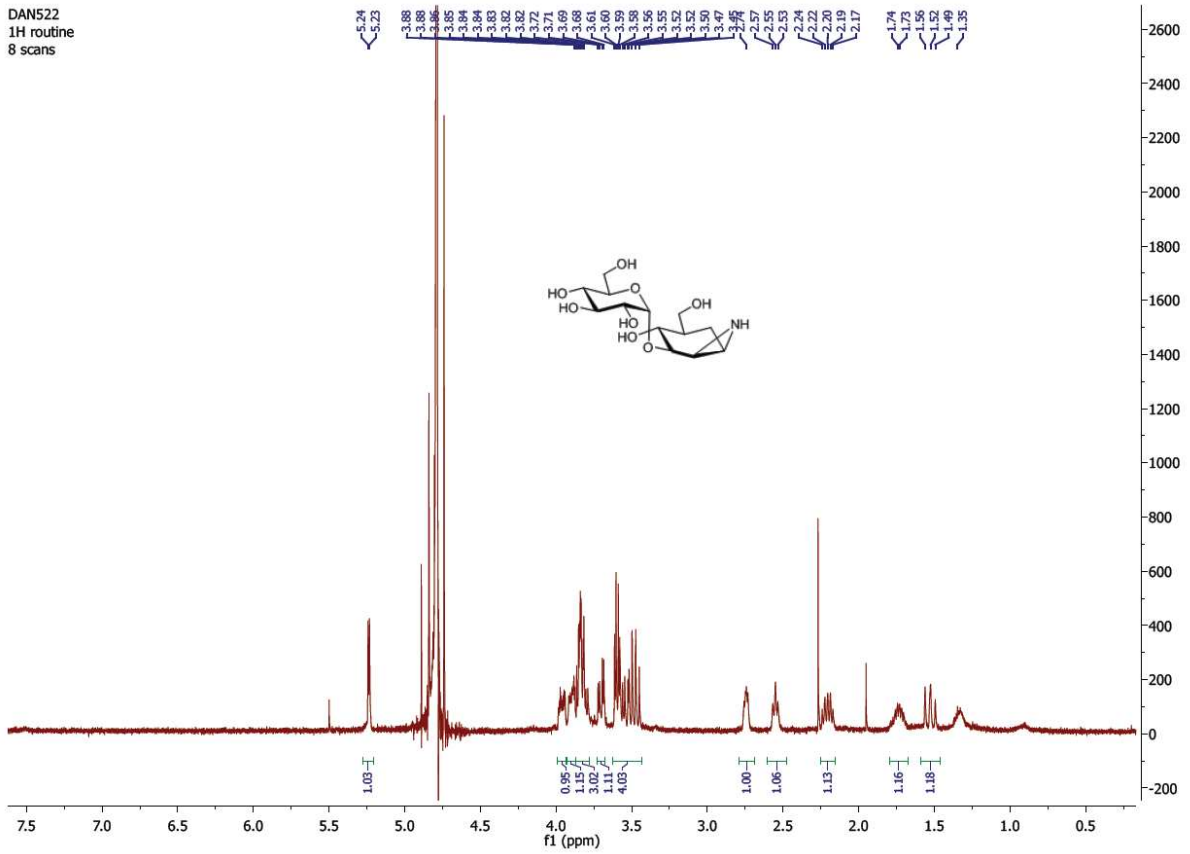

^{13}C NMR spectrum of compound **2** (100.6 MHz, D_2O)